การวิเคราะห์ทางเศรษฐศาสตร์และผลกระทบทางสิ่งแวดล้อมของกระบวนการผลิตดีเซลชีวภาพสังเคราะห์จากน้ำมันปาล์มผ่านกระบวนการไฮโดรทรีตติง

ECONOMIC AND ENVIRONMENTAL ANALYSIS OF PALM OIL HYDROTREATING PROCESS FOR GREEN DIESEL PRODUCTION

นายณัฐภัทร พงษ์บริบูรณ์

NATTAPAT PONGBORIBOON

วิทยานิพนธ์นี้เป็นส่วนหนึ่งของการศึกษาตามหลักสูตรปริญญาวิศวกรรมศาสตรมหาบัณฑิต

สาขาวิชาวิศวกรรมเคมี

คณะวิศวกรรมศาสตร์

สถาบันเทคโนโลยีพระจอมเกล้าเจ้าคุณทหารลาดกระบัง

พ.ศ.2566

KMITL-2023-EN-M-227-181

ECONOMIC AND ENVIRONMENTAL ANALYSIS OF PALM OIL HYDROTREATING PROCESS FOR GREEN DIESEL PRODUCTION

NATTAPAT PONGBORIBOON

A THESIS SUBMITTED IN PARTIAL FULFILLMENT
OF THE REQUIREMENT FOR THE DEGREE OF
MASTER OF ENGINEERING IN CHEMICAL ENGINEERING
SCHOOL OF ENGINEERING
KING MONGKUT'S INSTITUTE OF TECHNOLOGY LADKRABANG
2023

KMITL-2023-EN-M-227-181

Thesis	Economic and Environmental Analysis of Palm Oil Hydrotreating Process for Green Diesel Production
Student	Mr. Nattapat Pongboriboon
Student ID	64601051
Degree	Master of Engineering
Program	Chemical Engineering
Year	2023
Thesis Advisor	Assoc. Prof. Dr. Walairat Chandra-ambhorn

ABSTRACT

Green diesel is a second generation of biofuel obtained from renewable feedstocks with similar properties and molecule structure to petroleum diesel. Green diesel is produced through a hydrotreating of triglycerides, which consists of 3 main reactions: decarbonylation, decarboxylation and hydrodeoxygenation. The simulation for green diesel production has included heat integration and CO_2 capture unit to reduce the energy consumption and CO_2 emission. The current production process has a high conversion, and CO_2 removal based on simulation. This study has focused on the economic and environmental impact analysis of carbon neutral green diesel production process from crude palm oil (CPO). It focuses on analysing the propensity of gross profit using the actual purchase and selling data of a green diesel production comparing with petroleum diesel production. Moreover, this economic evaluation includes carbon prices that the trade carbon prices increase annually. It was found from the result from the approximation that the gross profit between CPO and the retail diesel price is too low to operate commercial production due to the high-priced hydrogen as the main raw material. However, the amount of CO_2 reduction through the CO_2 capture of green diesel production will reduce the higher CO_2 taxation in the future. In terms of environmental impact, green diesel contributes to carbon neutrality, with lower greenhouse gas emissions and reduced air pollution compared to fossil fuels.

Keywords: Economic analysis, palm oil, green diesel, hydrotreatment, heat integration, CO_2 capture and carbon emission

หัวข้อวิทยานิพนธ์	การวิเคราะห์ทางเศรษฐศาสตร์และผลกระทบทางสิ่งแวดล้อมของกระบวนการผลิตดีเซลชีวภาพสังเคราะห์จากน้ำมันปาล์มผ่านกระบวนการไฮโดรทรีตติง
นักศึกษา	นายณัฐภัทร พงษ์บริบูรณ์
รหัสประจำตัว	64601051
ปริญญา	วิศวกรรมศาสตรมหาบัณฑิต
สาขาวิชา	วิศวกรรมเคมี
พ.ศ.	2566
อาจารย์ที่ปรึกษาวิทยานิพนธ์	รศ.ดร.วลัยรัตน์ จันทรอัมพร

บทคัดย่อ

ดีเซลชีวภาพ (green diesel) เป็นเชื้อเพลิงชนิดที่สองที่ได้จากวัตถุดิบทดแทนที่มีคุณสมบัติและโครงสร้างโมเลกุลที่คล้ายกับดีเซลจากปิโตรเลียม ดีเซลชีวภาพถูกผลิตผ่านกระบวนการไฮโดร-ทรีตติง (hydrotreating) ที่มีสามปฏิกิริยาหลักคือ ดีคาร์โบนิเลชัน (decarbonylation) ดีคาร์บอกซิเลชัน (decarboxylation) และไฮโดรดีออกซีเจนเอชัน (hydrodeoxygenation) การจำลองกระบวนการผลิตดีเซลชีวภาพได้รวมการปรับปรุงเครือข่ายเครื่องแลกเปลี่ยนความร้อน (heat integration) และหน่วยดักจับคาร์บอนไดออกไซด์ เพื่อลดการใช้พลังงานและการปล่อยคาร์บอนไดออกไซด์ จากผลการจำลองกระบวนการผลิตปัจจุบันมีค่าปริมาณการเกิดปฏิกิริยาและการกำจัดคาร์บอนไดออกไซด์สูง ในการศึกษานี้มุ่งเน้นการวิเคราะห์ผลกระทบทางเศรษฐกิจและสิ่งแวดล้อมของกระบวนการผลิตดีเซลชีวภาพที่มีความเป็นกลางทางคาร์บอนจากน้ำมันปาล์มดิบ (crude palm oil, CPO) โดยให้ความสำคัญกับการวิเคราะห์แนวโน้มของกำไรขั้นต้นโดยใช้ข้อมูลจริงเกี่ยวกับการซื้อขายและการผลิตดีเซลชีวภาพเทียบกับการผลิตดีเซลจากปิโตรเลียม นอกจากนี้การประเมินทางเศรษฐกิจนี้รวมถึงราคาคาร์บอนที่เป็นมิตรซึ่งมีการเพิ่มขึ้นทุกปี ผลลัพธ์จากการประมาณนี้พบว่ากำไรขั้นต้นระหว่างน้ำมันปาล์มดิบ และราคาดีเซลปลีกสูงเกินไปที่จะดำเนินการผลิตทางการค้าเนื่องจากน้ำมันปาล์มดิบและไฮโดรเจนที่มีราคาสูงเป็นวัสดุดิบหลัก อย่างไรก็ตามปริมาณการลดคาร์บอนไดออกไซด์ที่เกิดขึ้นผ่านการจับกัดคาร์บอนไดออกไซด์ของกระบวนการผลิตดีเซลชีวภาพจะลดภาษีคาร์บอนไดออกไซด์ที่สูงขึ้นในอนาคต ในทางสิ่งแวดล้อมดีเซลชีวภาพมีส่วนร่วมในการทำให้คาร์บอนเป็นศูนย์ด้วยการลดการปล่อยก๊าซเรือนกระจกและลดมลพิษอากาศเมื่อเทียบกับเชื้อเพลิงธรรมชาติ

ACKNOWLEDGEMENTS

I would like to express my sincere gratitude to Prof. Wei Wu and Assoc.Prof. Walairat Chandra-ambhorn for their invaluable guidance, mentorship, and support throughout my academic journey. Their expertise, knowledge, and dedication have been instrumental in shaping my understanding of chemical engineering and have greatly contributed to the successful completion of this project. I am truly grateful for the time and effort that both advisors have invested in providing me with insightful feedback, constructive criticism, and encouraging discussions.

In addition, I would like to express my sincere gratitude to the committee members for their invaluable contribution and guidance throughout the project. Their expertise, insightful feedback, and constructive criticism have greatly enhanced the quality of this work.

I am also thankful for the department's resources, facilities, and opportunities that have enriched my educational experience. The collaborative and nurturing atmosphere within the department has fostered a strong sense of community and encouraged intellectual curiosity.

I would like to express my deepest gratitude to all the professors and the department for their continuous support, encouragement, and belief in my abilities.

Nattapat Pongboriboon

Table of Contents

Page

Table of contents (Cont.)

Page

Table of contents (Cont.)

Page

List of Tables

Page

List of Tables (Cont.)

Page

List of Figures

Page

List of Figures (Cont.)

Page

List of Figures (Cont.)

Page

CHAPTER 1
INTRODUCTION

1.1 Background

Environmental problems and carbon dioxide emissions pose significant challenges to the health of our planet. Human activities, particularly the burning of fossil fuels for energy production, transportation, and industrial processes, release vast amounts of carbon dioxide (CO_2) and other greenhouse gases (GHG) into the atmosphere. These emissions contribute to global warming, climate change, and a range of environmental issues. To address these challenges, reducing carbon emissions and transitioning to cleaner and more sustainable energy sources are essential. Biofuels are regarded as sustainable energy sources due to their renewable nature and potential to reduce greenhouse gas emissions. It is renewable fuels derived from biological sources such as plants, crops, or organic waste. Green diesel provides a viable alternative to traditional fossil fuels, contributing to the reduction of greenhouse gas emissions. The main types of biofuels include ethanol, biodiesel, biogas, and green diesel. As a renewable alternative, green diesel plays a crucial role in reducing reliance on fossil fuels and promoting a more sustainable and environmentally friendly transportation sector. Green diesels contribute to carbon neutrality as the CO_2 released during combustion is offset by the CO_2 absorbed during feedstock growth, forming a closed carbon loop.

To reduce CO_2 emissions in process design and economic analysis, a comprehensive strategy is crucial. It involves optimizing energy usage, considering renewable resources, and improving process efficiency. This strategy should assess the entire lifecycle of a product or process to identify emissions hotspots. Implementing carbon capture and storage, selecting sustainable materials, and enhancing supply chain practices are also vital. An economic analysis helps evaluate the feasibility of emission reduction initiatives. Compliance with environmental regulations, employee engagement, and a commitment to continuous improvement are essential elements of this strategy, ensuring a balance between environmental responsibility and economic sustainability.

Previous research delved into the hydrotreating process of palm oil for green diesel production [1]. This method yields high product rates, minimizes environmental

impacts, and reduces energy consumption, particularly when integrated with evacuated tube solar collectors. The use of renewable energy tends to be more cost-effective than relying on fossil fuels, concurrently diminishing external costs associated with air pollution's impact on human health and environmental harm from CO_2 emissions. While the initial design underwent enhancements through heat integration and process optimization. However, previous studies did not consider the economic analysis and environmental impact of the production process. Consequently, this study aims to evaluate the economic and environmental impacts, encompassing carbon revenue, greenhouse gas emissions, and overall environmental impact, utilizing the Life Cycle Assessment (LCA) technique. The investigation into the green diesel processes' environmental impact employs a midpoint impact based on the CML (Characterization, Midpoint, and Damage) method in SimaPro.

1.2 Objectives

1.2.1 To study green diesel production processes from palm oil using heat integration, CO_2 capture and integrating with an evacuated tube solar collector system.

1.2.2 To evaluate the economics of green diesel production process with and without CO_2 capture unit.

1.2.4 To evaluate the environmental impact of green diesel production process, including the environmental impacts analysis of palm oil plantation, as well as comparison of different process designs of green diesel production process.

1.3 Scopes of work

1.3.1 Simulate the green diesel production process with and without CO_2 capture unit by Aspen Plus®.

1.3.2 Validate the kinetic parameters of palm oil hydrotreating reaction.

1.3.3 Minimize the energy consumption by using Aspen Energy Analyzer.

1.3.4 Evaluate the economic analysis of green diesel production process.

1.3.5 Evaluate the environmental impact of green diesel production process.

1.4 Expected outputs

1.4.1 The design of green diesel production process aims to yield valuable products while minimizing energy consumption and environmental impacts.

1.4.2 The CO_2 capture process is expected to effectively reduce carbon emissions and mitigate environmental impacts.

1.4.3 Green diesel is expected to have favourable economic prospects, offering potential profitability and sustainability in the fuel market.

CHAPTER 2
LITERATURE REVIEW

2.1 Biofuel

Biofuel is a type of renewable energy derived from biological sources, such as plants, crops, or organic waste materials. It serves as an alternative to fossil fuels, with the potential to reduce greenhouse gas emissions and dependence on non-renewable energy sources. There are many types of a biofuel, including ethanol, biogas, biodiesel, and green diesel. Both biodiesel and green diesel are two types of alternative fuels that can be used as substitutes for traditional petroleum-based diesel fuel. Although both fuels are derived from renewable sources, they have different production processes and characteristics. They offer environmental benefits compared to petroleum diesel as they are derived from renewable feedstocks. They can help reduce greenhouse gas emissions, decrease dependence on fossil fuels, and promote sustainability in the transportation sector. The choice between biodiesel and green diesel depends on factors such as feedstock availability, production processes, desired fuel properties, and market availability.

Biodiesel is typically produced from vegetable oils, animal fats, or recycled cooking oil through a process called transesterification. Transesterification involves reacting the oil or fat with an alcohol, usually methanol, in the presence of a catalyst to convert the triglycerides into fatty acid methyl esters (FAME), which make up biodiesel. It can be blended with petroleum diesel at various ratios, such as B20 (20% biodiesel with 80% petroleum diesel). However, higher blends, such as B100 (100% biodiesel), may require some engine modifications or be used in specific dedicated vehicles.

Biofuel, particularly green diesel, serves as an environmentally friendly alternative to traditional diesel fuel. Derived from renewable biomass sources like crops, agricultural residues, and algae, green diesel offers significant advantages. It can be used seamlessly in diesel engines without requiring modifications to existing infrastructure or engines themselves. With its compatibility and versatility, green diesel can be either used in its pure form or blended with petroleum diesel. In addition to reducing carbon dioxide emissions and combatting global warming, biomass-derived green diesel boasts excellent cold flow properties, making it suitable for use in cold climates. Overall, green diesel stands as a promising solution in the quest for sustainable

and eco-friendly transportation fuel options. Green diesel stands out as a superior environmental alternative to biodiesel. Derived from waste materials, it often results in lower greenhouse gas emissions during production. Additionally, its chemical composition, closer to traditional diesel, ensures compatibility with existing engines, reducing the need for modifications and promoting a smoother transition to a more sustainable fuel source. The comparison of properties of petroleum diesel, biodiesel, and green diesel are shown in Table 2.1.

Table 2.1 Comparison of three types of diesels [2,3]

Properties	**Petroleum diesel**	**Biodiesel (FAME)**	**Green diesel (HVO)**
Carbon, wt.%	86.8	76.2	84.9
Oxygen, wt.%	0.0	11.2	0.0
Hydrogen, wt.%	13.2	12.6	15.1
Density at 15°C, g/ml	0.82 – 0.84	0.88	0.77 – 0.78
Flash point, °C	60 – 170	55 – 78	55 – 78
Pour point, °C	3 – 15	-15 to 16	-3 to 29
Cloud point, °C	-13 to 15	-3 to 17	-25 to 30
Cetane number	40 – 45	45 – 55	70 – 90
Viscosity at 40°C, mm2/s	2.0 – 4.5	4.5	2.5 – 3.5
LHV, MJ/kg	42 – 44	37 – 38	34 – 44
Sulphur content, ppm	<10	<1	<1
Change in NOx emissions a, %	–	+10	-10
Storage stability	Good	Medium	Good

2.1.1 Global production and consumption

In recent years, there has been a growing global interest in finding sustainable alternatives to traditional fossil fuels. Biofuels, which are produced from sustainable biomass sources like crops, agricultural residues, and algae, have emerged as a promising solution to combat climate change by reducing greenhouse gas emissions. The global production and consumption of biofuels have witnessed a significant surge, driven by increasing environmental concerns, volatile oil prices, and government policies promoting renewable energy. The transition to biofuels not only provides a

renewable and cleaner energy alternative but also brings forth economic opportunities for nations and plays a role in enhancing energy security. In the global shift towards a more environmentally sustainable future, gaining insights into the production and utilization of biofuels becomes crucial. Understanding the processes and applications of biofuels on a global scale is key to navigating the evolving landscape of energy choices and promoting sustainable practices. The global output of biofuel in 2023 was estimated to be 124 billion U.S. dollars [4]. The market value of biofuels is expected to keep growing and reach around 201.2 billion U.S. dollars by 2030 as shown in Figure 2.1. Therefore, the production of green diesel is expected to increase further.

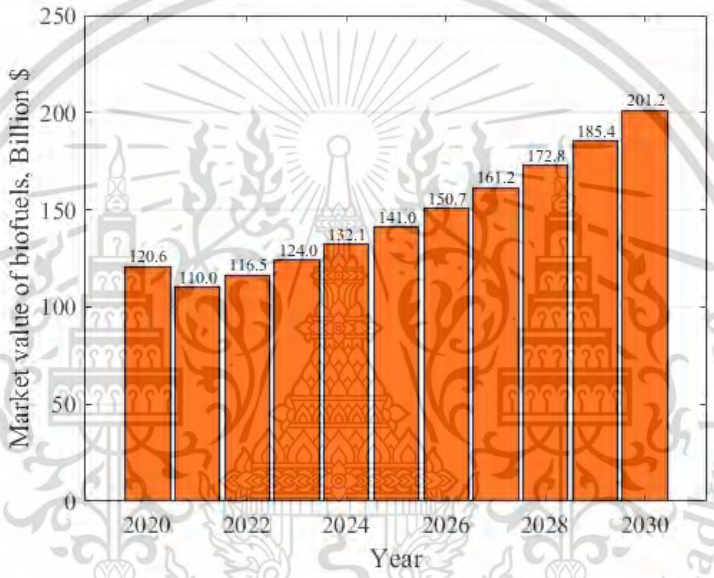

Figure 2.1 Biofuels market value 2021 with forecast until 2030 (data adopted from [4])

2.2 Green diesel

Green diesel, alternatively referred to as renewable diesel or hydrotreated vegetable oil (HVO), is generated via a hydrotreating process. This process involves hydrogenation, where animal fats, waste oils, or vegetable oils are reacted with hydrogen at high temperatures and pressures in the catalyst reactor. The hydrotreating process removes oxygen, sulphur, and other impurities, resulting in a high-quality diesel fuel. Green diesel has properties similar to petroleum diesel and meets the same specifications as shown in Table 2.1. It has a higher energy content compared to biodiesel, which can result in increased fuel efficiency. Green diesel is also low in sulphur and aromatics, leading to reduced emissions of pollutants. Due to its exceptional cold flow properties, it is well-suited for applications in cold climates.

2.2.1 Feedstocks for green diesel

The selection of feedstocks should consider their impact on land use, water resources, biodiversity, and food production to ensure sustainable and responsible production practices. Additionally, feedstock availability may vary depending on geographic location and regional agricultural practices. Green diesel can be produced from various feedstocks. Some common feedstocks used for green diesel production include vegetable oils, animal fat, cooking oils, and algal oils. Vegetable oils derived from oil crops such as canola (rapeseed), soybeans, jatropha, sunflower, and palm can be used as feedstocks for green diesel production. These oils contain triglycerides that can undergo hydrotreating to remove impurities and convert them into green diesel. In this research, palm oil is chosen as the raw material for the hydrotreating reaction due to its significance in the Thai economy. Thailand is currently ranked as the third-largest producer of palm oil globally. Palm oil is rich in various fatty acids, such as palmitic, stearic, oleic, linoleic, and more, as presented in Table 2.2.

Table 2.2 Composition of palm oil fatty acids

Fatty acids		Formular	Composition
Unsaturated	Oleic	$C_{18}H_{34}O_2$	36 - 44%
	Linoleic	$C_{18}H_{32}O_2$	9 - 12%
Saturated	Palmitic	$C_{16}H_{32}O_2$	39.3 - 47.5%
	Stearic	$C_{18}H_{36}O_2$	3.5 - 6%

2.2.3 Simple process flow sheet

A process design for the synthesis of green diesel starting from H_2 and crude palm oils is shown in Figure 2.2. The prepared feedstock undergoes pre-treatment, which may include processes such as heating, filtering, or centrifugation to remove impurities and moisture. The pre-treated feedstock is then subjected to hydrotreatment, also known as hydroprocessing. This process involves reacting the feedstock with hydrogen under high temperature and pressure conditions in the presence of a catalyst. Hydrotreatment removes impurities, sulphur compounds, and oxygenates from the feedstock, resulting in the production of green diesel. The hydrotreated mixture is then sent to a separation unit where various fractions are separated based on their boiling points. Green diesel, having a similar boiling point to petroleum diesel, is separated, and collected as the desired product. The collected green diesel may undergo further refining processes to

meet quality specifications and improve its properties. This may involve processes such as distillation.

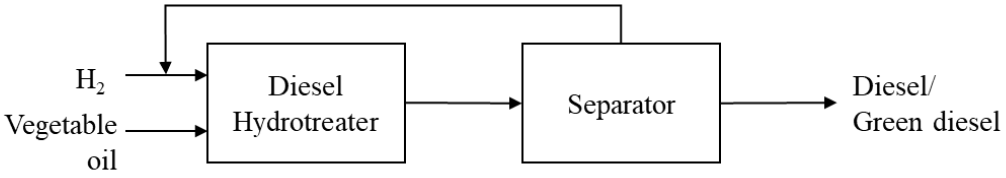

Figure 2.2 Process flow diagram to produce green diesel.

It's important to note that the actual process flow sheet for green diesel production can vary depending on the specific technology and plant design employed by different manufacturers. The steps outlined above provide a general overview of the typical processes involved in producing green diesel from biomass feedstock.

2.2.4 Advantage

- Green diesel possesses similar benefits to biodiesel, as it can be seamlessly utilized in diesel engines without necessitating any adjustments to the engine or infrastructure [4].
- Green diesel provides the versatility of being utilized either in its pure state or blended with conventional petroleum diesel.
- The production of green diesel fuel aids in the reduction of carbon dioxide emissions, contributing to the fight against global warming [5].
- Biomass-derived green diesel is compatible with existing diesel engines and presents the advantage of having a higher cetane number when compared to biodiesel.

2.3 Hydrotreating reaction

Hydrotreating of palm oil involves a crucial reaction process aimed at transforming the properties of the oil to improve its quality and stability. In this process, palm oil is subjected to a series of reactions under specific conditions, typically utilizing a $NiMoS_2/\gamma\text{-}Al_2O_3$ catalyst. The hydrotreating reaction facilitates the removal of impurities, such as sulphur, nitrogen, and oxygen compounds, as well as the saturation of double bonds present in the fatty acid chains of the triglycerides. Triglycerides are compounds found in palm oil that consist of three fatty acid chains attached to a glycerol backbone in an ester form. During the processing of these triglycerides, three main steps are involved [5] as shown in Figure 2.3.

- Saturation: The double bonds present in the hydrocarbon chains of triglycerides are converted into single bonds through a process called saturation.
- Separation: The triglycerides are separated from the glycerol backbone, resulting in the formation of propane as a by-product.
- Oxygen Removal: The remaining molecules containing oxygen are eliminated through a reduction process using hydrogen, effectively removing the oxygen atoms from the compound.

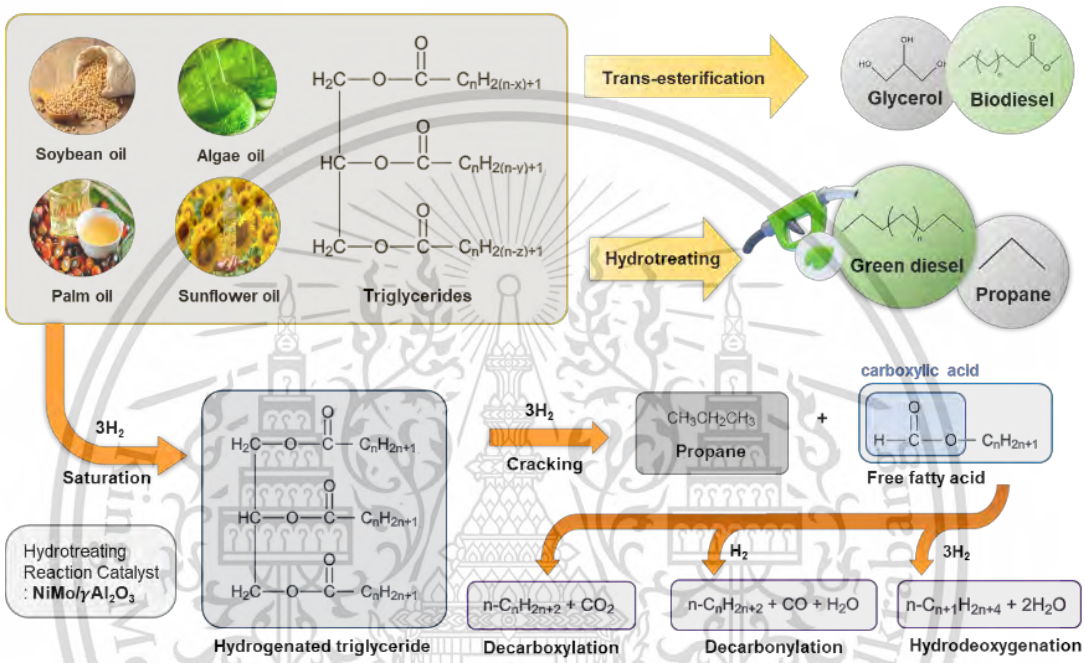

Figure 2.3 Pathway of hydrotreating reaction

2.3.1 Kinetic parameter

Kinetic parameters depend on several factors, including temperature, pressure, reactant concentrations, and reaction conditions such as residence time and reactor type. The kinetic parameters of the reactions are influenced not only by the reactor conditions, primarily temperature, but also by the specific catalyst system being used, as the reactions occur at the catalyst surface [6]. The $NiMoS_2/\gamma\text{-}Al_2O_3$ catalysts are commonly used in hydrotreating reactions due to their high conversion rates (100% conversion) as reported in various studies and publications [7], [8], [9], [10], [11], [12], [13]. The palm oil hydrotreating process is divided into three distinct stages, which include the hydrogenation, hydrodeoxygenation, and hydrodecarboxylation. These stages are illustrated in Table 2.3.

Table 2.3 The mechanism, kinetic expression, and kinetic data of palm oil hydrotreating process [5]

Reaction	**Kinetic expression**	**k_0** (1/s)	**Ea** (kJ/mol)
Hydrogenation of unsaturated triglyceride			
1. $C_{57}H_{98}O_6 + 6H_2 \rightarrow C_{57}H_{110}O_6$	$r_1 = k_1C_{Trilinolein}$	9.4×10^{11}	149.9
2. $C_{57}H_{104}O_6 + 3H_2 \rightarrow C_{57}H_{110}O_6$	$r_2 = k_2C_{Triolein}$	4.4×10^{13}	162.5
Hydrodeoxygenation			
3. $C_{51}H_{98}O_6 + 12H_2 \rightarrow 3C_{16}H_{34} + C_3H_8 + 6H_2O$	$r_3 = k_3C_{Tripalmitin}$	3.8×10^{10}	147.4
4. $C_{57}H_{110}O_6 + 12H_2 \rightarrow 3C_{18}H_{38} + C_3H_8 + 6H_2O$	$r_2 = k_4C_{Tristearin}$	5.6×10^{10}	149.1
Hydrodecarboxylation			
5. $C_{51}H_{98}O_6 + 3H_2 \rightarrow 3C_{15}H_{32} + C_3H_8 + 3CO_2$	$r_1 = k_5C_{Tripalmitin}$	1.4×10^{10}	150.6
6. $C_{57}H_{110}O_6 + 3H_2 \rightarrow 3C_{17}H_{36} + C_3H_8 + 3CO_2$	$r_2 = k_6C_{Tristearin}$	8.2×10^{11}	169.2

2.4 Initial economic potential

The economic potential (EP) is calculated according to the production amount of 1282.38 ton/year of green diesel. The economic potential assumes that the raw materials are converted completely into product (100% conversion) for all reactions in section 2.3. The initial economic potential can be calculated as follows:

$$EP = \text{Cost of products sold} - \text{Cost of raw materials} \quad (1)$$

The market price for green diesel was assumed to be equal to the selling price of petroleum diesel, resulting in Table 2.4 for economic potential.

Table 2.4 Initial Economic potential, flow rate and the price summary

Substance	Mass flow (kg/hr)	Price (USD/kg)	Cost (USD/hr)	Cost (USD/$kg_{Green\ diesel}$)
Hydrogen	36.69	3.30	121.08	0.11
CPO	1282.38	1.08	1388.81	1.28
LPG	42.20	1.20	50.64	0.05
GD	1083.08	1.35	1462.16	1.35
Economic Potential (EP)				**0.05**

2.5 Literature survey

There is much research that explored various feedstocks, catalysts, process conditions, and optimization strategies to improve the efficiency and yield of green diesel production. Additionally, comparisons with other biofuels, such as biodiesel, have been conducted to assess the performance and advantages of green diesel. The literature survey provides valuable insights into the current state of research, technological advancements, and the potential of green diesel as a sustainable alternative to conventional diesel fuel.

Kittisupakorn et al. [14] investigated energy optimization of palm oil hydrotreating process for green diesel production. The hydrotreating process by using $NiMoS_2/Al_2O_3$ is simulated. The production capacity and energy consumption of green diesel production process are 200,000 tonnes per year and 124,510 kW, respectively. The three designs of heat exchanger network (HEN) are investigated for minimize the energy consumption. The result showed that the use of all three HEN designs can reduce energy consumption by up to 89.36% or a value of 111,195kW.

Hilbers et al. [15] produced green diesel and jet fuel and evaluated the economics of green diesel production from crude palm oil (CPO). The results show the difference in price between crude palm oil and retail diesel is insufficient to support the operation of a financially sustainable process. Nevertheless, the production and use of biofuels are mandated by international regulations. Based on an assumed internal rate of return (IRR) of 15% and a depreciation period of ten years, a negative cash flow of 900 million dollars (M$) was calculated. In order for the palm oil-based process to be economically viable, the current diesel price of around 1.10 $/kg would need to increase to 1.35 $/kg. Alternatively, the price of palm oil would need to decrease from approximately 0.75 $/kg to less than 0.50 $/kg. These adjustments are necessary to create a favourable economic scenario for the utilization of palm oil in the process.

Wu et al. [1] investigated the development of palm oil-based polygeneration systems to produce green diesel and LPG. The fixed bed hydrotreating reactor (FBHTR) model optimization, CO_2 capture technologies, and heat integration designs contribute to achieving CO_2-negative emissions and the production of high-purity products. Further research and optimization of these designs hold promising potential for sustainable energy production from palm oil feedstock. Additionally, an amine-based CO_2 capture process is integrated with either pre- or post-separation systems to produce high-purity CO_2 as a by-product. The results show that design 3 further enhances the

CO_2 capture process by producing three high-purity products simultaneously: 98.3% of green diesel, 100% of LPG, and 99.9% of CO_2. In addition to achieving negative net CO_2 emissions, Design 3 incorporates a heat integration design to minimize the energy duties of hot/cold utilities.

CHAPTER 3
METHODOLOGY

The methodology of process simulation with economic and environmental analysis involves using computer-based models to simulate and analyse chemical or industrial processes. This methodology integrates economic and environmental analysis into the simulation to assess the financial feasibility and environmental impact of the process as shown in Figure 3.1. It starts with gathering relevant data on the process, including inputs, outputs, operating conditions, and cost parameters. The simulation model is then developed, which represents the process mathematically and simulates its behaviour over time. Economic analysis is performed by incorporating cost data, such as raw material prices, energy costs, labour expenses, and equipment costs, to evaluate the profitability and financial viability of the process. Environmental analysis involves considering environmental factors such as energy consumption, emissions, waste generation, and the use of environmentally friendly technologies or materials. By integrating economic and environmental considerations, this methodology enables decision-makers to identify optimal process configurations, evaluate the impact of different scenarios, and make informed decisions that balance economic efficiency and environmental sustainability.

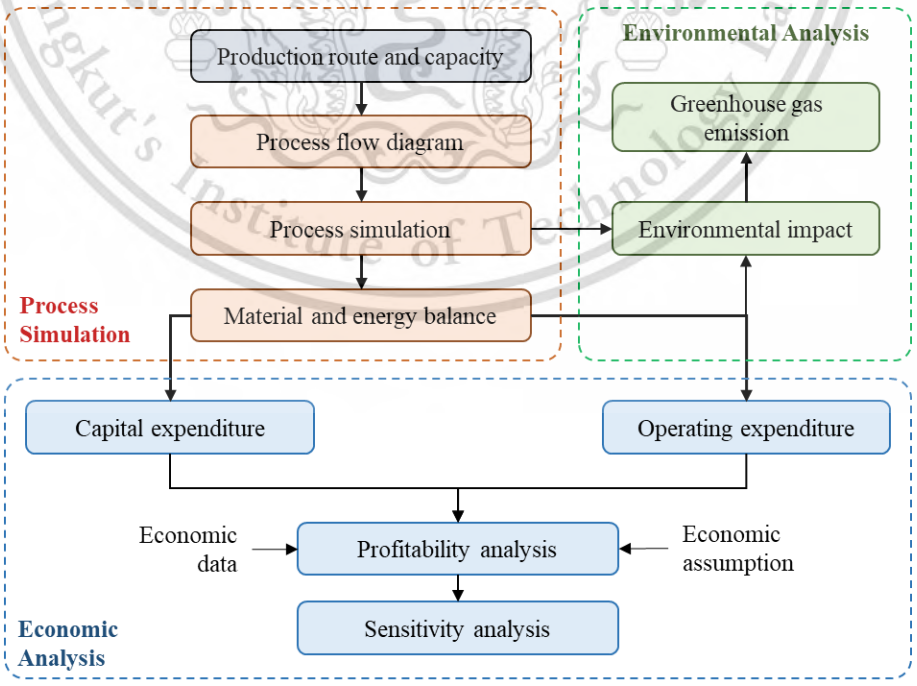

Figure 3.1 Methodology framework of green diesel production

3.1 Process Simulation

Green diesel is acknowledged as an eco-friendly fuel, and in order to create a more environmentally conscious system, the evacuated tube solar collector (ETSC) system is implemented to generate the thermal energy required for palm oil pre-treatment in green diesel production process. This section focuses on the process design and simulation of green diesel production using Aspen Plus® V14. The design of the ETSC system, including the number and arrangement of units, is determined through the utilization of a mathematical model. In addition, the process is integrated with CO_2 capture unit to further enhance its environmental sustainability. The incorporation of CO_2 capture technology allows for the separation and capture of carbon dioxide emitted during the green diesel production process. By capturing and effectively managing CO_2 emissions, the system aims to reduce its carbon footprint and contribute to the mitigation of greenhouse gas emissions. This integration of CO_2 capture underscores the commitment to creating a more environmentally friendly and sustainable green diesel production system. The objective is to establish an efficient and sustainable approach to green diesel production while minimising environmental impact.

3.1.1 Hierarchical decomposition

Hierarchical decomposition is a problem-solving approach that breaks down complex tasks or systems into smaller, more manageable components. By organising the problem into a hierarchical structure, it becomes easier to understand and tackle the different aspects of the problem. This method allows for a systematic analysis of the problem at various levels of detail, enabling a step-by-step approach to problem-solving. By breaking down the problem into smaller sub-problems, it becomes more feasible to identify and address specific issues, leading to a more efficient and effective solution. For the process design of the green diesel production, hierarchical decomposition is divided into four levels as follows:

Level 1: Decisions on batch versus continuous.

Deciding whether to use batch or continuous production for green diesel involves considering a few things. For smaller operations, batch production works well because it can handle different amounts and types of feedstocks. Otherwise, continuous production is better for larger operations because it keeps the process flowing without stopping. If the availability of feedstock is inconsistent, batch production is more suitable, while continuous production needs a steady supply. Continuous production is

more efficient and produces a consistent product, but it may cost more upfront. Batch production allows for more flexibility in adjusting the process, while continuous production is better for standardised products and larger market demands. Environmental impacts should be considered too, as continuous production may use more energy and batch production may have extra impacts during startup and shutdown. Ultimately, the choice depends on factors like scale, feedstock availability, efficiency, costs, product specifications, and environmental concerns. The production of green diesel can either be a batch or continuous process [16]. Therefore, the process plant of green diesel from hydrotreating of crude palm oil is considered to be continuous process.

Level 2: Decisions on input and output structure.

The composition of crude palm oil comprises 41.09 wt% triolein, 36.53 wt% tripalmitin, 13.81 wt% trilinolein, and 8.57 wt% tristearin [5]. These raw materials contain slight amounts of impurities. The number of impurities is relatively small and does not take part in either of the reactions, so it is not required to remove them before the reactors.

Level 3: Decisions on recycle structure and reactor.

The process involves one reactor, the reactions have 100% conversion so there will be one recycle stream for the unreacted reactants. In this green diesel production process, hydrogen is the residue of the reaction. The decision to recover unreacted hydrogen involves considering whether to collect and reuse hydrogen that remains unused after a chemical reaction. This decision depends on evaluating the economic, environmental, and technical factors associated with hydrogen recovery. Factors such as the cost-effectiveness of the recovery process, the availability of suitable technologies, and the potential benefits of reusing the unreacted hydrogen play a crucial role in determining whether recovery is viable. Therefore, the green diesel production process is decided to recover hydrogen as it is a costly substrate, and the recovery diagram is shown in Figure 3.2.

Level 4: Decisions on separation system.

The stream from the hydrotreating reactor exists in three phases and can be separated using *Flash3* model, with the unreacted reactants in gaseous phase, light liquid, and the green diesel product in liquid phase. The initial separator is designed to separate green diesel from water and gases. The gaseous phase from the first separator consists of hydrogen, propane, water, and CO_2. The presence of carbon dioxide as an

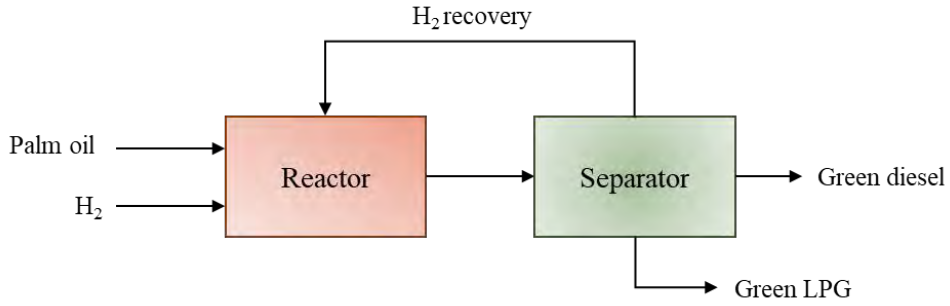

Figure 3.2 Decisions on recycle stream.

impurity in the product stream can lead to corrosion in valves, pipelines, and pressure vessels when it combines with water to form acids or acidic solutions. Therefore, this study will investigate a process design both with and without a CO_2 capture unit.

In a separation design without CO_2 capture unit as shown in Figure 3.3, the focus is on separating desired components while minimizing the separation of CO_2. This design aims to optimize the separation process for specific target substances or purification requirements, taking into account factors such as selectivity, efficiency, and energy consumption. On the other hand, in a separation design with CO_2 capture, an additional unit is integrated into the process to capture CO_2 from the gas stream as shown in Figure 3.4. Various methods can be employed for CO_2 capture, such as absorption, adsorption, or membrane separation. The design considers the specific characteristics of the system and aims to maximize CO_2 capture efficiency while minimizing energy consumption and overall process costs. The remaining hydrogen and hydrocarbon contents are separated by the cryogenic separator. Propane, which has a higher boiling temperature compared to hydrogen, is condensed and separated as a liquid.

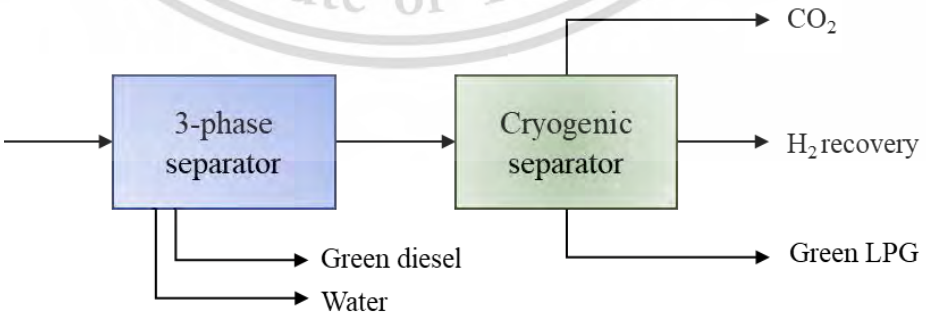

Figure 3.3 Separation design 1 of green diesel production (without CO_2 capture)

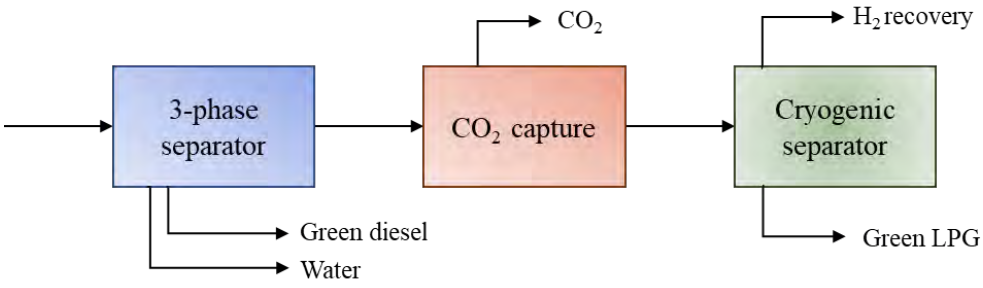

Figure 3.4 Separation design 2 of green diesel production

3.1.2 Addition of components

Process simulation of green diesel production started from adding components based on hydrotreating reactions. The components are specified in components-specification panel of Aspen Plus® as shown in Figure 3.5.

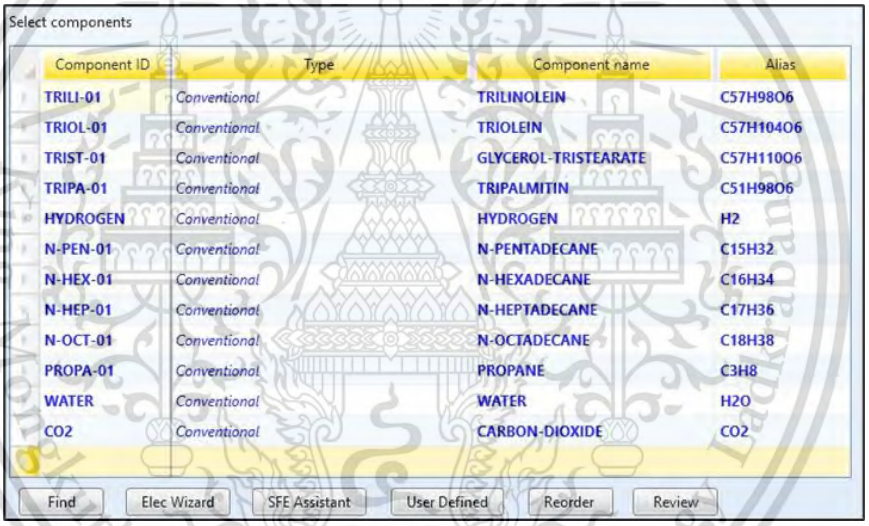

Figure 3.5 Components for hydrotreating reaction in Aspen Plus®

3.1.3 Thermodynamic model selection

The selection of a thermodynamic model is the most critical decision that significantly impacts the results when utilizing a chemical process simulation. Selecting an appropriate thermodynamic model depends on the specific system and the information required for analysis. When selecting a thermodynamic model, various factors need to be taken into account, including the behaviour of different phases, the temperature range, and the pressure range. In this study, Peng-Robinson model and electrolyte non-random two liquid model were chosen to be used as thermodynamic models in the green diesel and carbon dioxide capture processes, respectively.

The Peng-Robinson model is an equation of state (EOS) commonly used in thermodynamics and chemical engineering to calculate the properties of fluid mixtures. It provides an estimation of the thermodynamic properties of both pure components and mixtures, including vapour-liquid equilibrium (VLE) calculations. It is particularly useful for hydrocarbon systems, such as those encountered in the petroleum, petrochemical, and natural gas industries. Literature suggests the utilization of the Redlich-Kwong or Peng-Robinson equations of state for estimating thermophysical properties in hydrocarbon mixtures [6], [17]. Thus, the Peng-Robinson model (PENG-ROB) is chosen to effectively capture the characteristics of high-pressure gas phase systems, while the non-polar nature of triglycerides allows for an approximation of ideal liquid behaviour.

The electrolyte non-random two liquid model (ELCL-NRTL) model for electrolyte solutions can provide information about various properties, including activity coefficients, vapour-liquid equilibrium, liquid-liquid equilibrium, and excess enthalpy. It is commonly used in chemical engineering and process design for simulating and predicting the behaviour of electrolyte solutions in various industrial processes, such as chemical reactions, separation processes, and solvent extraction. Therefore, ELEC-NRTL is used for explaining the electrolytic interaction of carbon dioxide and MEA-water solution in CO_2 capture process.

3.1.4 Model validation

To ensure the accuracy of the kinetic model in the hydrotreating reaction, a kinetic validation step was taken before initiating the process design. This step involved validating the kinetic parameters of the reactions, which included the determination of the reaction rate constant and activation energy. The purpose of this validation is to ensure the accuracy, reliability, and precision of the kinetic model. By verifying these parameters, the accuracy of the kinetic model for hydrotreating reaction is guaranteed. The design of the reactor section in the green diesel production process aimed to closely resemble the actual process implemented in the green diesel plant, as illustrated in Figure 3.6.

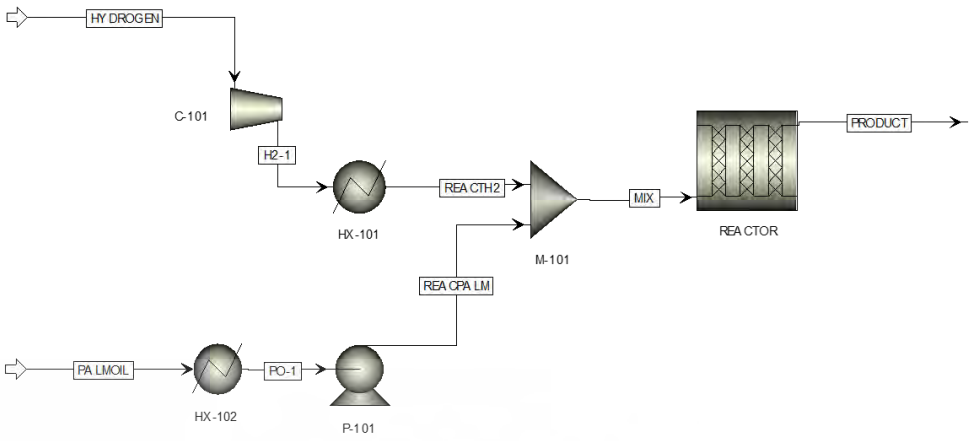

Figure 3.6 The green diesel production process flowsheet of reactor for validation.

The parameters for the reactor setup are shown in Table 3.1. The reactor used in the study was classified as an isothermal reactor, as the temperature was maintained at a specified value throughout the reaction. The operating conditions of the reactor, including temperature and pressure, were determined based on experimental observations. The dimensions of the reactor and the amount of catalyst loaded were designed to align with the experimental reactor [18]. It is worth noting that the reactor length was relatively short, leading to negligible pressure drop across the reactor.

Table 3.1 The parameters for the reactor in a model validation [18]

Parameters	**Value**
Reactor type	Reactor with specified temperature
Reactor diameter (cm)	7
Reactor length (cm)	30
Catalyst weight, $NiMoS_2/\gamma\text{-}Al_2O_3$ (g)	8.5
Catalyst density (kg/m^3)	717.15
Pressure drops (bar)	None
Reaction phase	Vapour-liquid

3.1.5 Equipment design

The equipment design for green diesel production involves various key components to ensure an efficient and reliable process. It typically includes reactors, separators, heat exchangers, pumps, compressor, and evacuated tube solar collector (ETSC). The reactors are designed to accommodate the specific reaction conditions required for the hydrotreating process, where the catalyst is employed to facilitate the conversion of feedstock into green diesel. Separators are utilized to separate different

components, such as propane, hydrogen, and purified green diesel, based on their different physical properties. Heat exchangers are incorporated to optimize heat transfer and maintain the desired temperatures throughout the process. Pumps and compressors are responsible for fluid circulation and maintaining adequate pressure levels. The equipment design takes into consideration factors such as safety, efficiency, and adherence to regulatory standards, ensuring the smooth operation of the green diesel production process.

1) Reactor

The reactor section of the green diesel production process was designed to replicate the actual operations of green diesel plant. Before entering the hydrotreating reactor, palm oil and hydrogen undergo heating and pressurization to meet the required operating conditions. This process involves a heater and various pressure control devices such as pumps and compressors. The reactor employs a plug flow configuration to ensure efficient vapour-liquid reactions. The optimal values for the hydrotreating temperature, hydrogen pressure, LHSV and H_2/oil ratio are 323.81 °C, 30.04 bar, 1.001 h^{-1} and 1,186.07 cm^3/cm^3, respectively. These values resulted in a 100% conversion and 84.40% yield [1]. The operating conditions for the feed in the industry and the dimensions of the fixed-bed reactor were established as illustrated in Table 3.2.

Table 3.2 The parameters for the large-scale reactor

Parameters	**Value**
Reactor type	Reactor with specified temperature
Reactor diameter (m)	0.625
Reactor length (m)	10.15
Catalyst weight, $NiMoS_2/\gamma\text{-}Al_2O_3$ (g)	2,232
Catalyst density (kg/m^3)	717.15
Pressure drops (bar)	None
Reaction phase	Vapour-liquid

2) Three-phase separator

In the gas and oil industry, a three-phase separator is commonly employed for the separation of mixed products into gas, oil, and water phases. This separator utilizes the gravity separation technique. As the products enter the vessel, they encounter the inlet diverter, causing an immediate separation of gases from liquids. The buoyancy force facilitates the removal of gases at the top of the vessel. The remaining oil and

water descend to the bottom of the vessel under the influence of gravity and undergo a rapid separation, forming two distinct layers. An emulsion layer may also form above the water layer. The levels of oil and water are carefully maintained through the use of a level controller. The oil spills over a weir, enabling its separation from the water. Both liquids can then be efficiently removed from the vessel by controlling the appropriate control valves.

During the simulation process, Aspen Plus® utilizes the *Flash3* unit to perform Vapour, light liquid, and heavy liquid separation. This unit combines the functionalities of the *Flash2* and Decanter units. Hence, *Flash3* was chosen as the appropriate unit for separating green diesel from gases and water. The three-phase separator operates at elevated pressures, which effectively raises the boiling temperature of the components and reduces cooling consumption, resulting in improved energy efficiency.

3) Cryogenic

Cryogenic technology offers several advantages in handling hydrocarbons and hydrogen (C_3H_8 and H_2). It enables efficient transportation and storage, allowing for greater quantities to be transported in liquid form compared to their gaseous state. One significant advantage of the cryogenic technique is its capability to directly produce liquefied gas, which is highly advantageous for transportation purposes. By transforming the gas into its liquid state, it becomes more efficient to store and transport, offering increased storage capacity and reduced space requirements. This makes the cryogenic technique particularly valuable in industries where the transportation of liquefied gases, such as propane, is essential. Therefore, in this green diesel production, cryogenic is selected to separate propane from the gas mixture.

For the simulation process, the *Flash2* in Aspen Plus® is chosen to replicate the functionality of the propane separator. This selection is based on the difference of boiling temperatures between hydrogen and propane. Operating the separator at high pressure contributed to increased component boiling temperatures, resulting in reduced cooling requirements from the refrigeration system. This approach offered a cost-effective and energy-efficient solution for the separation process.

4) CO_2 capture unit

The hydrotreating reaction in the production process generates carbon dioxide (CO_2) as an impurity in the gas product stream. Removing carbon dioxide from the gas products is crucial for several reasons. Firstly, it reduces the volume of gas for

transportation, making it more efficient and cost-effective. Secondly, it increases the calorific value of the final gas product, improving its energy content. Additionally, controlling the concentration of carbon dioxide in the gas products is essential to prevent pipeline corrosion issues during transportation. The CO_2 capture technologies are shown in Figure 3.7. The choice of CO_2 capture technology depends on factors such as the type of facility, emissions characteristics, and economic considerations. Among these technologies, chemical scrubbing stands out as a suitable option for the gas and oil industry. It offers high product purity, low product losses, and cost-effective operation.

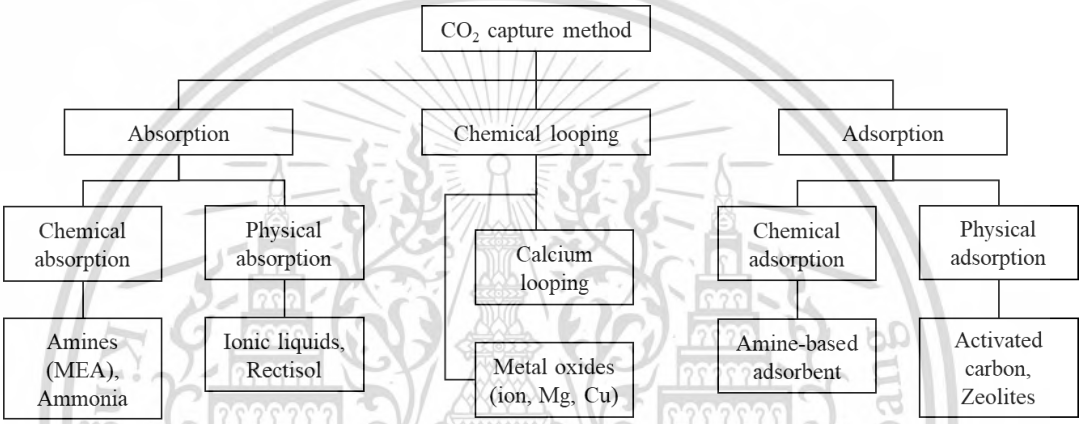

Figure 3.7 CO_2 capture method [19]

The simulation of CO_2 capture unit, 35%wt of monoethanolamine (MEA) is chosen as solvent due to its high selectivity in capturing carbon dioxide (CO_2) from gas streams. In Aspen Properties®, carbon dioxide, water and MEA are selected as base components for generating the ions as shown in Figure 3.8. The software generates 11 components as the ions and salts for CO_2-MEA-H_2O system by using the Electrolytes Wizard as shown in Figure 3.9. Furthermore, the software generates a series of ionic equilibrium reactions, which are used to analyse and determine the compositions involved in the given process. In this study, the set of ionic reactions in the following equation have been considered.

$$H_2O + MEA^+ \rightleftharpoons MEA + H_3O^+ \quad (2)$$

$$H_2O + MEACOO^- \rightleftharpoons MEA + HCO_3^- \quad (3)$$

$$2H_2O \rightleftharpoons OH^- + H_3O^+ \quad (4)$$

$$H_2O + HCO_3^- \rightleftharpoons CO_3^{2-} + H_3O^+ \quad (5)$$

$$2H_2O + CO_2 \rightleftharpoons HCO_3^- + H_3O^+ \quad (6)$$

These reactions are specified in the reaction panel as shown in Figure 3.10.

The CO_2 post-combustion capture process utilizing monoethanolamine solutions involves a two-step operation: absorption and stripping. In the absorption section, carbon dioxide is absorbed from the vapour phase into the liquid phase through a reactive absorption process facilitated by the solvent. The absorbed CO_2 then undergoes regeneration in the stripping section, where the amine is separated from the CO_2, allowing it to be transferred back into the gaseous phase. The two sections are connected by a cross heat-exchanger, which facilitates the transfer of heat between the absorption and stripping processes. A simplified diagram of the system can be seen in Figure 3.11. The flue gas, which contains a high concentration of CO_2, enters the absorber from the bottom and flows in the opposite direction to the liquid solvent. After the absorption process, the exhaust gas exits the top of the column and, after recovering the solvent, is released through the stack. The solvent, enriched with CO_2, is pumped from the bottom of the absorber to the cross heat-exchanger, where it is heated. It is then directed to the top of the stripper for further processing. The stripper operates with

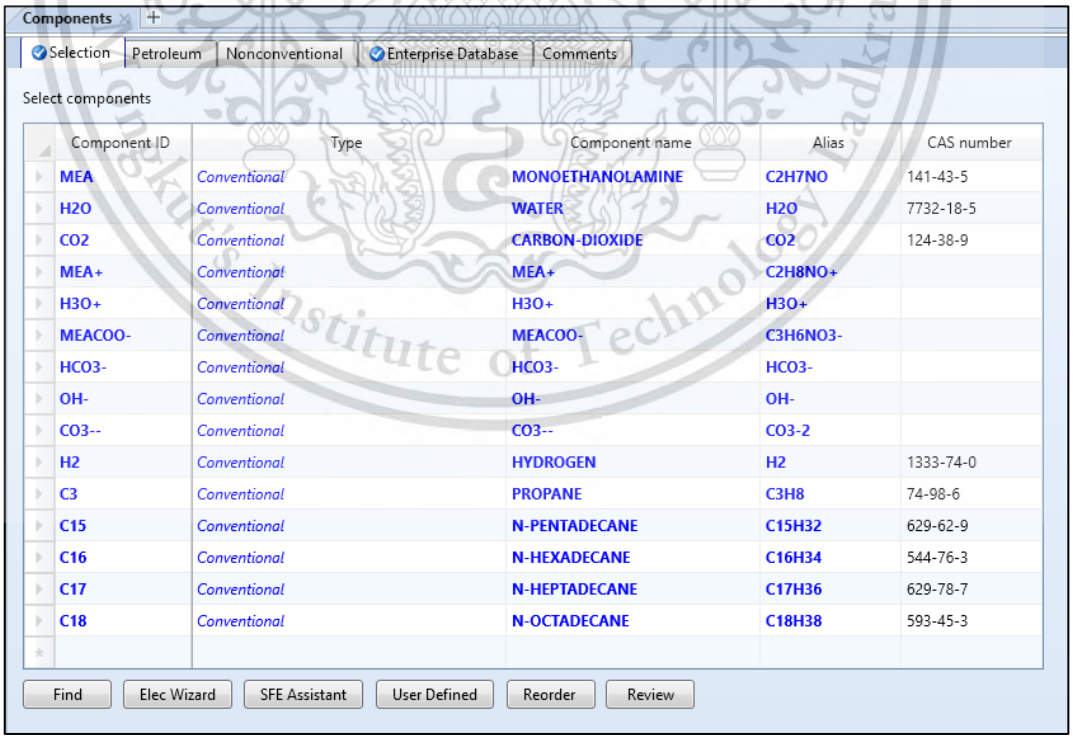

Figure 3.8 The 11 components as the ions and salts for CO_2-MEA-H_2O system

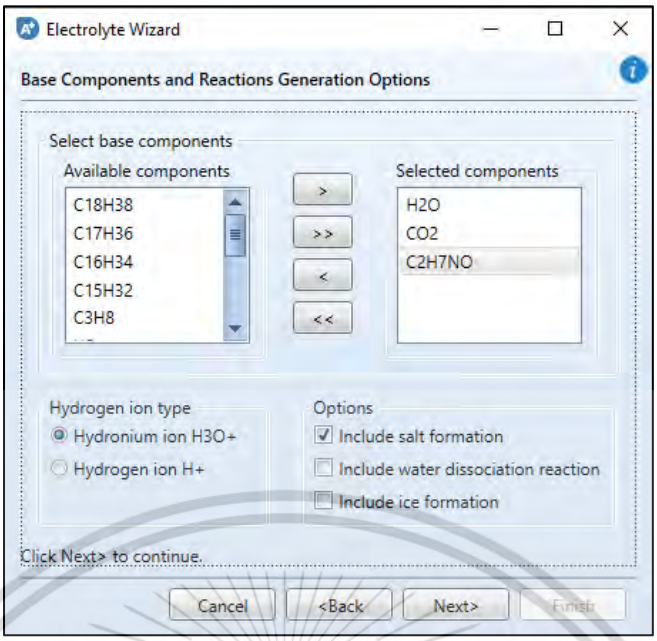

Figure 3.9 The electrolyte wizard panel in Aspen Plus®.

liquid and vapour flowing in opposite directions. The top section of the stripper produces a mixture of CO_2 and water vapour, which is subsequently sent to a partial condenser. In the condenser, the CO_2 is concentrated as a gas, while the water is recovered as a liquid. The concentrated CO_2 gas is subsequently sent for compression, while the liquid phase containing water is further processed for recovery purposes.

In Aspen Simulation, the reactive absorption-stripping was performed using a modelling known as *RadFrac*™ model as shown in Figure 3.12. This model enables the accurate representation and simulation of the absorption and stripping processes,

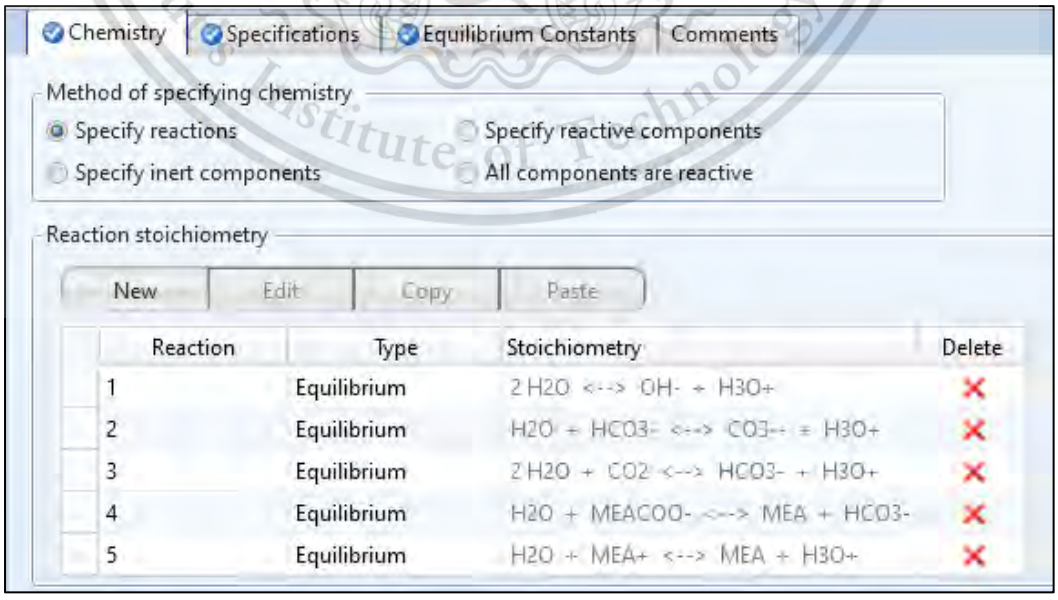

Figure 3.10 The set of ionic equilibrium reactions in the reaction panel

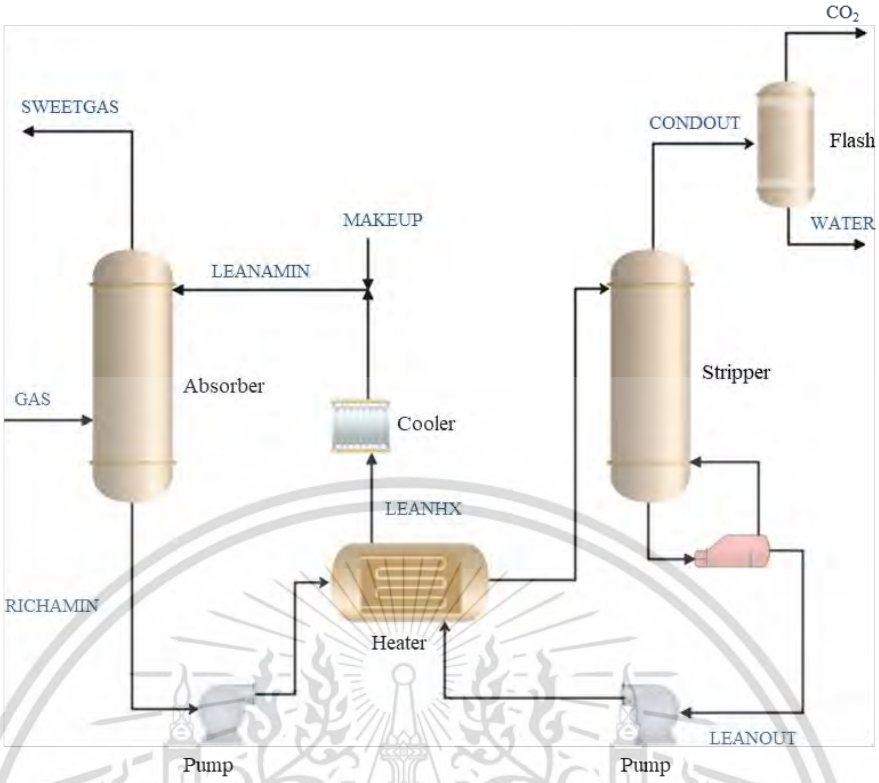

Figure 3.11 Representation of the MEA flowsheet in the present study

taking into account the chemical reactions that occur within them. By utilizing the *RadFrac*™ model, the complex interactions and dynamics of the system can be effectively captured, facilitating a comprehensive analysis, and understanding of the absorption and stripping processes with chemical reactions. Absorption column and stripping column are generally chosen for packed column due to the higher gas-liquid contact area and lower pressure drop. The stripper condenser is a partial condenser since complete liquid phase is not necessary from the top of the column. The reboiler was specified as a kettle. The column and packing feature for both absorber and stripper are shown in Table 3.3.

Table 3.3 Column and packing feature for both absorber and stripper.

Parameter	**Absorber**	**Stripper**
Packing type	Metal Pall Rings	Metal Pall Rings
Size (mm)	50	50
Packing factor (m^{-1})	66	66
Superficial area (m^2/m^3)	115	115

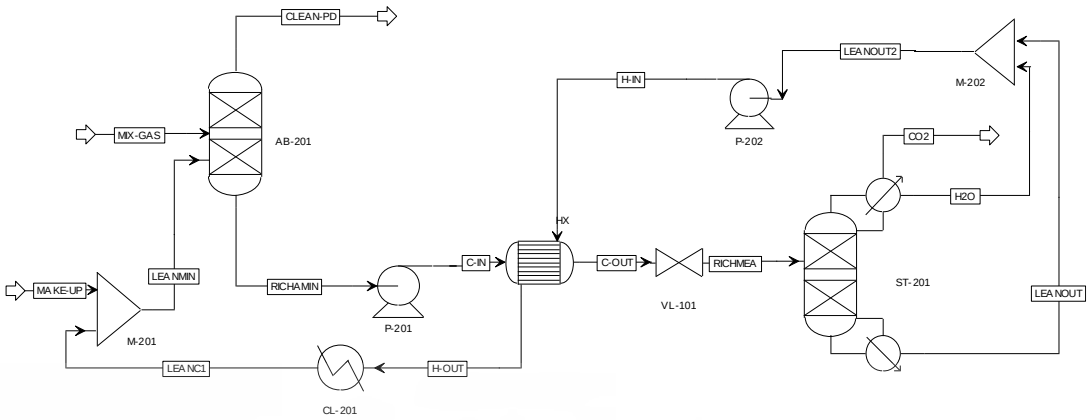

Figure 3.12 MEA flowsheet for the CO_2 reactive absorption-stripping of design 2 in Aspen Plus®

The summary design of the green diesel production process is shown in Figure 3.13 and Figure 3.14. The specifications and operating conditions of units in Designs 1 and Design 2 are presented in Table 3.4.

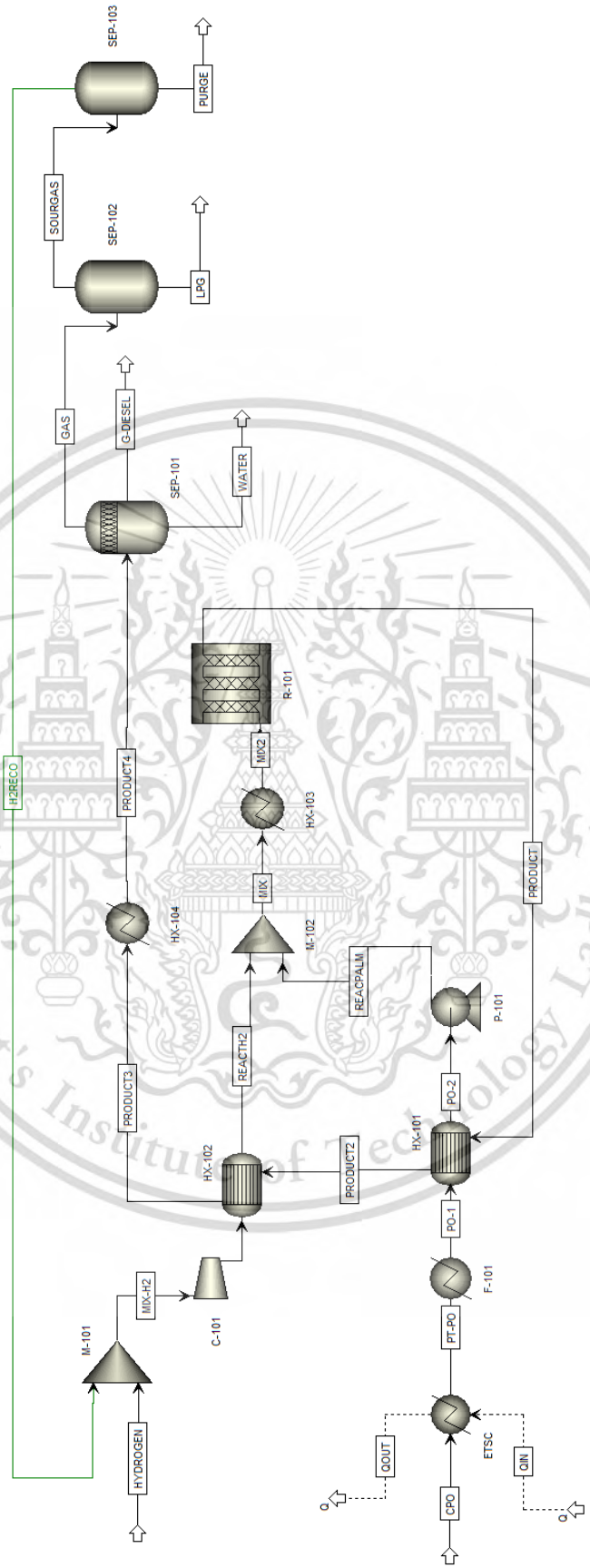

Figure 3.13 Overall process simulation of green diesel production design 1

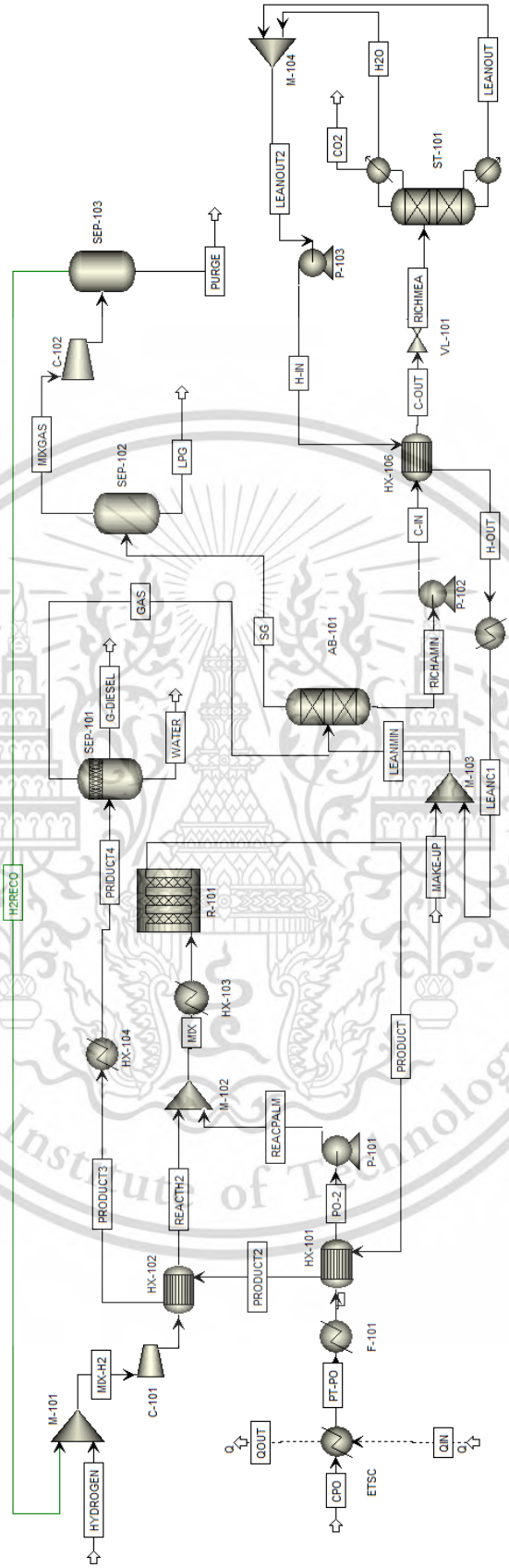

Figure 3.14 Overall process simulation of green diesel production design 2

Table 3.4 The specifications and operating conditions of units in simulation

Equipment	Module	Specification
STC	Heater	Pressure = 1 bar
		Temperature = 80 ºC
		Operating time of ETSC/heater = 8/16 hours/day
FBH reactor	RPlug	Isothermal, Vapor-liquid phase
		Reactor diameter = 0.625 m
		Reactor length = 10.15 m
		Catalyst: NiMoS2/γ-Al2O3
		Weight = 2,232 kg, Density = 717.15 kg/m3
		Pressure = 30 bar, Temperature = 324 ◦C
3-phase separator	Flash3	Pressure = 30 bar
		Temperature = 52 ºC
Cryogenic (SEP-102)	Flash2	Design 1: Pressure = 29.9 bar, Temperature= -80 ºC
		Design 2: Pressure = 10 bar, Temperature= -0 ºC
Cryogenic (SEP-103)	Flash2	Design 1: Pressure = 29.7 bar, Temperature= -80 ºC
		Design 2: Pressure = 30 bar, Temperature= -100ºC
Absorber	RadFrac	Pressure = 1 bar
		Number of stages = 6 stages
		Section packing height = 6.34 m
		Diameter = 0.32 m
		Amount of MEA solvent = 427 kg/h
		Condenser: none
		Reboiler: none
		Packing type: Metal Pall Rings, Size = 50 mm, Packing factor = 66 m^{-1}, Superficial area = 115 m^2/m^3
Stripper	RadFrac	Pressure = 1.97 bar
		Number of stages = 10 stages
		Section packing height = 3.94 m
		Diameter = 0.30 m
		Condenser: Partial-Vapour
		Reboiler: Kettle
		Packing type: Metal Pall Rings, Size = 50 mm, Packing factor = 66 m^{-1}, Superficial area = 115 m^2/m^3

3.1.6 Addition of utilities

The addition of utilities in Aspen Plus® is a critical step in process simulation and design. It can accurately measure and analyse the consumption of essential utilities such as energy, cooling, and water, which are directly associated with operational expenditures. The list of the utilities is shown in Table 3.5.

Table 3.5 Inventory of utilities provided to the green diesel production process in Aspen Plus®.

Equipment number	Equipment	Utility
F-101	Heater	Fired heater
HX-103	Heater	LP steam
HX-104	Cooler	Cooling water
HX-105	Cooler	Cooling water
ST-101	Condenser	Cooling water
ST-101	Reboiler	HP steam
C-101	Compressor	Electricity
C-102	Compressor	Electricity
P-101	Pump	Electricity
P-102	Pump	Electricity
P-103	Pump	Electricity
SEP-102	Flash2	Refrigerant
SEP-103	Flash2	Refrigerant

3.2 Economic analysis

Estimating the total capital investment requires a thorough analysis of each equipment in process and consideration of various factors specific to the equipment such as material and size of equipment. It is often beneficial to consult experts, conduct market research, and use historical data to make accurate estimates. Regular review and updating of the capital investment estimate throughout the project's lifecycle can help in identifying potential cost variations and adjusting the financial plan accordingly. The total capital investment and operational costs are estimated by utilizing a preliminary process design in Section 3.1.

In this study, the Guthrie preliminary estimate method was applied to determine the cost following the development of an optimal process design. Considering regional

factors, feedstock availability, government policies, and market conditions is crucial as they can significantly impact the economic evaluation of green diesel production. To ensure well-informed decisions regarding the green diesel production and utilization as a financially viable and sustainable fuel alternative, it is essential to conduct a thorough and comprehensive assessment of these factors. Therefore, the carbon revenues are also considered in the total annual income due to the financial sustainability of emission reduction effort.

3.2.1 Capital investment

The capital investment required to establish a green diesel production facility is an important consideration. It includes costs related to construction, equipment, engineering, permits, and other associated expenses. The scale of the plant, production capacity, and the chosen technology can significantly influence the capital investment.

Vessel, chemical reactor, and tower (for distillation, absorption, and stripping)

Vessels with or without internal (empty vessel) are widely used in processing plants, for example mixing vessels, fixed-bed adsorption, storage drums and chemical reactors. Most of the empty vessels are cylindrical in shape with connection to the two ellipsoidal heads at opposite ends. Moreover, the empty vessels include nozzles, manholes, and connections for relief valves. In calculating the purchase cost of vessel ($C_{P,V}$), the diameter and length of the vessel obtained from Aspen Plus® must be used.

In Aspen Plus® simulation, *Flash2* and *Flash3* were used for simulating the three-phase separator and cryogenic separator that did not provide the length and diameter of vessel. It is necessary to find these values to calculate the equipment cost by assuming residence time and L/D ratio. In general, the residence time (τ) for mixing, liquid-liquid extractors, and in the pressure-vessel are less than 5 mins. Therefore, the vessel volume (V) is determined by considering a liquid holdup time of five minutes and equal volume of Vapour in vessel.

$$V = \frac{2F_L\tau}{\rho_L} \tag{7}$$

where F_L is the liquid flow rate exiting the vessel, ρ_L is density of liquid, and τ is residence time. Horizontal vessels are commonly used as surge tanks, settling drums, distillations, and reactors. The ratio of vessel length to vessel diameter (L/D ratio) for horizontal vessel is normally four. The vessel volume with L/D ratio of four can be calculated according to Equation 8.

$$V = \pi D^3 \tag{8}$$

where D is the inside diameter of vessel.

The purchase cost of vessels ($C_{P,V}$) in the Equation 9 includes carbon-steel vessel cost ($F_M = 1$), platform and ladders cost.

$$C_{P,V} = F_M C_V + C_{PL} + V_P C_{PK} + C_{DR} \tag{9}$$

where F_M is material factor as shown in Table 3.6, V_P is volume of packing (ft^3), C_{PK} is an installed cost of packing, and C_{DR} is an installed cost of high-performance liquid distributors. The last two terms ($V_P C_{PK} + C_{DR}$) can be neglected if internal packing is not considered. The cost of vessels (C_V) is based on the weight of the shell of the vessel. The cost of platforms and ladders (C_{PL}) depends on the inside diameter (D_i) and length (L) of the vessel in feet. There are many factors that affect the purchase cost, it differs between vertical and horizontal vessels and can be calculated as follows:

For horizontal vessels,

$$C_V = \exp\{5.6336 + 0.4599 [\ln(W)] + 0.00582 [\ln(W)]^2\} \tag{10}$$

$$C_{PL} = 2275(D_i)^{0.2094} \tag{11}$$

For vertical vessels,

$$C_V = \exp\{7.1390 + 0.18255 [\ln(W)] + 0.02297 [\ln(W)]^2\} \tag{12}$$

$$C_{PL} = 410(D_i)^{0.73960}(L)^{0.70684} \tag{13}$$

For the tower used in the separation process, such as the absorption, stripping, and distillation. They consist of packing or/and plate and take into account multiple feeds. The purchase cost of the vessel of vertical tower (C_V) that includes a skirt, nozzle, manholes, does not included packing or/and plate can be calculated according to the following equation.

$$C_V = \exp\{10.5449 - 0.4672 [\ln(W)] + 0.05482 [\ln(W)]^2\} \tag{14}$$

$$C_{PL} = 341(D_i)^{0.63316}(L)^{0.80161} \tag{15}$$

For packing tower, the total purchase of packing tower for absorber and stripper are given by Table 3.7. The cost of installed for dumped packing (C_{PK}) is given in Table 3.7. The liquid distributors in the packing tower should be located at every feed point and every 20 ft. The installation cost of liquid distributors (C_{DR}) is assumed to be \$140/ft^2 of column cross-sectional area. The weight of the shell (W) in the correlation depends on the wall thicknesses (t_S) and can be approximated by Equation 16.

$$W = \pi (D_i + t_S)(L + 0.8D_i)\, t_S \rho \quad (16)$$

where t_S is shell thickness (in inches) assumed to be the same throughout the shell, and ρ is density of material. The term $(L+D_i)$, it is the length of the vessel which includes the cylinder length (L) and two heads ($0.8D_i$). The minimum wall thicknesses are shown in Table 3.8.

Table 3.6 Materials factors for vessels

Material of construction	Material factor
Carbon steel	1.0
Low-alloy steel	1.2
Stainless steel 304	1.7
Stainless steel 316	2.1

Table 3.7 The installed costs for dumped packings

Packing	Installed cost ($/ft^3)			
	1.0 in.	1.5 in.	2.0 in.	3.0 in.
Berl saddles				
Ceramic	50	40	32	
Raschig rings				
Carbon steel	50	50	30	30
Stainless steel	150	116	80	80
Ceramic	20	20	20	20
Pall rings				
Carbon steel	56	42	36	
Stainless steel	160	130	100	
Polypropylene	50	30	20	18

Table 3.8 Minimum wall thicknesses

Vessel inside diameter (ft)	Minimum wall thicknesses (in.)
Up to 4	1/4
4-6	5/16
6-8	3/8
8-10	7/16
10-12	1/2

Centrifugal pumps

The purchase cost of pump ($C_{P,P}$) in Equation 17 includes pump type factor (F_T) and material factor of pump (F_M), as listed in Table 3.9 and Table 3.10, respectively.

$$C_{P,P} = F_T F_M C_{B,P} \tag{17}$$

Where $C_{B,P}$ is bare cost of pump, which can be determined using Equation 18 and 19. The cost covers the base plate and driver coupling but does not include the electric motor. The cost includes a size factor (S), which recognises the capability of a given centrifugal pump to function across a flow rate (Q) and head combinations (H).

$$C_B = \exp\{12.1656 - 1.1448[\ln(S)] + 0.0862[\ln(S)]^2\} \tag{18}$$

$$S = Q(H)^{0.5} \tag{19}$$

Table 3.9 Centrifugal pump type factor

Number of stages	Shaft rpm	Flow Rate Range (gpm)	Pump Head Range (ft)	Maximum Motor Hp	F_T
1	3,600	50-900	50-400	75	1.0
1	1,800	50-3,500	50-200	200	1.5
1	3,600	100-1,500	100-450	150	1.7
1	1,800	250-5,00	50-500	250	2.0

Table 3.10 Materials factors for centrifugal pump

Material of construction	Material factor
Carbon iron	1.00
Ductile iron	1.15
Cast steel	1.35
Bronze	1.90
Stainless steel	2.00
Hastelloy C	2.95
Monel	3.30
Nickel	3.50
Titanium	9.70

Compressors

The purchase cost of compressor ($C_{P,C}$) in Equation 20 includes electric motor drive (F_D) and material factor of compressor (F_M).

$$C_{P,C} = F_D F_M C_{B,P} \tag{20}$$

Where electric motor drive factor (F_D) is 1.15 for a steam turbine drive and 1.25 for a gas turbine drive, material factor of compressor (F_M) is 2.5 for stainless steel and 5.0 for nickel alloy. The bare cost of compressor ($C_{B,P}$), comprising an electric motor drive, is intended for cast iron or carbon-steel construction as shown in Equation 21.

$$C_{B,C} = \exp\{9.1553 + 0.63[\ln(P_c)]\} \tag{21}$$

Where P_C is Consumed power in horsepower (Hp)

Fired heater

The purchase cost of fired heater ($C_{P,H}$) in Equation 22 includes material factor (F_M) and pressure factor (F_P).

$$C_{P,H} = F_P F_M C_{B,H} \tag{22}$$

Where F_M represents material factor of fired heater, which is 1.4 for tubes of Cr–Mo alloy steel and 1.7 for stainless steel. $C_{B,H}$ represents the bare cost of a fired heater, which can be calculated using Equation 23. The pressure factor can be calculated using Equation 23 for the pressure (P) range of 500 to 3000 psig.

$$C_{B,H} = \exp\{-0.15241 + 0.785[\ln(Q)]\} \tag{23}$$

$$F_P = 0.986 - 0.0035\left(\frac{P}{500}\right) + 0.0175\left(\frac{P}{500}\right)^2 \tag{24}$$

Where Q represents the heat duty absorbed by the process stream in Btu/hr.

Heat exchangers

The purchase cost of heat exchangers ($C_{P,Hx}$) is determined from Equation 25. The bare cost of U-type and kettle vaporizer shell-and-tube heat exchanger is calculated by Equation 26 and 27, respectively.

$$C_{P,Hx} = F_P F_M F_L C_{B,Hx} \tag{25}$$

$$C_{B,Hx-u} = \exp\{11.5510 - 0.9186[\ln(A)] + 0.0979[\ln(A)]^2\} \tag{26}$$

$$C_{B,Hx-k} = \exp\{12.3310 - 0.8709[\ln(A)] + 0.09005[\ln(A)]^2\} \tag{27}$$

Where A represents tube outside surface area, F_M represents a material factor for various combinations of tube and shell materials, as provided in Table 3.11, based on

the surface area (A) in ft^2 in Equation 28. The pressure factor (F_P) is determined by the shell-side pressure (P, in psig) and it is defined by Equation 29. F_L is a tube-length as follows Table 3.12.

$$F_M = a + \left(\frac{A}{100}\right)^b \tag{28}$$

$$F_P = 0.9803 - 0.018\left(\frac{P}{100}\right) + 0.0017\left(\frac{P}{100}\right)^2 \tag{29}$$

Where the constants a and b are determined based on the materials of construction for the shell-and-tube, as presented in Table 3.11.

Table 3.11 Materials factors for heat exchanger

Materials of construction (shell/tube)	**a**	**b**
Carbon steel/carbon steel	0.00	0.00
Carbon steel/brass	1.08	0.05
Carbon steel/stainless steel	1.75	0.13
Carbon steel/titanium	5.20	0.16
Carbon steel/Cr-Mo steel	1.15	0.05
Stainless steel/stainless steel	2.70	0.07
Titanium/titanium	9.60	0.06

Table 3.12 Tube-length factor of heat exchanger

Tube Length (ft)	**F_L**
8	1.25
12	1.12
16	1.05
20	1.00

3.2.2 Bare-module costs

As mentioned in Section 3.2.1, the purchase cost contains only the piece of equipment. It does not include the cost from installation of equipment such as piping, concrete, and electrical wiring price. The estimated installed costs are obtained using the factored-cost method proposed by Guthrie. The factored-cost method considers both direct and indirect costs. The direct costs include purchasing land, buildings, equipment, machinery, vehicles, and any assets required for the operation. Additionally,

direct costs may also involve expenses related to permits, legal fees, licenses, and initial marketing activities. Indirect costs refer to the expenses that are not directly tied to specific assets but are necessary for the project's success. This may include costs related to project management, professional fees, research, and development. When these costs are added to purchase cost, it is known as the bare-module cost that can be calculated according to the Equation (30).

$$C_{BM} = C_P F_{BM} \tag{30}$$

Where C_P is purchasing cost (in Section 3.2.1), F_{BM} is bare-module factors that can be seen in Table 3.13.

However, all the data provided in Section3.2.1 and Section3.2.2 are based on 2013. Generally, the price of these equipment increases over time. To account inflation, the update bare-module cost is calculated as follows:

$$\text{update bare module cost} = C_{TBM} \frac{I_{\text{Present}}}{I_{Base}} \tag{31}$$

where C_{TBM} is total bare-module cost, and I is the cost index. The cost index for the green diesel production based on the chemical engineering plant cost index (CEPCI), in 2013 it was 567, and in April 2022 is equal to 821.11.

Table 3.13 Bare-Module factors (F_{BM})

Equipment	**Bare-module factors (F_{BM})**
Furnaces	1.86
Shell-and-tube heat exchangers	3.17
Double-pipe heat exchangers	1.80
Fin-tube air coolers	2.17
Vertical pressure vessel	4.16
Horizontal pressure vessel	3.05
Pumps and drivers	3.30
Gas compressor	2.15
Centrifuges	2.03

3.2.3 Total capital investment

The total capital investment (C_{TCI}) is based on the individual factor's method of Guthrie. It includes various components such as the cost of land, construction,

equipment, machinery, infrastructure, permits, licenses, and other expenses associated with setting up the venture. Total capital investment is a comprehensive measure that takes into account all the financial resources needed to initiate and operate the project, ensuring its successful implementation and sustainability. To apply this method, the purchase cost and bare-module cost of each equipment must be calculated. The total bare-module investment (C_{TBM}) is obtained by adding the costs of on-site equipment to the bare-module costs. In addition, there are other investment costs such as site preparation cost (C_{site}), industrial building cost ($C_{building}$), offsite facilities cost ($C_{offsite\ facilities}$) and working capital cost (C_{WC}). The equation for the total capital investment by the Guthrie method as shown in the following equation.

$$C_{TCI} = 1.18\ (C_{TBM} + C_{site} + C_{building} + C_{offsite\ facilities}) + C_{WC} \quad (32)$$

The working capital cost (C_{WC}) for one month period of plant operation refers to the amount of money required to cover the day-to-day operational expenses and maintain sufficient liquidity during that specific time frame. It includes costs such as raw materials, inventory, utilities, labour, maintenance, marketing, and other operational expenses that occur within the monthly operational cycle. The working capital cost is based on the following assumptions.

- A reserve of cash equivalent to thirty days is set aside to cover expenses related to raw materials, operations, utilities, operating overhead, maintenance, property taxes, insurance, and depreciation. This reserve represents approximately 8.33% of the annual cost of manufacture (COM), assuming that 30 days is equivalent to one-twelfth of a year.
- A reserve of inventories equivalent to a seven-day period, based on their sales price, is maintained for liquid and solid products. This assumes that these products are shipped once a week. The inventory reserve accounts for approximately 1.92% of the annual sales of liquid and solid products, assuming that 7 days is equivalent to 1/52 of a year.
- An accounts receivable equivalent to a thirty-day period is established for products at their sales price. This reserve represents approximately 8.33% of the annual sales of all products.
- A reserve for accounts payable, covering a thirty-day period, is established by the company for the purchase of feedstocks. This reserve represents approximately 8.33% of the annual feedstock costs.

3.2.4 Operating expenditures

Operating Expenditures (OPEX) refer to the ongoing costs associated with operating and maintaining chemical processing plants and facilities. These expenditures include expenses related to raw materials, utilities, equipment maintenance, labour, safety measures, process control, and other operational costs. Thers values are included in the cost sheet in Table 3.14. Assuming a 5-year catalyst lifespan [20], its cost is evenly distributed in the OPEX, added annually.

The modified accelerated cost recovery system (MACRS) is a depreciation method used for tax purposes. It determines the allowable depreciation deductions for qualifying assets over their respective recovery periods. MACRS uses two main depreciation methods: the general depreciation system (GDS) and the alternative depreciation system (ADS). The asset type differences are classified into various classes under MACRS, each with its own assigned recovery period or class life. These class lives can vary from as short as 3 years to as long as 50 years, depending on the type of the asset as shown in Table 3.15. For the new chemical plant project, a class life of 5 and 7 is recommended.

C_{TDC} in Table 3.14 is Total depreciable capital (TDC) investment for the desired production rate and year, which can be calculated using Equation 33.

$$C_{TDC} = C_b \left(\frac{\text{Production rate}}{\text{Production rate}_b} \right)^{0.6} \left(\frac{I}{I_{Base}} \right) \tag{33}$$

The calculation of TDC for green diesel is derived from biodiesel data, as there is limited available data specific to green diesel. The total depreciable capital investment for a plant to produce 10,000 ton/year of biodiesel was $3.52 million in 2004 [25].

Table 3.14 Operating Expenditures (OPEX)

Cost factor	Annual cost
Feed stocks	
Hydrogen	3.30 $/kg
Crude palm oils [21][22]	0.47 - 0.81 $/kg
MEA solvent [23]	1.38 $/kg
Catalyst (lifetime 5 years) [24]	7.5 $/kg
Utilities	
Water	0.067 $/1000kg
Refrigeration	0.190 $/1000kg
Electricity	0.120 $/kWh
Steam, 572 psia	29.970 $/1000kg
Operations (O)	
Direct wages and benefit (DW&B)	$40/operator-hr
Direct salaries and benefits	15% of DW&B
Operating supplies and services	6% of DW&B
Technical assistance to manufacturing	$60000/(operator/shift)-yr
Control laboratory	$65000/(operator/shift)-yr
Maintenance (M)	
Wages and benefits (MW&B)	3.5% of C_{TDC}
Fluid handling process	4.5% of C_{TDC}
Solid-fluid handling process	5.0% of C_{TDC}
Salaries and benefits	25% of MW&B
Material and services	100% of MW&B
Maintenance overhead	5% of MW&B
Operating overhead	
General plant overhead	7.1% of M&O-SW&B
Mechanical department services	2.4% of M&O-SW&B
Employee relations department	5.9% of M&O-SW&B
Business services	7.4% of M&O-SW&B
Property taxes and insurance	2.0% of C_{TDC}
Depreciation	
Direct plant	8.0% of (C_{TDC} - 1.18 C_{alloc})
Allocated plant	6.0% of 1.18 C_{alloc}
COST OF MANUFACTURE (COM)	**Sum of above**
General Expenses	
Selling expense	1.0% of sales
Direct research	4.8% of sales
Allocated research	0.5% of sales
Administrative expense	2.0% of sales
Management incentive compensation	1.25% of sales
TOTAL GENERAL EXPENSES (GE)	
TOTAL PRODUCTION COST (C)	**COM+GE**

Table 3.15 Class life in year and assets for MACRS depreciation method

Asset types	Class life (years)
Special manufacturing and handling devices (e.g., tractors, horses)	3
Most road vehicle, computer, copy and duplicating equipment, and manufacturing equipment	5
Office furniture, farm machinery, petroleum or natural gas equipment, and all other property not assigned to another class	7
Vessels and water transportation equipment, petroleum refining, agriculture production processing, and shipbuilding	10
Telephone distribution plants, land improvement, landscaping, and municipal sewage treatment plants	15
Municipal sewers, farm building, and power production equipment	20
Residential rental property (does not include hotels and motels)	27.5
Non-residential real property	39

3.2.5 Carbon revenue

Investing in renewable energy projects or adopting clean technologies can result in reduced CO_2 emissions. Depending on the region and the incentives provided, organizations may receive financial incentives, subsidies, or tax credits for generating clean energy or using low-carbon technologies. These financial benefits can be considered as a form of CO_2 revenue. Carbon revenue refers to the potential income generated by selling or trading carbon dioxide emissions allowances or offsets. It is a financial incentive for organizations or entities that reduce their greenhouse gas emissions and contribute to mitigating climate change.

Referring to the emission trading scheme (ETS) for prediction of China's carbon price in the next 30 years [26] as shown in Figure 3.15. Carbon revenue (ΔP_i) is taken into the annual income as a positive value and can be calculated according to Equation 34.

$$\Delta P_i = Di \times P_{t,i} + B_i \tag{34}$$

where $P_{t,i}$ is the traded carbon price, D_i is the amount of CO_2 reduction achieved through the process of CO_2 capture and utilization (CCU), B_i is the incentives provided by the government for CCU assumed to be 15,000 USD.

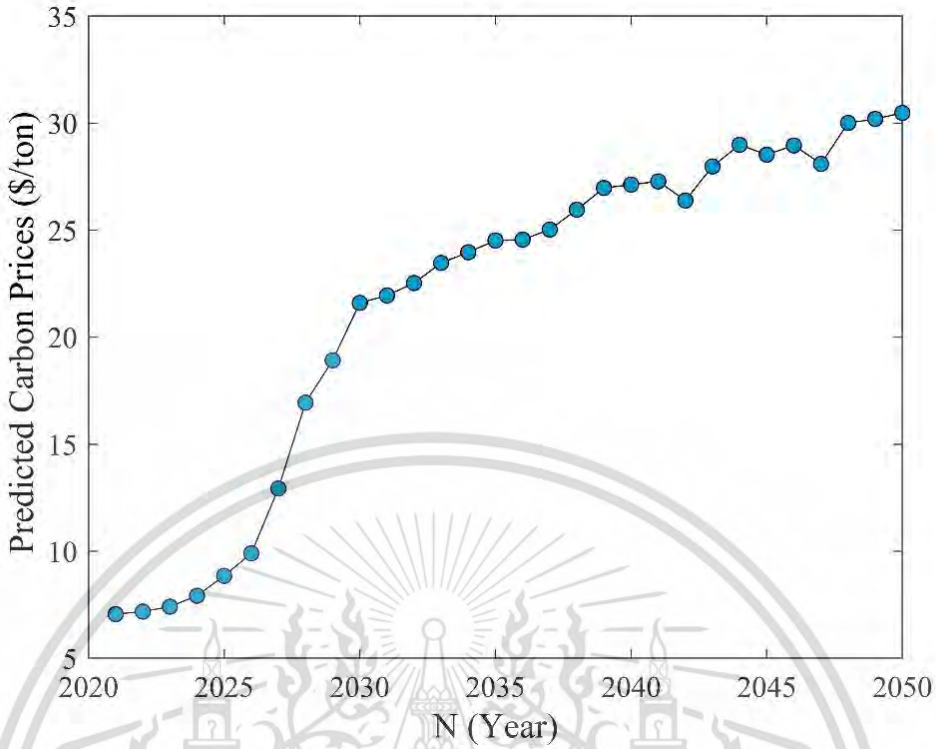

Figure 3.15 Forecasts for China's carbon price

3.2.6 Profitability analysis

Profitability analysis refers to the process of evaluating the financial performance and potential profitability of a business, project, or investment. It involves assessing the revenues generated, costs incurred, and the resulting profit or loss. It involves analysing various financial metrics and ratios, such as gross profit margin, net present value (NPV), return on investment (ROI), and payback period (PBP).

Net present value

When estimating capital investment, it is crucial to consider the effects of inflation and the time value of money. Future expenses should be adjusted to account for inflation, and the value of money over time should be discounted to reflect the present value of the cash flows. The net present value (NPV) Provides the present value of all payments according to a given rate of return and project lifetime. It can be calculated according to Equation 50.

$$NPV = -C_I + NP \cdot (1 - (1 + i)^{-n}) / i \tag{35}$$

where C_I is the capital investment, NP is the net profit, i is interest rate, and n is project lifetime.

Return on investment.

Return on Investment (ROI) measures the profitability of an investment by comparing the gain or loss from the investment relative to its cost. It is expressed as a percentage and helps assess the efficiency and profitability of capital investments. ROI is a measure of profitability that compares the net profit generated from an investment to the initial investment amount. A higher ROI indicates a more profitable investment, while a lower ROI suggests a lower return relative to the initial investment. The ROI can be calculated by using the following formula:

$$\text{ROI} = \frac{\text{Net earnings}}{\text{Total capital investment}} \tag{36}$$

Internal rate of return

The internal rate of return (IRR) is a financial metric used to evaluate the potential profitability of an investment or project. It represents the discount rate at which the net present value (NPV) of all future cash flows from the investment becomes zero. In other words, the IRR is the rate at which an investment breaks even, and any discount rate higher than the IRR would result in a negative NPV, indicating that the investment is not economically viable. The IRR is an essential tool for assessing the attractiveness and feasibility of various investment opportunities, as it helps determine whether the expected returns justify the initial investment cost. IRR is calculated using the following equation:

$$\text{NPV} = \sum \left(\frac{CF_t}{(1+IRR)^t} \right) = 0 \tag{37}$$

where CF_t represents the cash flow at time t, and t represents different time periods, typically starting from t=0 for the initial investment and continuing for each subsequent period.

Payback period

The payback period (PBP) is the length of time required for an investment to generate cash flows or profits that equal the initial cost of the investment. It is a straightforward metric used by businesses and investors to assess the time it will take to evaluate the feasibility of a project and determine the time required to recover their initial investment. However, the payback period does not take into account the time value of money or consider cash flows beyond the payback period, limiting its

usefulness as a standalone metric. The payback period can be calculated by using the following formula:

$$\text{PBP} = \frac{\text{Cost of investment}}{\text{Average annual cash flow}} \tag{38}$$

3.2.7 Sensitivity analysis

Sensitivity analysis is a technique used in economic analysis to assess the impact of changes in key variables or assumptions on the outcomes of a project or investment. Evaluating the sensitivity of profitability to changes in key factors, such as sales price of product, purchase price of raw material, capital and operational costs, or market conditions. It helps to understand the sensitivity of economic indicators, such as net present value (NPV), internal rate of return (IRR), or payback period, to different scenarios or changes in input parameters.

3.3 Environmental impact analysis

Environmental impacts refer to the consequences of human activities on the natural environment. These impacts can manifest in positive or negative forms and can influence diverse components of the ecosystem, such as air, water, land, biodiversity, and climate.

3.3.1 Environmental impact

In this study, the environmental impact is developed by using the life cycle assessment (LCA) in SimaPro software. The CML (baseline) is selected as an impact assessment method in SimaPro software as shown in Figure 3.16. The categories of CML environmental impact are shown as follows:

- Abiotic depletion potential (ADP)
- Global warming potential (GWP)
- Ozone layer depletion potential (ODP)
- Human toxicity potential (HTP)
- Terrestrial ecotoxicity potential (TEIP)
- Acidification potential (AP)
- Eutrophication potential (EP)
- Fresh water aquatic ecotoxicity potential (FAETP)
- Marine aquatic ecotoxicity potential (MAETP)
- Photochemical oxidation potential (POCP)

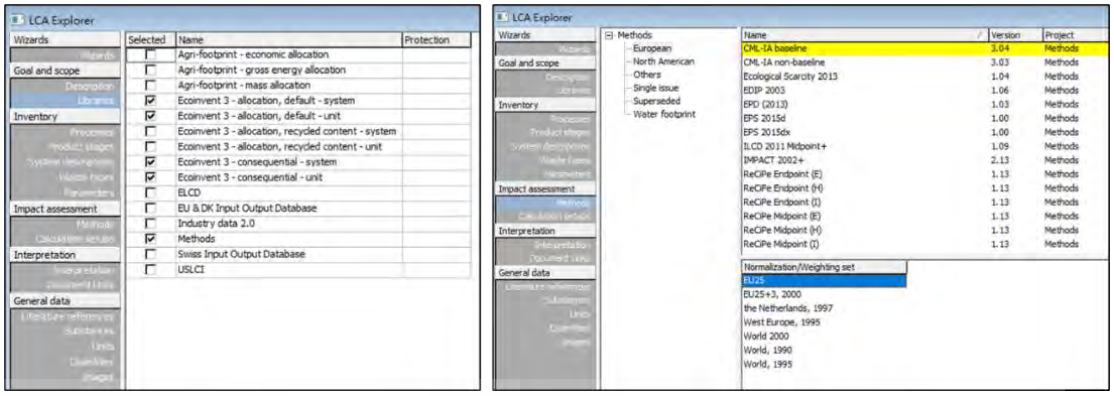

Figure 3.16 Overview SimaPro Explorer.

This environmental impact assessment (EIA) considers planning, harvesting, collection, and hydrotreating process of palm oil as shown in Figure 3.17. The EIAs of green diesel process were not included in the impact from transportation and equipment construction. The system boundary of crude palm oil refers to all the stages involved in its production. This includes planting and nurturing oil palm trees, to processing the oil and getting it ready for distribution. The boundary encompasses activities such as preparing the land, using fertilizers and pesticides, and harvesting. It also covers processes such as oil extraction and refining. Throughout these stages, the waste management, energy usage, and emissions are considered. The materials and energy consumed during the production of green diesel serve as inputs for the LCA analysis, sourced from Aspen Plus version 14.

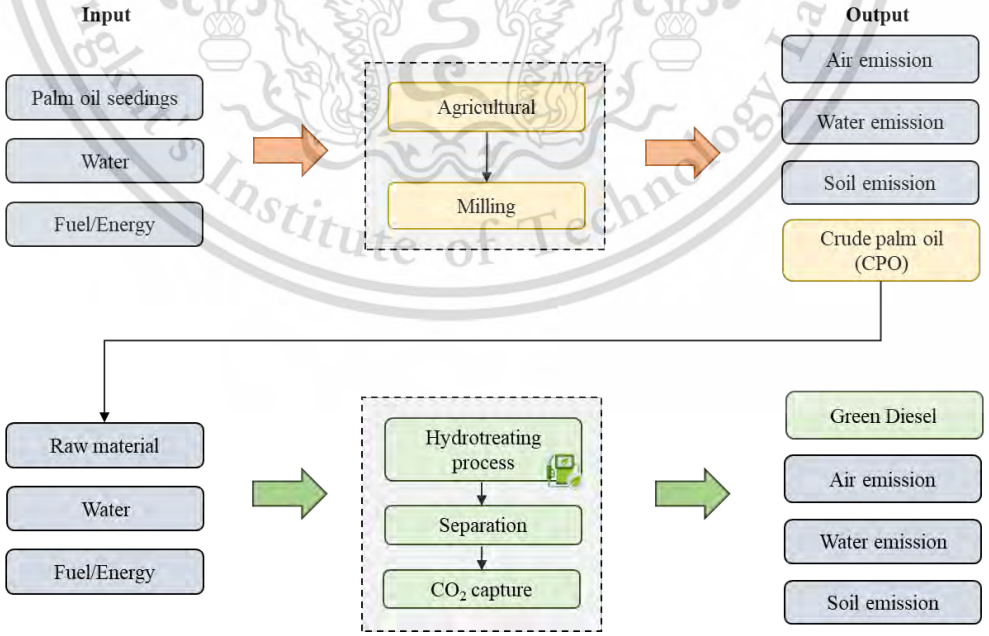

Figure 3.17 System boundary of green diesel production process from CPO.

Table 3.16 Impact categories and indicator for the CML baseline environmental impact method

Environmental impact category	Abbreviation	Unit
biotic depletion	ADP	kgSb eq.
Abiotic depletion (fossil fuels)	ADP fossil.	MJ
Global warming	GWP	kgCO_2 eq.
Ozone layer depletion	ODP	kgR-11 eq.
Human toxicity	HTP	kg1,4-DB eq.
Fresh water aquatic ecotoxicity	FAETP	kg1,4-DB eq.
Marine aquatic ecotoxicity	MAETP	kg1,4-DB eq.
Terrestrial ecotoxicity	TETP	kg1,4-DB eq.
Photochemical oxidation	POCP	kgC_2H_4 eq.
Acidification	AP	kgSO_2 eq.
Eutrophication	EP	kgPO_4 eq.

3.3.2 Greenhouse gas emission assessment

The emission of greenhouse gases (GHG), primarily carbon dioxide from burning fossil fuels, and contributes to climate change. Increased concentrations of GHG in the atmosphere, leading to the world global warming. Greenhouse gas emissions are calculated by carbon tracking option on Aspen Plus® in each utility panel using the United States Environmental Protection Agency Rule of E9-5711 (US-EPA-Rule-E9-5711) method of evaluation [27], [28]. In this study, natural gas is used as the fuel source for carbon tracking as seen in Figure 3.18.

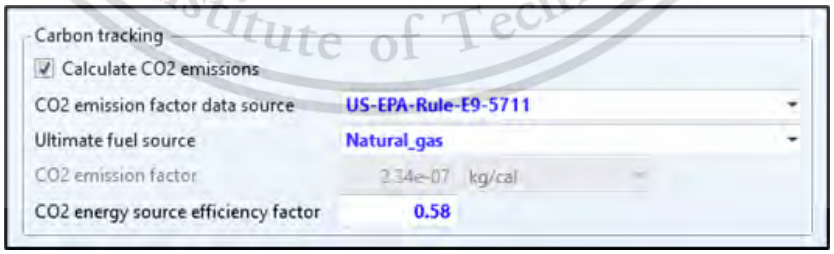

Figure 3.18 Carbon tracking panel in Aspen Plus®

The utilities used in the green diesel production include cooling water, electricity, refrigeration, and steam. The CO_2 energy source efficiency factor for each utility is shown in Table 3.17.

The sequestration impact of palm trees can vary depending on their size, age, and environmental conditions. Older and larger palm trees tend to sequester more

carbon over time. Additionally, the overall carbon sequestration capacity of palm trees can be influenced by factors such as climate, soil conditions, and land management practices. Therefore, in this study, CO_2 sequestration calculations are based on data from Rivera-Mendez et al [29]. 606 kilograms of carbon dioxide are generated per ton of palm oil production. The complete CO_2 emissions resulting from the biodiesel production process amounted to 1,750 kilograms of CO_2 equivalent per ton of palm oil. These emissions are attributed to various stages within the palm oil preparation process, which are divided into five sub-processes: 1.41% for land preparation, 1% for seeding, 1.3% for planting, 1.23% for harvesting, and 22.9% for palm oil mills. The net CO_2 sequestration can be determined by using Equation 54 and 55.

$$CO_2\ sequetration = (w_{CO_2,captured} - w_{CO_2,emitted}) \times \frac{F_{PO}}{1000} \tag{39}$$

$$w_{CO_2,emitted} = (\alpha_{land} + \alpha_{seeding} + \alpha_{planting} + \alpha_{harvesting} + \alpha_{mill}) \times w_{total\ CO_2,emitted} \tag{40}$$

where $w_{CO_2,captured}$ is weight of carbon dioxide captured to produce one ton of palm oil (in kg), $w_{CO_2,emitted}$ is weight of carbon dioxide emitted to produce one ton of palm oil (in kg), α is CO_2 emission factor from palm oil production process.

Table 3.17 The CO_2 energy source efficiency factor for each utility

Utility type	CO_2 energy source efficiency factor
Steam	0.85
Fired heater	0.85
Electricity	0.58
Refrigeration	1

3.4 Evacuated tube solar collector

The evacuated-tube solar collector (ETSC) is a renewable energy system that converts solar energy into usable thermal energy, reducing pollutant emissions and costs compared to fossil fuels. It collects solar energy and stores it for various applications, including water heating, power generation, and industrial processes.

Using ETSC in small industries is eco-friendly and cost-effective. It efficiently harnesses solar energy, even in limited sunlight conditions, reducing reliance on fossil fuels, saving energy costs, and lowering carbon emissions. Its high efficiency ensures a reliable source of hot water or process heat for industrial needs. The modular design

allows for easy scalability, empowering small industries to contribute to a greener future with renewable energy.

3.4.1 System configuration

The schematic of cross-sectional view of evacuated tube collector is shown in Figure 3.19.

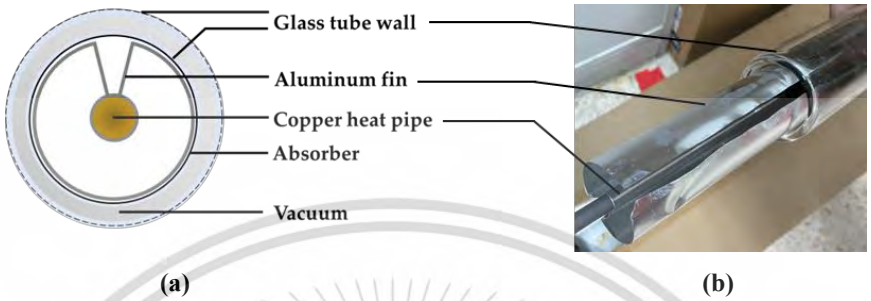

Figure 3.19 (a) Schematic diagram of an HP-ETSC cross section (b) Components inside an HP-ETSC.

A space between concentric glass tubes is vacuumed to reduce thermal energy loss from conduction and convection. The copper heat pipe is held om aluminum fin to mechanically support the heat transfer of copper heat pipe. The principle of evacuated tube solar collector is shown in Figure 3.20.

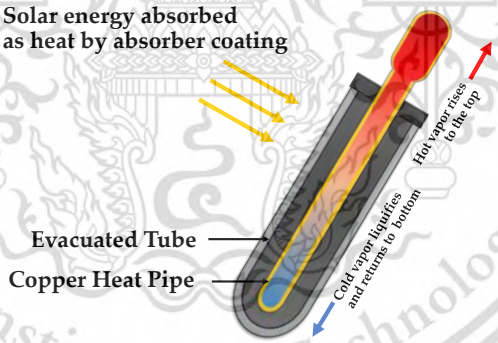

Figure 3.20 Principle of a single evacuated tube solar collector.

The evacuated tube solar collector absorbs solar thermal energy. Solar thermal energy is transferred through aluminum fin to the copper heat pipe inside the evacuated tube by conduction. The copper heat pipe contains working fluid that is a 10%mol of ethylene glycol in water. The working fluid in the evaporator section evaporates and creates a Vapour pressure to flow to the condenser section. After releasing latent heat, cold fluid in the storage tank is pumped into the manifold to receive the latent heat from the tip of copper heat pipe released from ethylene glycol. Hot fluid is returned to the storage tank for storing heat energy. The heat transfer fluid in the condenser section is

condensed and returned to the evaporator section. In order to study the performance of the evacuated tube solar collector, the following assumptions are considered as follows:

- Heat loss at the pipes in the system are neglected.
- Hear loss by radiation between storage wall and insulator is neglected.
- Temperature drop between storage tank and inlet manifold is neglected.

3.4.2 Experimental setup

The experimental arrangement depicted in Figure 3.21a was established to record the temperatures of the heat pipe tips. This experiment was conducted at the School of Engineering, King Mongkut's Institute of Technology Ladkrabang in Bangkok, situated at latitude 13°43′35″ N and longitude 100°46′20″ E. On the other hand, the experimental setup illustrated in Figure 3.21b was configured to assess the performance of the heat pipe evacuated-tube solar collector.

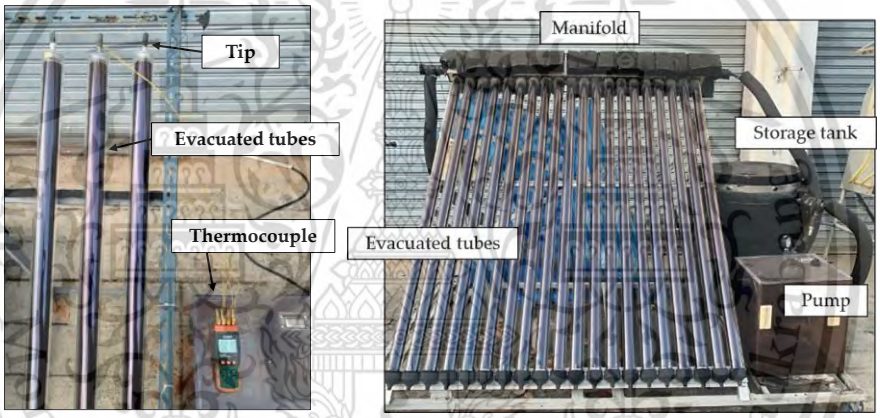

(a) (b)

Figure 3.21 Experimental configuration for (a) investigating the influence of solar intensity on the tip temperature of HP-ETSC, (b) evaluation the performance of HP-ETSC.

The first experiment in Figure 3.21a involved three individual evacuated tubes exposed to sunlight simultaneously to ensure data reliability due to the uncontrollable climate. Each evacuated-tube solar collector utilized a copper heat pipe containing a mixture of 10 mol% ethylene glycol in water as the working fluid. This mixture vaporized completely at 138.7 °C, an ideal temperature for efficient solar thermal energy absorption. K-type thermocouples with an accuracy of ±1 °C were connected to the heat pipe tips to measure their temperatures, with data recorded by a data logger. Solar intensity was monitored from 9:00 a.m. to 4:00 p.m. using a solar power meter with an accuracy of less than ±5% error.

To evaluate the performance of the evacuated-tube solar collector, a setup similar to Figure 3.21b. This setup featured 20 evacuated-tube solar collectors tilted at a 45° angle from the horizontal, connected to a storage tank containing palm oil with varying capacities from 50 to 160 L. The palm oil was circulated through the system with a constant mass flow rate of 1.92 kg/min. Insulation with thermal insulators was applied to the manifold, pipes, and palm oil storage tank to enhance thermal efficiency. The experiment involved circulating palm oil within the system while measuring and recording several parameters every hour from 9:00 a.m. to 4:00 p.m. These parameters included solar intensity, manifold inlet temperature, manifold outlet temperature, ambient temperature, and the temperature of the palm oil inside the storage tank.

3.4.3 Governing equation

Evacuated tube domain

The evacuated tubes absorb solar thermal energy from sunlight which can be as follows.

$$\dot{Q}_{rad} = I_G A_{ETC} \tag{41}$$

where Q_{rad} represents the solar thermal energy stored in the absorber surface, I_G is the solar intensity and A_{ETC} is gross area of evacuated tube solar collector.

Manifold domain

Heat from the working fluid in the condenser is transferred to the palm oil that flows through the manifold by convection. The heat transfer from copper pipe tip in the manifold to palm oil heating medium can be calculated as follows.

$$Q_{man} = \dot{m} c_p (T_{out,man} - T_{tank}) = h A_{tip} \Delta T_{lm} \tag{42}$$

where ΔT_{lm} is the logarithmic mean temperature difference between the tip and the palm oil heating medium. ΔT_{lm} is given by:

$$\Delta T_{lm} = \frac{(T_{tank} - T_{man})}{\ln[(T_{tip} - T_{man}) / (T_{tip} - T_{tank})]} \tag{43}$$

In manifold that consist of a number of evacuated tube's tip (N) in series. The outlet palm oil temperature from the manifold can be written as:

$$T_{man,out} = T_{tip} - (T_{tip} - T_{tank}) \exp\left(\frac{-N A_{tip} h}{\dot{m} c_p} \right) \tag{44}$$

where A_{tip} is outer surface area of single tip that assumed to be a sphere.

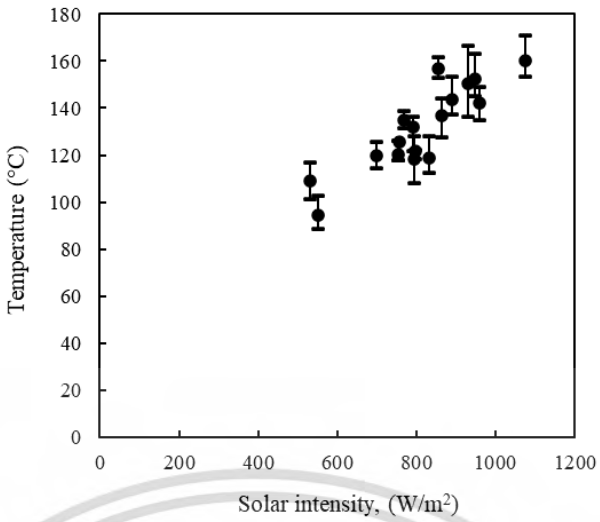

Figure 3.22 The temperature at the tip of the heat pipe varies with different levels of solar intensity.

To study the relationship between heat pipe tip temperature and solar intensity, the experiment conducted measurements over multiple days in September 2020. These measurements were taken from 9:00 a.m. to 4:00 p.m. using the experimental setup depicted in Figure 3.23a. The experimental results on Figure 3.22 were collected to establish the correlation between the tip temperature and solar intensity, as represented by Equation 45.

$$T_{tip} = 11.5 + 236.9\left(\exp\left(\frac{-496.6}{I_G} \right) \right) \tag{45}$$

Heat transfer coefficient (h) can be determined through the Nusselt number, that is the ratio of convective to conductive heat transfer at a boundary in a fluid. Flow through tube banks is studied in this work. The Nusselt number correlation has been proposed by Zukauskas et al. [30] as shown in Equation 46.

$$Nu = \frac{hD}{k} = fC\,\mathrm{Re}^{m}\,\mathrm{Pr}^{n}(\mathrm{Pr}/\,\mathrm{Pr}_s)^{0.25} \tag{46}$$

where C, m, and n are coefficients that vary based on the Reynolds number (Re) range of the fluid passing through the tube banks, as indicated in Table 3.18, and f is a correction factor for one-line in-line tube banks which is equal to 1 for Re < 1000 and equal to 0.7 for Re > 1000. Heat loss from manifold can be calculated by considering the thermal resistance of each component in manifold as shown in Figure 3.23. The thermal resistance of manifold can be calculate by Equation 47.

Table 3.18 The certain constants in Nusselt number correlation of Zukauskas' equation.

Range of Re	Constant		
	C	***m***	***n***
0–100	0.900	0.40	0.36
100–1000	0.520	0.50	0.36
1000–200,000	0.270	0.63	0.36

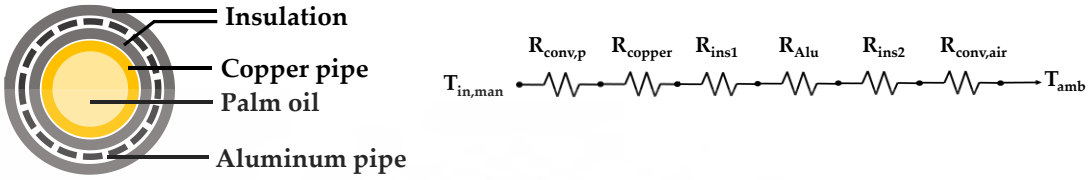

(a) (b)

Figure 3.23 The equivalent thermal resistances network (R) and temperatures (T) of the manifold heat losses surrounded by insulation (a), modelled as an electrical current (b).

$$R_{man} = R_{conv,p} + R_{copper} + R_{ins1} + R_{alu} + R_{ins2} + R_{conv,air} \tag{47}$$

For unit area the overall heat transfer coefficient is equal to invers of the total thermal resistant.

$$\dot{Q}_{man,loss} = \frac{T_{tank} - T_{amb}}{R_{man}} \tag{48}$$

Storage tank domain

Palm oil outlet of the manifold flowing to storage tank and heat accumulation in storage tank can be calculated as follows:

$$\frac{dQ_{tank}}{dt} = \dot{Q}_{man} - \dot{Q}_{loss} \tag{49}$$

where Q_{tank} is heat accumulation of the palm oil in the storage tank and can be expressed as Equation 50.

$$\frac{dQ_{tank}}{dt} = \frac{\rho V c_p dT_{tank}}{dt} \tag{50}$$

The storage tank temperature (T_{tank}) based on the derived expression can be calculated as follows:

$$\frac{dT_{tank}}{dt} = \frac{1}{(mC_p)_{tank}}[mC_p(T_{man} - T_{tank}) - UA_{tank}(T_{man} - T_{amb})] \tag{51}$$

where U is the overall heat transfer coefficient of the storage tank and A_{tank} is surface area of the storage tank.

The thermal resistance of storage tank is used to determine the heat loss from storage tank as shown in Figure 3.24 and can be calculate as follows:

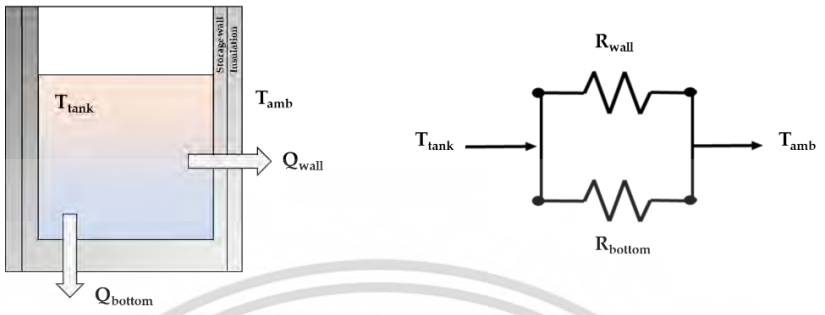

(a) (b)

Figure 3.24 The equivalent thermal resistances network (R) and temperatures (T) of the storage tank heat losses surrounded by insulation (a), modelled as an electrical current (b).

$$R_{wall,tank} = \frac{1}{h_p A_{in,tank}} + \frac{\ln(r_{out,tank} / r_{in,tank})}{2\pi k_{tank} L} + \frac{\ln(r_{out,ins} / r_{in,ins})}{2\pi k_{ins} L} + \frac{1}{h_{air} A_{out,ins}} \quad (52)$$

$$R_{bottom,tank} = \frac{1}{h_p A_{in,tank}} + \frac{r_{out,tank} - r_{in,tank}}{k_{tank} A_{out,tank}} + \frac{1}{h_{air} A_{ins}} \quad (53)$$

where $R_{wall,tank}$ is the heat losses resistance of wall of storage tank that includes the convection losses of palm oil to inner storage tank wall, the conduction losses between inner-outer storage tank wall, the conduction losses of between inner-outer insulator, the convection losses outer insulator to ambient. $R_{bottom,\ tank}$ is the heat losses resistance of bottom of storage tank. h_p and h_{air} are heat transfer coefficient of palm oil and air, respectively. k_{tank} and k_{ins} are thermal conductivity of tank and insulation, respectively. r is a radius. So, the total equivalent resistance of storage tank (R_{tank}) can be expressed by:

$$R_{tank} = \frac{R_{bottom,tank} \times R_{wall,tank}}{R_{bottom,tank} + R_{wall,tank}} \quad (54)$$

where $Q_{loss,tamk}$ is the storage tank heat loss to the ambient which is calculated by:

$$\dot{Q}_{loss,tank} = UA(T_{tank} - T_{amb}) = \frac{(T_{tank} - T_{amb})}{R_{tank}} \quad (55)$$

where T_{amb} is ambient temperature.

CHAPTER 4
RESULTS AND DISCUSSION

4.1 Mass balance and energy consumption

Mass balance has been verified to confirm whether desired number of products have been produced and the validity of mass balance. The mass balances of design 1 and design 2 are shown in Table 4.1 and Table 4.2, respectively.

Table 4.1 Compositions and conditions of feed and product streams in Design 1

Composition	**Palm oil**	**H_2**	**Green diesel**	**Green C3**	**CO_2**	**Water**
Temperature, °C	30	30	51.51	-80	-140	51.51
Pressure, bar	1	20	30.04	30.04	30.04	30.04
Phase	Liquid	Vapour	Liquid	Liquid	Liquid	Liquid
Flow rate, kg/h	1,282.38	36.82	1,102.05	52.34	41.39	122.51
Trilinolein	177.10					
Triolein	526.93					
Tristearin	109.90					
Tripalmitin	468.45					
Hydrogen		36.82	0.27	0.02	0.01	
Pentadecane			74.18	0.003		
Hexadecane			315.10	0.005		
Heptadecane			145.91			
Octadecane			547.88	0.001		
Propane			13.81	44.26	7.99	
Carbon dioxide			2.52	5.28	33.39	
Water			2.41	2.77		122.51
Summary	**1,319**		**1,319**			

The difference between the mass out and mass in of design 1 and design 2 is 0.067 and 0.00 percent, respectively, which is insignificant. The small difference is due to the calculation margins set by Aspen plus V14. The palm oil and hydrogen flow rates for two designs are set at 1,282.38 kg/h and 106.96 kg/h, respectively. For Design 1, the fresh hydrogen input is 36.82 kg/h, and the recovery is 70.14 kg/h, the high purity of the green diesel fuel (98.27 wt%) at a flow rate of 1,102.05 kg/hr contrasts with the lower purity of green propane (84.56 wt%) at 52.34 kg/hr and carbon dioxide (80.67 wt%) at 41.39 kg/hr. Despite the inferior purity, green propane can still be utilized as a fuel in the furnace. However, due to the low purity of carbon dioxide, it cannot be used

and is emitted as pollution. For Design 2, the fresh hydrogen input is 36.69 kg/h, and the recovery is 70.27 kg/h, the purity of the green diesel fuel (98.27 wt%) remains unchanged. However, the purity of green propane increases to 100 wt%, and the purity of carbon dioxide increases to 99.43 wt% at 38.38 kg/hr.

Table 4.2 Compositions and conditions of feed and product streams in Design 2

Composition	**Palm oil**	**H_2**	**MEA Make-up**	**Green diesel**	**Green C3**	**CO_2**	**Water**	**Purge**
Temperature, ºC	30	30	40	51.51	-80	78.13	51.51	25
Pressure, bar	1	20	2	30.04	30.04	1.97	30.04	15
Phase	Liquid	Vapour	Liquid	Liquid	Liquid	Vapour	Liquid	Liquid
Flow rate, kg/h	1,282.38	36.69	48.30	1,102.05	51.82	38.38	122.52	52.60
Trilinolein	177.10							
Triolein	526.93							
Tristearin	109.90							
Tripalmitin	468.45							
Hydrogen		36.69		0.24				
Pentadecane				74.18				
Hexadecane				315.10				
Heptadecane				145.91				
Octadecane				547.88				
Propane				13.81	51.82			
Carbon dioxide				2.52		38.16		9.76
Water			46.98	2.41		0.22	122.52	42.60
MEA			1.32					0.21
Summary	**1357**			**1357**				

The analysis of heat integration using Pinch theory for Designs 1-2 has provided valuable insights into the optimization of energy utilization in the production process, as depicted in Figures 4.1 and 4.2.

In Design 1, the heat exchanger network (HEN) demonstrates effective heat integration. The hot stream from the FBH reactor undergoes sequential exchanges with a cold stream of palm oil at HX-101 and then with a cold stream of hydrogen at HX-102. This configuration aims to maximize heat recovery and minimize energy consumption. The efficiency of this network in transferring heat between process streams is crucial for improving overall energy efficiency.

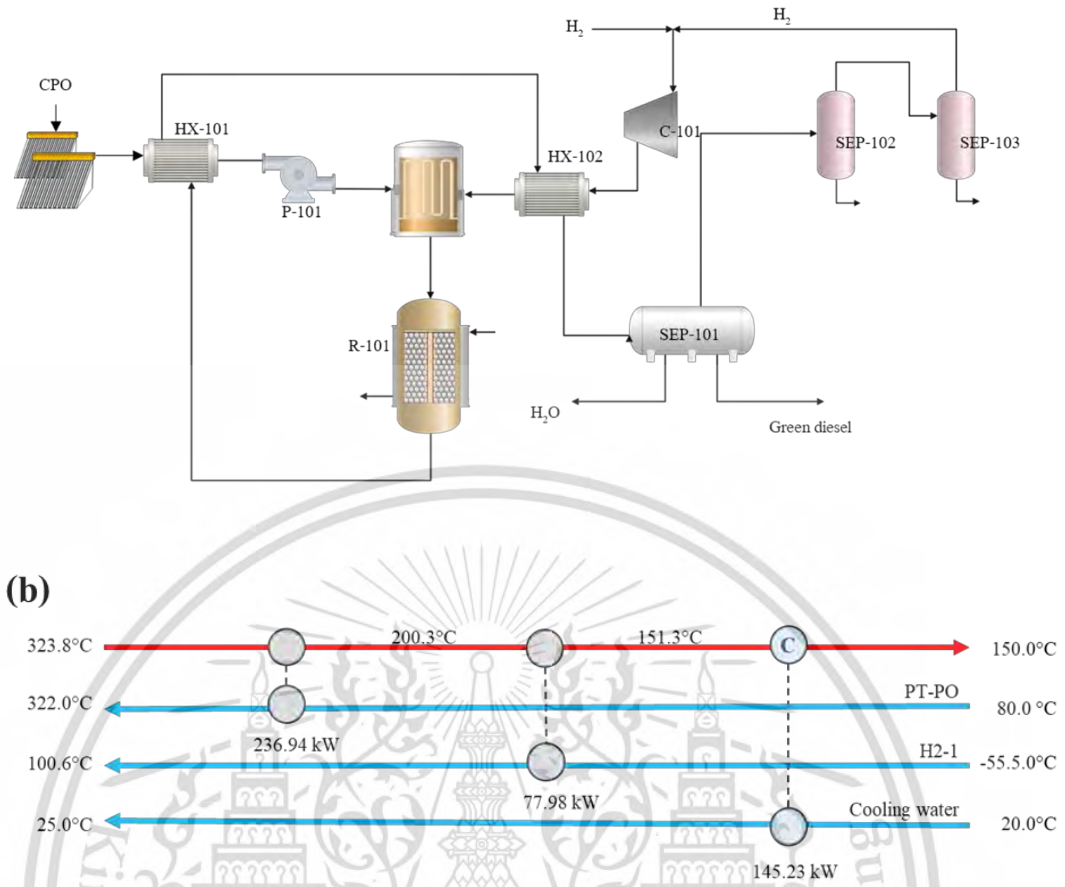

Figure 4.1 The heat integration of Design 1 through (a) the process flow diagram and (b) the heat exchanger network.

Design 2 follows a similar HEN as Design 1 but with a variation in the cold streams involved. The hot stream from the FBH reactor is exchanged with a cold stream of palm oil at HX-101 and a cold stream of hydrogen at HX-102. Additionally, the cold stream of rich MEA is exchanged with the hot stream of lean MEA at HX-106. Comparing Design 2 to Design 1 allows for an assessment of the impact of variations in the heat exchanger network on energy efficiency.

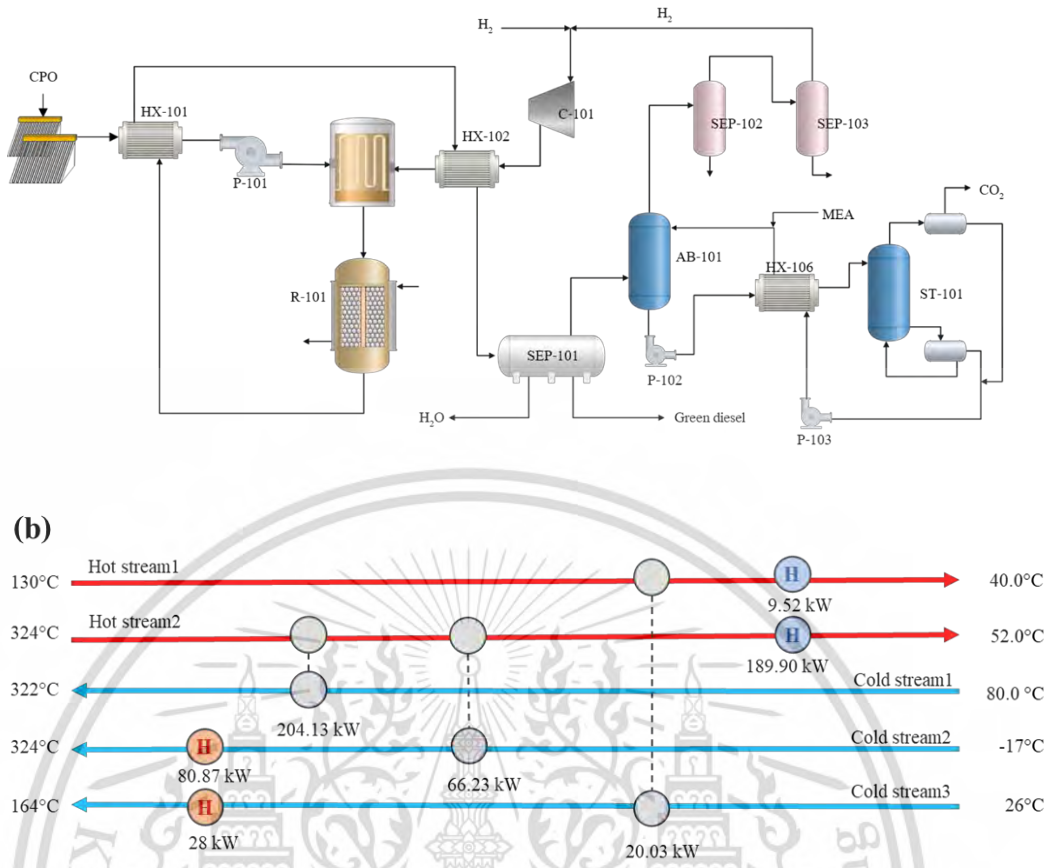

Figure 4.2 The heat integration of Design 2 through (a) the process flow diagram and (b) the heat exchanger network.

The results indicate that heat integration across both designs significantly reduce the heat consumption from specific heaters. Cooling consumption in HX-104 demonstrates a reduction of energy consumption, decreasing from 405.78 kW to 135 kW in both designs. For Designs 2, the heat integration of the CO_2 capture unit reduces energy use in the cooler (HX-105) from -27.28 kW to -9.53 kW. The net energy consumptions for Designs 1 and 2 exhibit a substantial reduction, decreasing from initial values of 950.91 kW and 1,022.92 kW to 460.49 kW and 510.88 kW, respectively. This significant decline underscores the efficacy of the implemented heat integration strategies in enhancing overall energy efficiency across the three designs.

Table 4.3 The energy consumption following the heat integration of green diesel production in Design 1 and Design 2.

No.	Equipment	Energy	Energy consumption, kW	
			Design 1	Design 2
P-101	Pump1	Electricity	5.13	5.13
P-102	Pump2	Electricity	-	0.04
P-103	Pump3	Electricity	-	0.00
C-101	Compressor1	Electricity	13.76	16.23
C-102	Compressor2	Electricity	-	15.40
F-101	Furnace	Heating	85.19	80.87
HX-101	Heat Exchanger1	None	236.94	204.14
HX-102	Heat Exchanger2	None	77.98	66.23
HX-103	Heater	Heating	96.51	80.23
HX-104	Heater	Cooling	-135.56	-135.42
HX-105	Cooler	Cooling	-	-9.53
HX-106	Heat Exchanger4	None	-	20.03
ST-101	Condenser	Condenser	-	7.28
ST-101	Reboiler	Heating	-	28.00
SEP-101	Separator1	Cooling	-54.46	-54.48
SEP-102	Separator2	Cooling	-21.72	-35.25
SEP-103	Separator3	Cooling	-48.16	-43.02
R-101	Reactor	None	-343.75	-343.75

4.2 Green diesel simulation

The validation of the kinetic model for hydrotreating reactions, ensuring its accuracy, was conducted using the liquid product compositions from Srifa et al [18]. This involved assessing the impact of operating parameters such as hydrotreating temperature, hydrogen pressure, liquid hourly space velocity (LHSV), and H_2/oil ratio. The influence of hydrotreating temperature was assessed within the range of 270-330°C, while maintaining fixed values for other operating parameters at a pressure of 50 bar, LHSV of 1.0 h^{-1}, and H_2/oil ratio of 1,000 cm^3/cm^3, as illustrated in Figure 4.3(a). The impact of hydrogen pressure on liquid product compositions contributes to the optimization of operating conditions for economic efficiency. Hydrogen pressure was

studied within the range of 30-80 bar, while maintaining fixed values for other operating parameters at a temperature of 300 °C, LHSV of 1.0 h^{-1}, and H_2/oil ratio of 1,000 cm^3/cm^3, as depicted in Figure 4.3(b). Liquid hourly space velocity (LHSV) represents the ratio of the mass flow rate to the volume of the packed catalyst. It is inversely proportional to residence time. The study varied LHSV within the range of 0.5-5 h^{-1}, while keeping other operating parameters fixed at a temperature of 300°C, pressure of 50 bar, and H_2/oil ratio of 1,000 cm^3/cm^3, as depicted in Figure 4.3(c). The H_2/oil ratio significantly influences both economic aspects and hydrotreating reactions. This study explored the H_2/oil ratio within the range of 500-2,000 cm^3/cm^3, while maintaining fixed values for other operating parameters at a temperature of 300°C, pressure of 50 bar, and LHSV of 1 h^{-1}, as depicted in Figure 4.3(d).

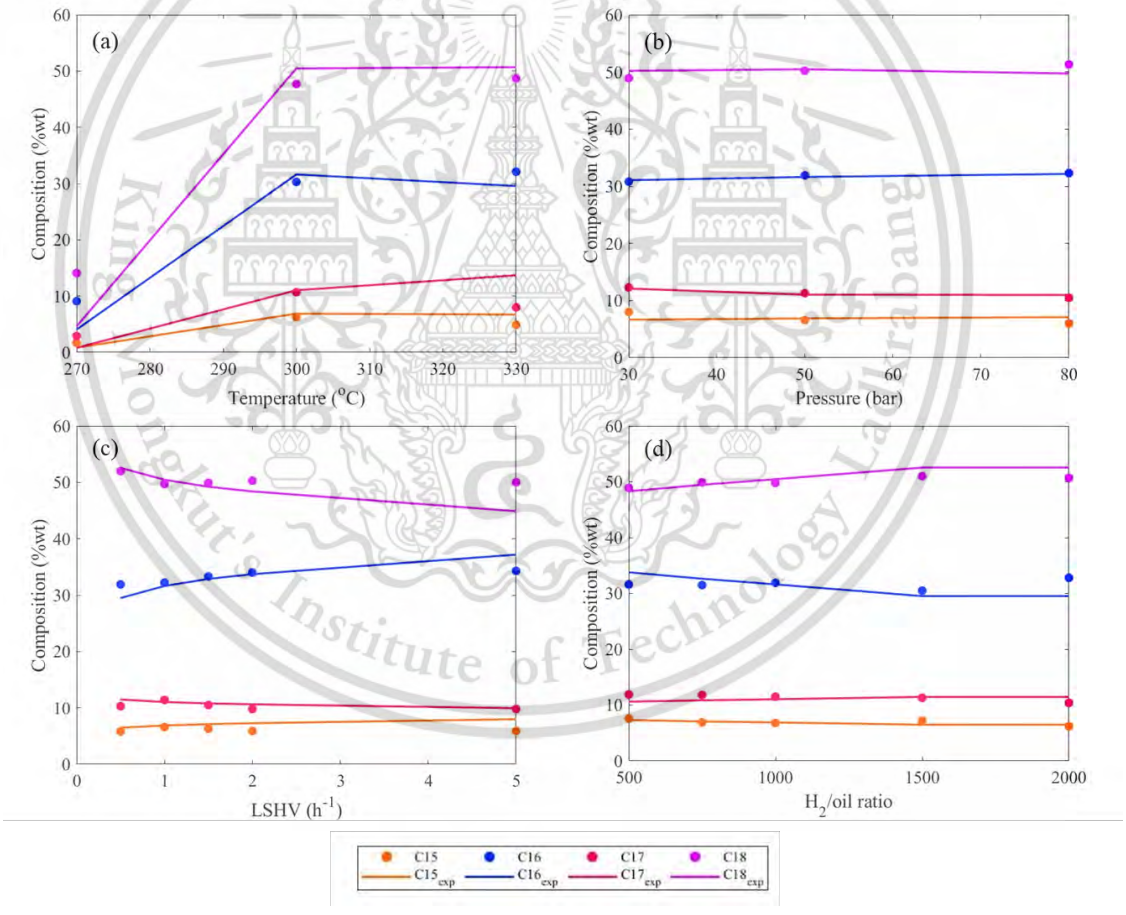

Figure 4.3 The validation of the mass fraction of green diesel (C15-C18) was conducted with respect to (a) Temperature, (b) Pressure, (c) LHSV, and (d) H_2/ratio.

In the simulation, the thermodynamic models PENG-ROB and ELEC-NRTL, available in ASPEN PLUS V14, were employed to simulate the data from Srifa et al [18]. The results are depicted in Figure 4.4. As observed, the model accurately predicted the green diesel product, demonstrating a RMSE of 4.21%.

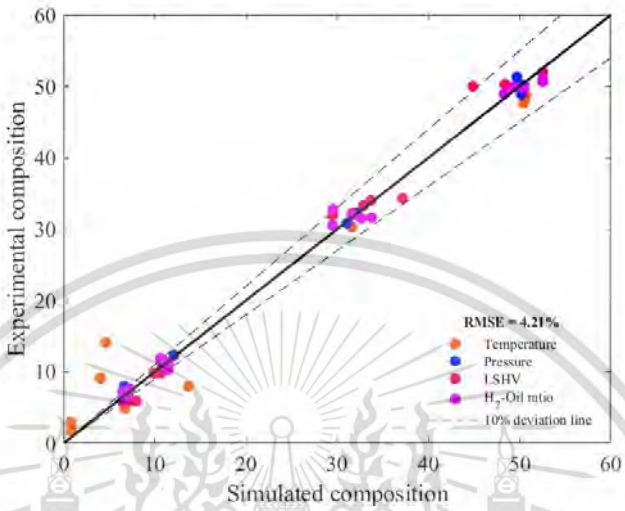

Figure 4.4 Comparison of experimental compositions (C15-C18) [18] with the simulated values obtained in this study.

The number of stages analysis is investigated to determine the optimal number of stages as reported in Table 4.4. The performance evaluation is represented by percentage of CO_2 removal at the same amount of rich solvent loading. From the result, increasing the number of stages from 15 to 30 increases CO_2 removal by only 0.03%. On the other hand, investigating absorption column profile is another way to ensure the optimum number of stages selection by using sensitivity analysis. Make a plot of the liquid mole fraction of the interesting components such as H_2O, H_2, CO_2, and MEA as shown in Figure 4.5. The flat regions shows that those stages are not very active and unnecessary. Therefore, it can be removed stages during the flat regions. Moreover, considering the lean solvent feed rate and number of stages is an optimization process capital and operating cost.

Table 4.4 Number of stages in absorber (AB-201)

Performance	**Number of segments**				
	6	**15**	**30**	**45**	**60**
CO_2 removal %	98.563	98.563	98.564	98.566	98.569

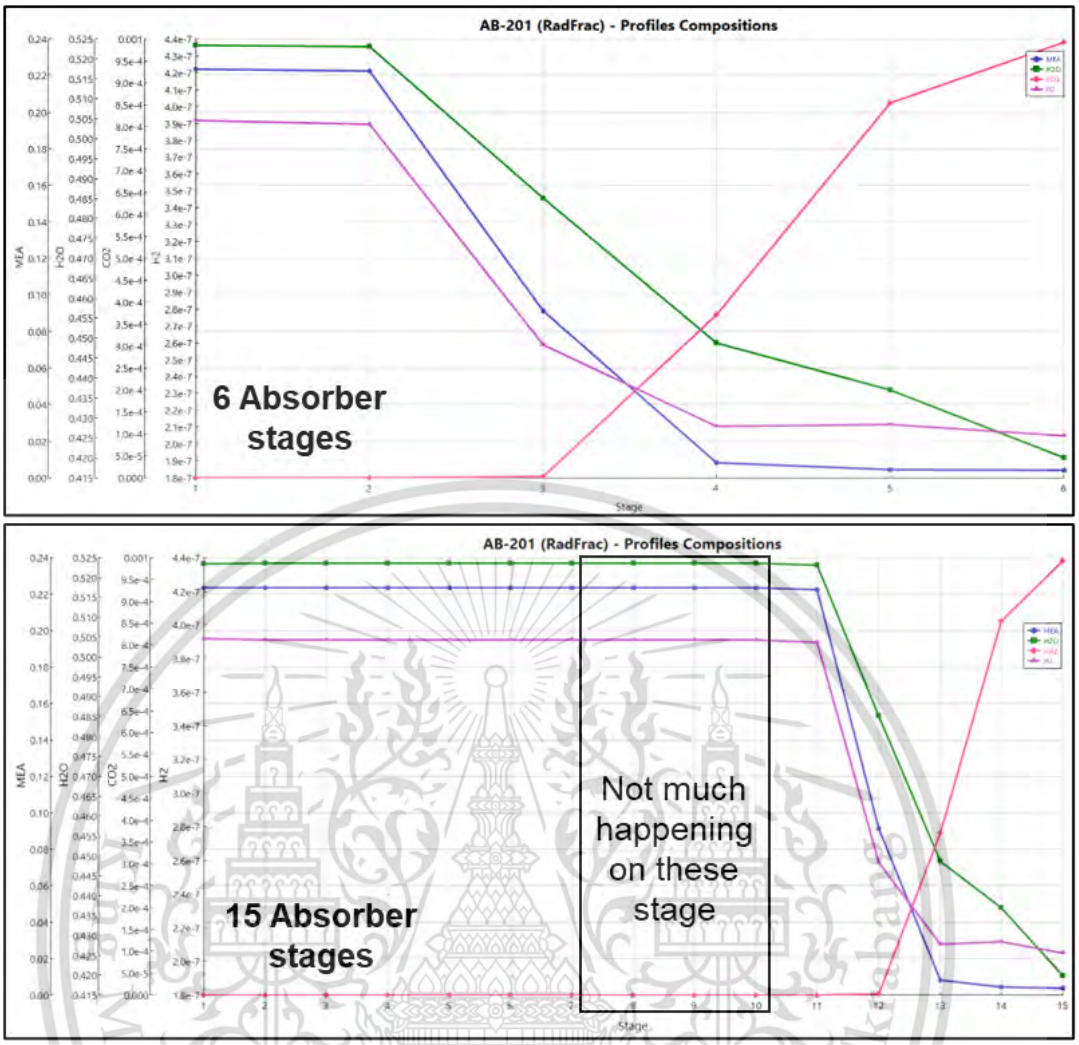

Figure 4.5 The column profile of the absorber to achieve 98.56% removal of CO_2 from the gas stream.

Once the evaluation of the minimum number of stages in the absorber is complete, the minimum lean solvent feed rate is determined through the utilization of sensitivity analysis on Aspen Plus®. The determination CO_2 removal percentage by varying the lean solvent feed rate, it was found that the solvent rate that caused the removal percentage up to 99.9% was 427 kg/hr of lean solvent as shown in Figure 4.6.

The design parameters of absorber and stripper columns are shown in Table 4.5. The reflux ratio and the reboiler duty are optimized by using sensitivity analysis to obtain lower operating cost due to low energy consumption, and high purity of CO_2 product.

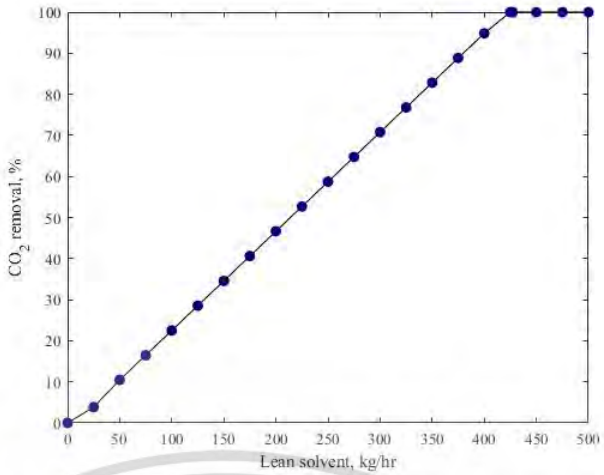

Figure 4.6 Sensitivity analysis varying the amount of lean solvent.

Table 4.5 Absorption and Stripping columns parameter (*RadFrac*^{TM})

Parameter	**Absorption**	**Stripper**
Number of stages	6	10
Section packing height, m	6.34	3.94
Diameter, m	0.32	0.3
Amount of solvent, kg/h	427	-
Condenser	None	Partial Vapour
Reboiler	None	Kettle
Reflux ratio	-	4.5
Reboiler duty, kW	-	28
Pressure, bar	1	1.97

4.3 Evacuated tube solar collector model

The performance of an evacuated tube solar collector was studied to assess its effectiveness and calculate the heat required for integration into the green diesel production process. This investigation aims to understand how well the solar collector performs in capturing and utilizing solar energy and to determine its potential contribution to meeting the heat needs of the green diesel production process. The evaluation involves analysing key performance metrics, such as solar energy absorption and heat transfer efficiency, with the ultimate goal of exploring the feasibility and benefits of integrating solar energy into the production process of green diesel.

Figure 4.7 illustrates a comparison between the measured and predicted temperatures of both inlet and outlet palm oil at different palm oil capacities. The comparison is made in two scenarios, one without applying the correction factor and the other with the correction factor. In the graph, the dashed lines represent the calculated results when the correction factor is not utilized in the heat transfer coefficient correlation, while the solid lines depict the calculated results after incorporating the correction factor into the correlation. This comparison allows for an assessment of the impact of the correction factor on the accuracy of temperature predictions.

The comparison between calculated and experimental results for water is presented in Figure 4.8a-d. The experimental data is divided into two categories based on water inlet temperatures. The first category covers the low inlet temperature case, ranging from 32 to 40°C, as shown in Figure 4.8a,b. The second category represents the high inlet temperature case, with temperatures ranging from 53 to 85°C, as displayed in Figure 4.8c,d. This division allows for a more detailed assessment of the accuracy of the calculations across different temperature ranges.

Figure 4.9 shows the percentage errors of the predicted heating medium outlet temperatures. For palm oil heating medium (Figure 4.7a), the average percentage deviations (A-PD) for various storage capacities fall within the range of 4.52% to 7.75%, with an overall absolute percentage deviation (ABS-PD) of 6.41% and a maximum deviation (MAX-PD) of 11.78%. For water heating medium (Figure 4.8b), the maximum error exhibited an increase with higher water mass flow rates, specifically 1.83% at 0.03 kg/s, 4.50% at 0.065 kg/s, 6.14% at 0.11 kg/s, and 15.23% at 0.3 kg/s. Meanwhile, the overall absolute percentage deviation was 4.76%. This implies that as the Reynolds number increases, the error also rises. This phenomenon may be attributed to discrepancies in the predicted heat transfer coefficient by the correlation coefficient. While there was a suggestion to incorporate a correction factor of $f = 0.7$ into the correlation for cases involving fluid flow with Reynolds numbers exceeding 1000, it's worth noting that this correction factor may not remain constant across the entire range but could vary with changes in the Reynolds number.

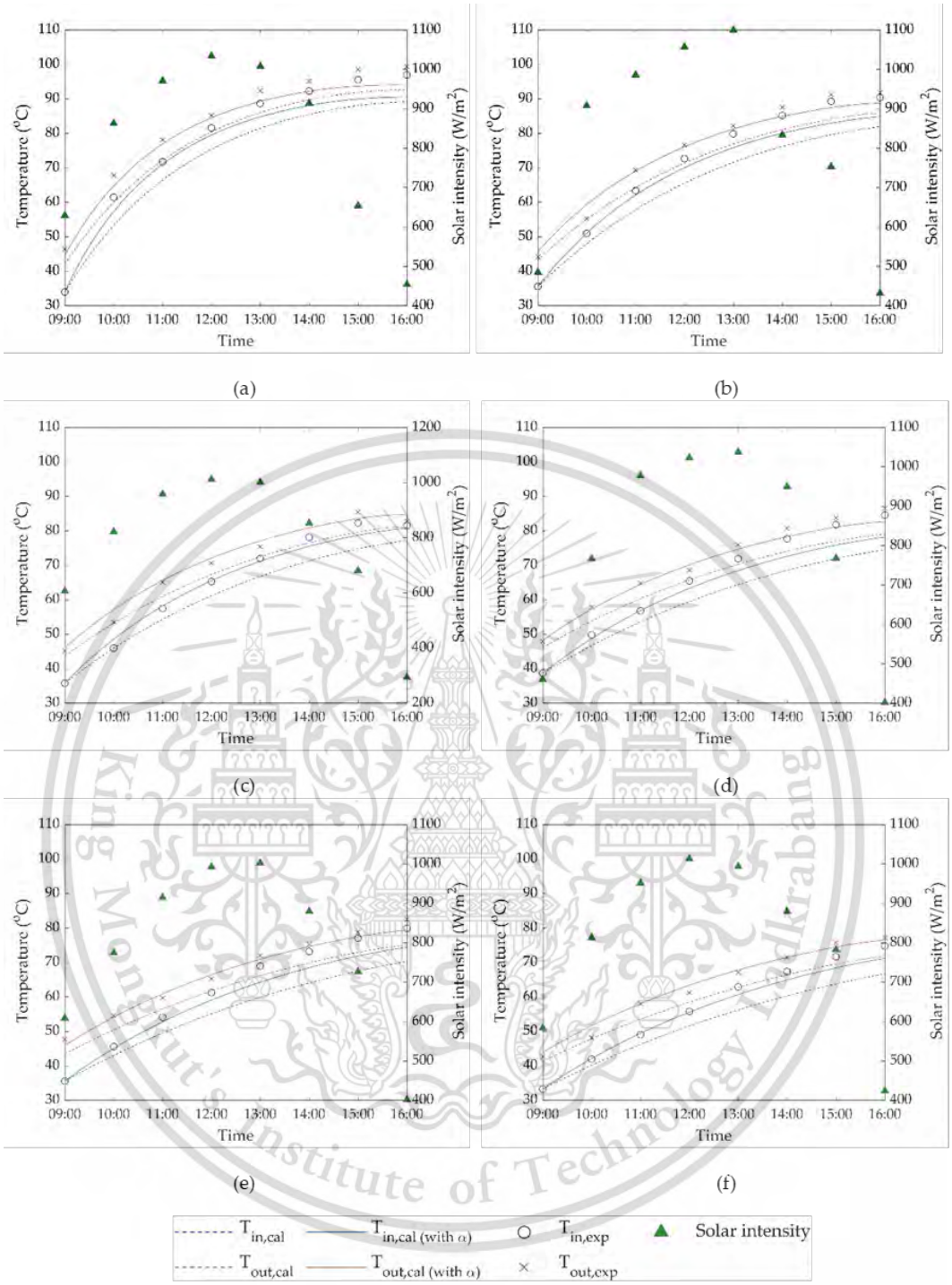

Figure 4.7 Experimental and calculated palm oil inlet and outlet temperatures at different storage capacities. Quantities of (a) 50 L, (b) 80 L, (c) 100 L, (d) 120 L, (e) 140 L and (f) 160 L.

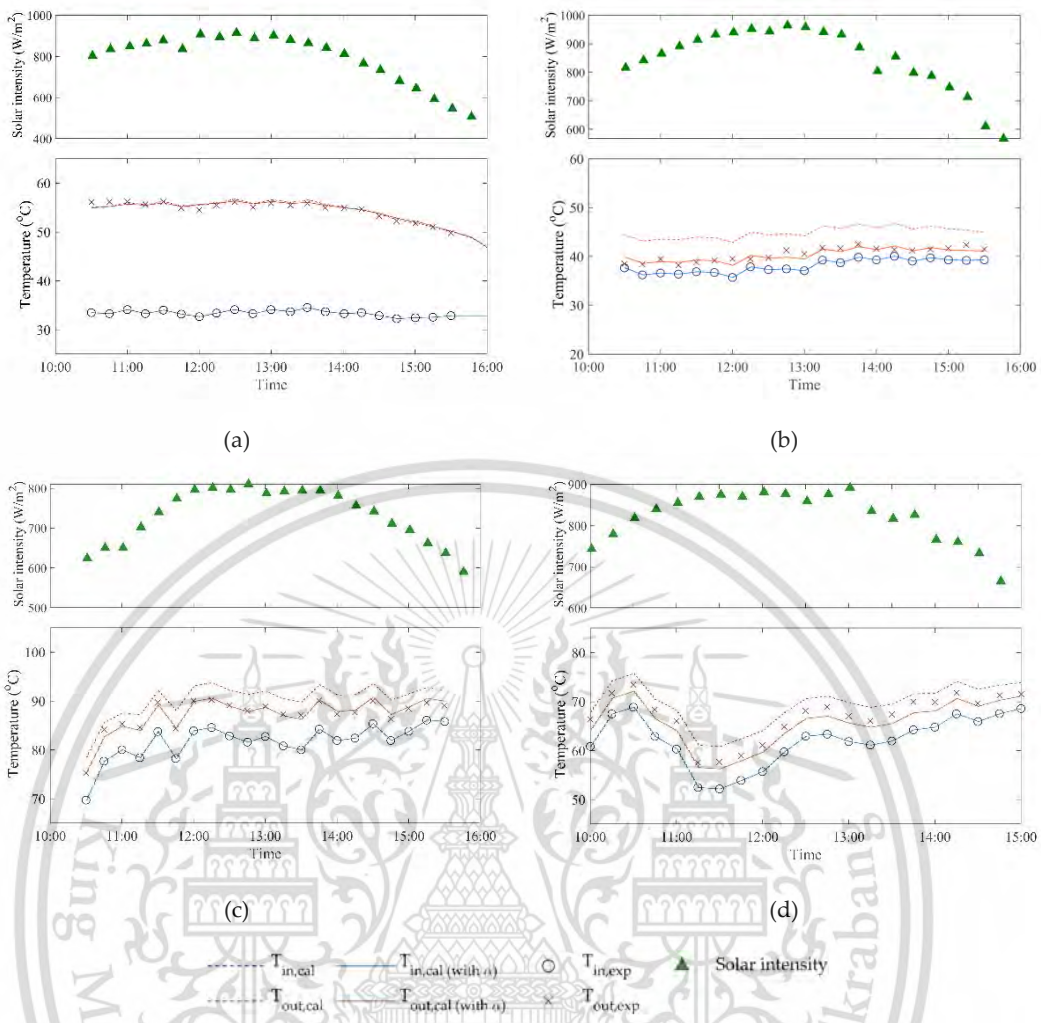

Figure 4.8 The comparison of water manifold inlet and outlet temperatures measured from the experiments reported by Elsheniti et al. [12] and the calculated results at the water mass flow rates of (a) 0.03 kg/s, (b) 0.3 kg/s, (c) 0.065 kg/s and (d) 0.11 kg/s.

The observed trend shows that the prediction deviation shifts from under-prediction at lower Reynolds numbers to over-prediction as Reynolds numbers increase, with the degree of over-prediction escalating as the Reynolds number rises. It's worth noting that the equation used to calculate heat pipe tips was established based on measurements taken with heat tips in ambient air. In this context, the heat from the heat pipe tips is transferred to nearly stagnant air.

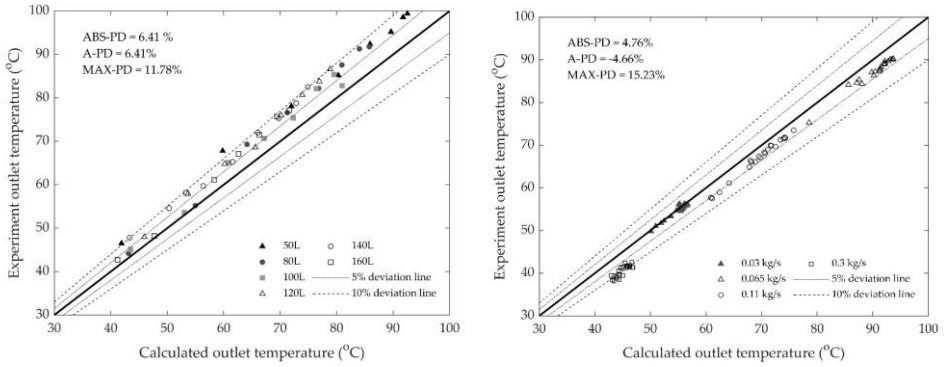

(a) (b)

Figure 4.9 Percentage errors of (a) predicted palm oil outlet temperatures and (b) predicted water outlet temperatures at different mass flow rates.

Consequently, the heat release rate from the heat pipe tips and the heat absorbed from sunlight should be considerably lower than those occurring in the manifold, where the heating medium fluid circulated. Moreover, a higher Reynolds number of the fluid leads to an increased heat transfer rate. Building upon the previous observation, a correction factor denoted as α was developed and incorporated into Nusselt correlation to offset the deviation, resulting in:

$$Nu = \frac{hD}{k} = \alpha f C \,\mathrm{Re}^{m}\,\mathrm{Pr}^{n}\,(\mathrm{Pr}/\,\mathrm{Pr}_{s})^{0.25} \tag{56}$$

$$\text{where} \quad \alpha = \frac{2400}{\mathrm{Re}} \quad \text{for Re} < 2{,}500 \tag{57}$$

$$\text{and} \quad \alpha = \frac{5500}{\mathrm{Re}} \quad \text{for Re} > 2{,}500 \tag{58}$$

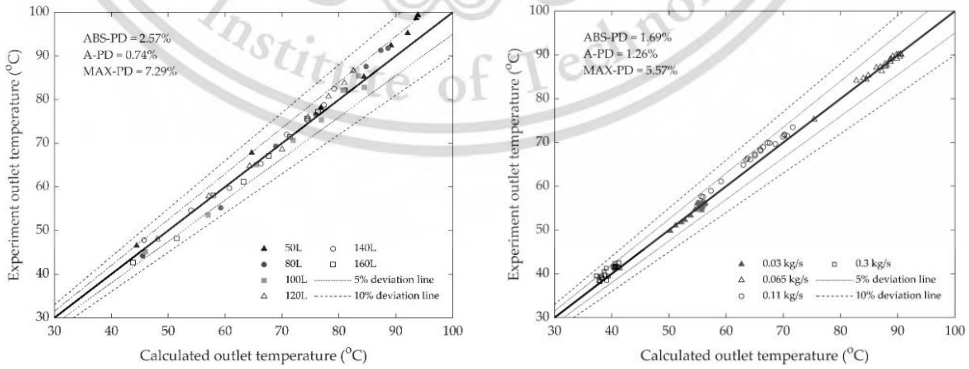

(a) (b)

Figure 4.10 Percentage errors of (a) predicted palm oil outlet temperatures and (b) predicted water outlet temperatures at different mass flow rates after adding the correction factor, α.

Figure 4.10 shows the percentage errors of the predicted heating medium outlet temperatures after applying the correction factor α. It is seen that the prediction is obviously more accurate for both palm oil and water cases. The incorporating correction factor α to the mathematical model reduce the maximum percentage error between theoretical and experimental values to 7.29% and 5.57% compared to 11.78% and 15.23% of the palm oil case and water case respectively.

4.3.1 Integrating of ETSC the green diesel production process

In this study, the ESTC system is integrated into palm oil pretreatment unit of the green diesel production process to reduce energy consumption and CO_2 emissions. This mathematical model was employed to assess the feasibility of implementing the ETSC within the pretreatment unit of the green diesel production process. The pretreatment unit operates at 80°C and requires an inflow of 1.67 kg/s of palm oil at 100°C from the ETSC system. The simulation results show that the heat exchange energy required from the ESTC unit is 255 MW per year. However, the system can only exchange heat for 8 hours per day. To provide 24 hours of operation, another 16 hours of heat exchanger is required. The optimal results for the 80°C target temperature and 85 MW/year (Operate 8 hr/day) obtained from the model are shown in Table 4.6.

Table 4.6 Design parameters of the ETCS employed for the pretreatment unit.

Design parameters	**Value**
Heating medium	Palm oil
Total mass flow rate	1.67 kg/s
Inlet temperature	90 ºC
Outlet temperature	100 ºC
Production rate	85 MWh/year
Number of parallel paths	8 lines
Number of tubes in series	240 tubes
Total number of tubes	1920 tubes
Gross surface area	288 m^2
Capital investment	$64000

4.4 Economic analysis

The economic evaluation based on the dimensions of equipment in Aspen Plus® involves considering the size and specifications of the equipment modules within the

process simulation. The size of equipment has a notable impact on its cost. Larger equipment generally requires more materials, higher construction and installation costs, and increased maintenance expenses. The size of the unit was established on the Guthrie's method. The size of each equipment was obtained from Aspen Plus®. The design parameters required to calculate the CAPEX are shown in Table A.1-16.

In the economic analysis of a green diesel production plant, critical assumptions are established as shown in Table 4.8. The plant construction time is set at 3 years, determining the construction duration and initial capital investments. The operating time is assumed to be 300 days per year, shaping revenue and operational expenses. The plant life is projected to be 20 years, influencing depreciation schedules and asset valuation. The depreciation period is determined as 7 years, affecting financial statements. A 30% of income tax rate in Thailand is applied to taxable income, impacting tax liability and cash flows. Additionally, an interest rate of 15% guides financing decisions and the project's overall financial feasibility. These assumptions collectively underpin financial modelling and are central to project evaluation.

Table 4.7 Summary of assumptions in economic evaluation

Assumptions	**value**
Plant construction time	3 years
Operating time	300 days/year
Plant life	20 years
Depreciation period	7 years
Income tax rate	30%
Interest rate	15%
Crude palm oil [21][22]	0.47 - 0.81 $/kg
Hydrogen	3.30 $/kg
MEA [23]	1.38 $/kg
Diesel	1.13 $/kg – 1.98 $/kg
Carbon dioxide	0.4 $/kg
Propane [31]	0.82 $/kg

4.4.1 Capital Expenditures (CAPEX)

The distribution of CAPEX is indicated in Figure 4.11 for the hydrotreating process in Design 1 and Design 2 were computed at 1.75 million dollars and 4.20 million dollars, respectively. Observing the cost breakdown, it becomes evident that in

Design 1, the hydrotreating reactor is the costliest equipment, accounting for a significant 34.98% of the CAPEX. On the other hand, Design 2 is primarily characterized by compressors, making up 38.44% of the CAPEX. In Design 2, a compressor is required to raise the pressure from 1 bar to 10 bar between the 3-phase separator and the first cryogenic unit, and then from 10 bar to 30 bar between the first and second cryogenic separators. The higher power requirements of compressors in Design 2 demand more expensive and durable components, such as larger motors, stronger materials, and intricate designs.

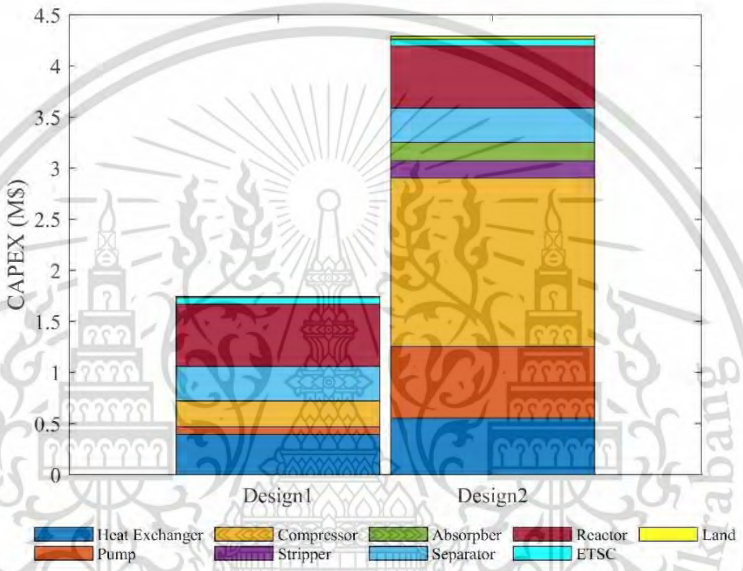

Figure 4.11 CAPEX of the hydrotreating process

The summary of the total capital investment is presented in Table 4.9. The working capital represents the funds required to operate the plant if there are delays in payment and maintenance of inventories. The working capital is calculated according to one month of the total manufacturing costs. Site, building, and offsite facility is 15% of total BMC.

Table 4.8 Summary of capital investment

Cost		**Value (M$)**	
		Design 1	**Design 2**
Total bare module cost, BMC		1.746	4.198
Site, building and offsite facility	15% BMC	0.260	0.630
Working capital	1 month of MC	2.881	2.947
Total capital investment		5.235	8.644

4.4.2 Operating Expenditures (OPEX)

OPEX were calculated by factor method of Busche as shown in Table 3.14. Figure 4.12 provides a detailed breakdown of each OPEX item, including Feedstocks, Utilities, Operations, Maintenance, Overhead, Taxes, Insurance, and Depreciation. The operational expenditures (OPEX) for Design 1 and Design 2 amount to 16.11 M$ and 16.55 M$, respectively. The predominant contributors to the OPEX in both designs are the raw materials, constituting 55.84% for Design 1 and 54.38% for Design 2. These figures highlight the substantial impact of raw material costs on the overall operational expenses of both designs.

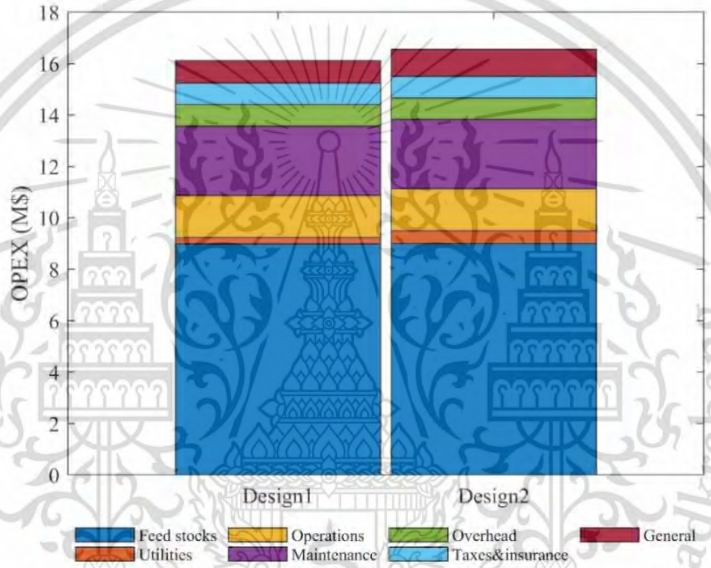

Figure 4.12 OPEX of the hydrotreating process

4.4.3 Profitability analysis

The evaluation of the plants NPV is shown from 2023 to 2038. It is assumed that green diesel production plants will be constructed in three years by dividing the total capital expenditure into three equal parts. NPV can be expanded to include not only capital and operational expenditures but also potential revenue with carbon emissions reductions.

In economic analysis, the carbon revenue can be incorporated into cash flows to account for the financial advantage linked to the reduction of carbon emissions or engagement in carbon credit trading markets. This income can be viewed as an extra source of revenue for a project that has implemented measures to reduce its carbon footprint. The carbon price for green diesel in Design 2 is shown in Figure 4.13.

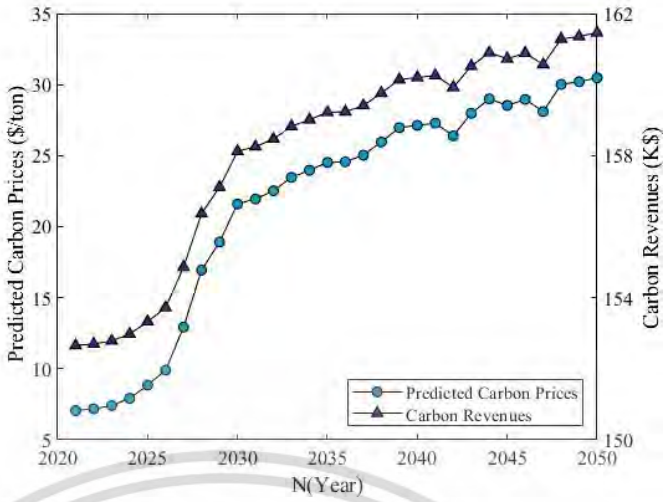

Figure 4.13 Carbon revenue of green diesel production

The results presented in Figure 4.14 reveal that after 15 years, NPV would stand at -28.1 million dollars for Design 1 and -30.2 million dollars for Design 2. The negative NPV for both Design 1 and Design 2 indicate that the green diesel plant is not expected to generate sufficient cash flows to cover its initial investment and provide a positive return.

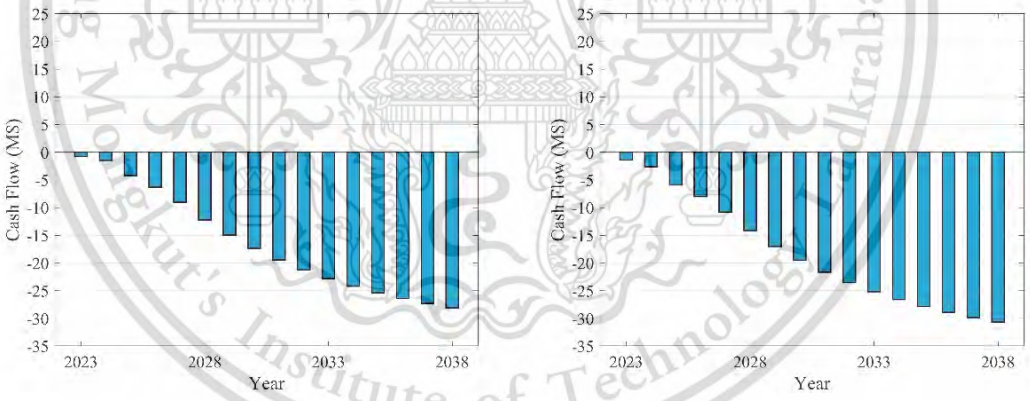

Figure 4.14 Cumulative cash flow diagram for green diesel processing plant (a) design 1 and (b) design 2

In the case of a project with a negative NPV, the net gain from investment is negative, indicating that the project is not expected to generate returns that exceed the initial investment. The results in Table 4.10 show a negative ROI, which indicates a poor or unprofitable investment. Moreover, the payback period (PBP) for such a project may not exist or may be infinitely long, meaning that the project may never recoup its initial investment.

Table 4.9 Profitability analysis of green diesel processing plant

Method		Specify		Specify		Calculated	
		item	value	item	value	item	value
Design 1	**NPV**	*i*	15%	n	15	NPV	-28.1 M$
	ROR	n	15	NPV	0	*i*	-181.7
	PBP	*i*	15%	NPV	0	n	-
Design 2	**NPV**	*i*	15%	n	15	NPV	-30.2 M$
	ROR	n	15	NPV	0	*i*	-182.1
	PBP	*i*	15%	NPV	0	n	-

4.4.4 Sensitivity analysis

The sensitivity analysis is conducted to ascertain the impact of various key factors might influence the concept's profitability. This is accomplished through the manipulation of raw material and product prices, where intentionally set them to deviate within a predefined range of ±100% from the current market price. Figure 4.15 illustrates the fluctuations in NPV resulting from alterations in the prices of raw materials, products, utilities, and equipment. The variability in diesel prices has the most substantial influence on NPV because it directly impacts the equivalent green diesel selling price, which subsequently affects the generated revenue. Conversely, the CPO price also wields a significant influence on NPV, given that it serves as the primary raw material used in the green diesel production process.

As the production volume increases, negotiate with suppliers for better pricing based on economies of scale. Larger quantities of feedstocks may lead to more favourable pricing agreements. From the result of sensitivity analysis, for both designs to achieve a 15-year payback period based on production, the cost of purchasing crude palm oil is 0.47 $/kg$_{CPO}$ (lowest price in September 2019) [21], and the price for selling green diesel price is 1.98 $/kg$_{GD}$. The NPV of both designs after adjusting the purchase price and selling price is shown in Figure 4.16.

After adjusting the purchase price of palm oil and the selling price of the green diesel, It is observed that the payback periods for Designs 1 and 2 reduced to 6.7 and 9.5 years, respectively.

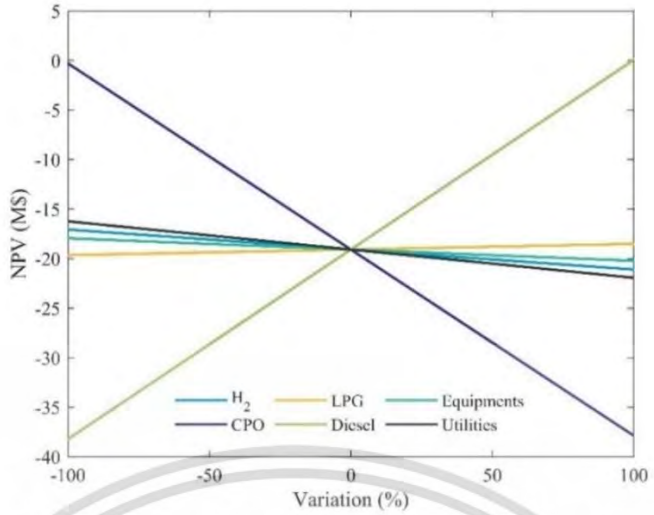

Figure 4.15 Effect on the NPV by variation in purchasing price of raw materials, selling price of products, utility, CAPEX and OPEX for the 15-year production project.

In summary, the process is technically feasible, but its large-scale implementation would necessitate additional funding or government incentives, contingent upon the prevailing diesel prices. Government incentives and subsidies may come from the use of renewable feedstocks. Additionally, large-scale producers can sometimes wield significant market power, which may allow to influence prices. Larger palm oil plantations may benefit from economies of scale, which can lead to lower production costs per unit of CPO. This can make more competitive and potentially maintain or even reduce prices.

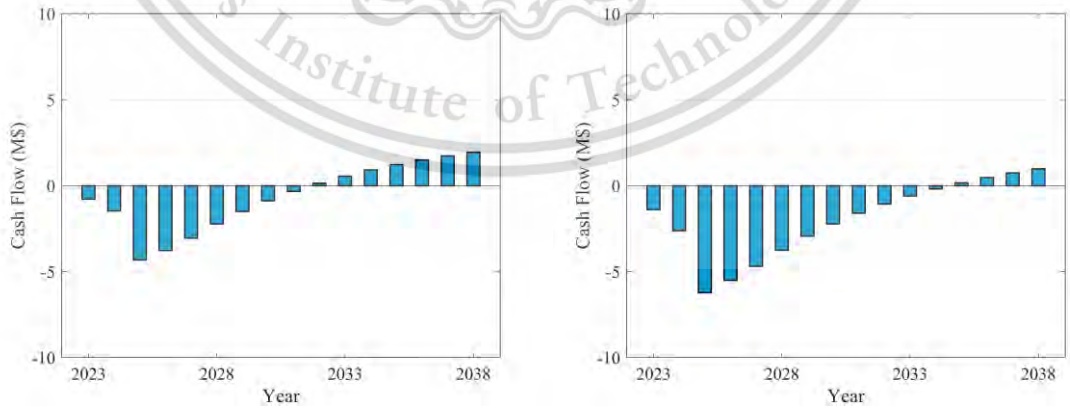

(a) (b)

Figure 4.16 Cumulative discounted cash flows of (a) design 1 and (b) design 2

4.5 Environmental Impact

Simapro is a life cycle assessment (LCA) software tool used to evaluate the environmental impact of products and processes. By conducting LCAs, Simapro helps identify the environmental consequences of various activities, such as manufacturing, transportation, and energy production. The software analyses the entire life cycle of a product or process, including raw material extraction and production, to quantify its environmental footprint. The main objective of this investigation is to compare the environmental impact of the two designs.

4.5.1 LCA

The environmental impact comparison between Design 1 and Design 2 for 1 kg of green diesel is illustrated in Figure 4.17. The normalization findings revealed that TEIP had the greatest influence on the environmental footprint of green diesel production, accounting for 74.45% in design 1 and 74.78% in Design 2, primarily due to palm oil plantation activities. The second greatest significant impact was attributed to FATEP, amounting to 16.18% in design 1 and 16.23% in Design 2. Figure 4.18 presents a graphical representation of the three-endpoint environmental impacts associated with the production and use of 1 kg of green diesel.

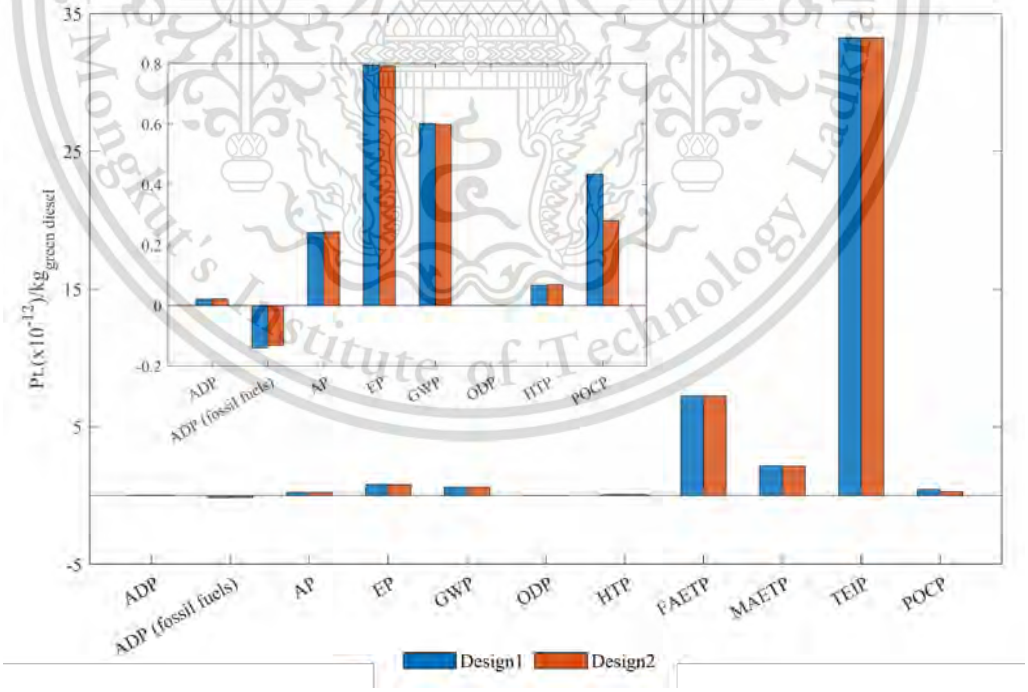

Figure 4.17 Environmental impacts of 1 kg Green Diesel

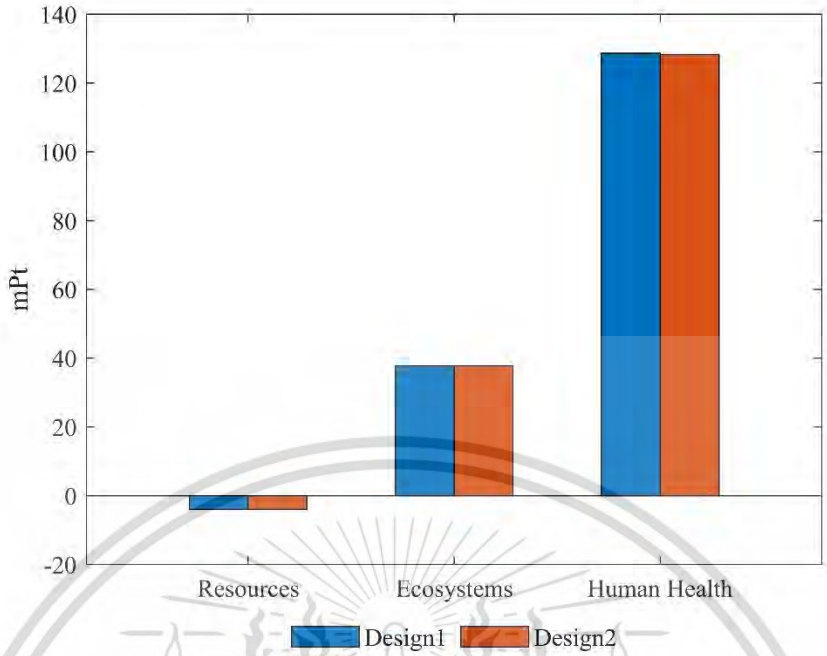

Figure 4.18 Three-endpoint environmental impacts of 1 kg green diesel

4.5.2 Greenhouse gas emissions

The study focused on the analysis of CO_2 emissions using greenhouse gas (GHG) emissions as shown in Figure 4.19. Large amounts of CO_2 emission in Designs 1 and Design 2 occur from furnace (HX-103). Design 1 exhibits higher CO_2 emissions compared to design 2 due to the cryogenic separation process, the carbon dioxide obtained had a lower level of purity. Therefore, a significant portion of the carbon dioxide was emitted into the environment, contributing to pollution. In Design 1, the total CO_2 emissions from 1 kg of green diesel are estimated to be 0.0705 kg, while in Design 2, the emissions are reduced to 0.0617 kg. However, the CO_2 emissions from green diesel production remain relatively low when contrasted with the 0.21 kg_{Carbon}/kg associated with petroleum diesel [32].

The CO_2 sequestration capacity of palm oil is 159 kg $CO_{2,\,eq}$/h (0.155 kg CO_2/ kg green diesel), which is sufficient to ensure the carbon footprint balance of both Designs 1 and 2. This CO_2 sequestration value allows the CO_2 emission of both designs to be completely captured by palm tree.

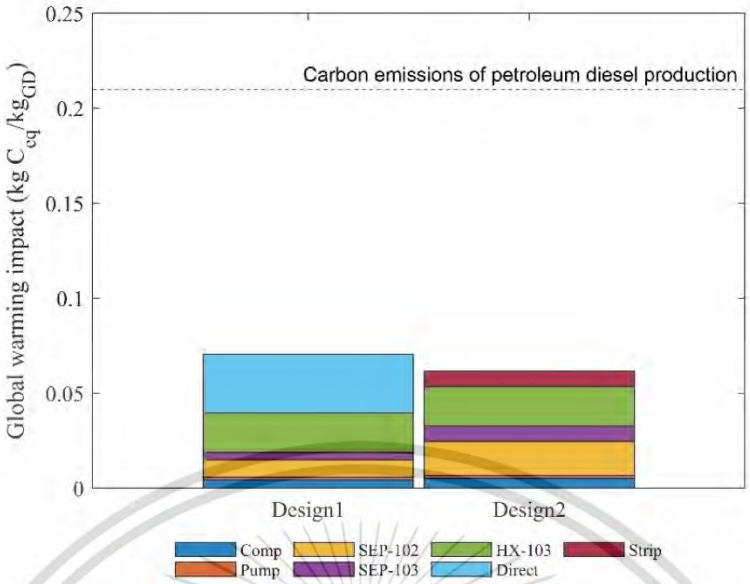

Figure 4.19 The environmental assessment result of green diesel production in term of global warming impact

In summary, carbon dioxide emissions have harmful environmental consequences. Therefore, it is advisable to integrate a process with a carbon capture unit to minimize unnecessary carbon dioxide emissions.

CHAPTER 5
CONCLUSIONS AND RECOMMENDATIONS

5.1 Conclusions

The green diesel production process was presented in two designs: Design 1 with ETSC and without CO_2 capture integration and Design 2 with ETSC and post-separation CO_2 capture. The performance of the green diesel production process was assessed through mass balance, energy consumption analysis, heat integration, and CO_2 emission analysis. The green diesel product from both designs had a production rate of 1,083 kg/h with a purity of 98.27 wt%. By-products from Design 2 are green propane and CO_2. The net energy consumptions for Design 1 and Design 2 after heat integration exhibit a substantial reduction, decreasing from initial values of 950.91 kW and 1,022.92 kW to 460.49 kW and 510.88 kW, respectively.

Economic evaluation is performed by Guthrie preliminary estimate method. The total capital investment and operating cost of Design 1 are found to be 5.223 M$ and 16.11 M$, respectively, while the Design 2 has total capital investment and operating cost, which are 8.64 M$ and 16.55 M$, respectively. A cumulative cash flow analysis revealed a negative NPV in year 15 of -28.1 M$ for Design 1 and -30.2 M$ for Design 2. In terms of techno-economic sensitivity analysis, it is notable that the selling price of green diesel and the cost of purchasing CPO have the most significant impact on the NPV. After increasing the selling price of green diesel from 1.13 to 1.98 $/kg$_{GD}$ and decreasing the cost of purchasing CPO from 0.81 to 0.47 $/kg$_{CPO}$, the NPV becomes positive, reaching 1.9 M$ and 0.9 M$ in year 15 for Design 1 and Design 2, respectively. As a result of these changes, the payback periods for Design 1 and Design 2 decreased to 6.7 years and 9.5 years, respectively.

The environmental analysis is conducted through the utilization of Life Cycle Assessment (LCA) techniques, encompassing various stages, including planning, harvesting, collection, and the hydrotreating process of palm oil. The results indicate that TEIP has the most significant environmental impact in both designs. This is likely since the cultivation of oil palm plantations often entails the extensive use of pesticides and agrochemicals. Green diesel contributes to carbon neutrality because the CO_2 emissions generated during combustion are balanced by the CO_2 absorbed during feedstock growth, creating a closed carbon loop. The carbon sequestration of palm oil,

which is -159 kg CO_{2eq}/h, can ensure the carbon footprint equilibrium in Design 2. In comparison to fossil fuels, green diesel typically exhibits lower net greenhouse gas emissions and can play a role in reducing air pollution. The carbon emissions from petroleum are approximately 0.21 kg of carbon per kg, while the CO_2 emissions from green diesel are 0.075 and 0.0617 for Design 1 and Design 2, respectively.

The comparison between green diesel and petroleum diesel highlights the intricate balance between economic and environmental considerations. Green diesel presents environmental advantages, such as reduced carbon emissions and improved air quality, making it a more sustainable and eco-friendly option. However, its production cost is often higher, which can be mitigated through government incentives and subsidies. Petroleum diesel, though economically competitive, carries environmental drawbacks due to its association with higher carbon emissions and resource depletion.

5.2 Recommendation

Integrating co-production into the green diesel production process can yield several notable benefits. This approach enhances resource efficiency by utilizing feedstocks more effectively, thereby reducing waste and conserving valuable resources. By co-producing valuable byproducts alongside green diesel, the overall economic viability of the plant is strengthened. This synergistic approach not only contributes to a more sustainable and environmentally friendly production process but also bolsters the economic bottom line through the extraction of additional value from the same raw materials.

REFERENCES

[1] W. Wu, R. Supankanok, W. Chandra-Ambhorn, and M. I. Taipabu, "Novel CO2-negative design of palm oil-based polygeneration systems," *Renew Energy*, vol. 203, pp. 622–633, Feb. 2023, doi: 10.1016/j.renene.2022.12.103.

[2] S. K. Hoekman, A. Broch, C. Robbins, E. Ceniceros, and M. Natarajan, "Review of biodiesel composition, properties, and specifications," *Renewable and Sustainable Energy Reviews*, vol. 16, no. 1. pp. 143–169, Jan. 2012. doi: 10.1016/j.rser.2011.07.143.

[3] D. Garraín, I. Herrera, Y. Lechón, and C. Lago, "Well-to-Tank environmental analysis of a renewable diesel fuel from vegetable oil through co-processing in a hydrotreatment unit," *Biomass Bioenergy*, vol. 63, pp. 239–249, 2014, doi: 10.1016/j.biombioe.2014.01.035.

[4] Jessica Aizarani, "Global biofuels market size 2020-2030." Accessed: Jun. 05, 2023. [Online]. Available: https://www.statista.com/statistics/217179/global-biofuels-market-size/

[5] J. Moreno Fernández-Villamil and A. Hurtado De Mendoza Paniagua, "Preliminary design of the green diesel production process by hydrotreatment of vegetable oils."

[6] A. Tirado, J. Ancheyta, and F. Trejo, "Kinetic and Reactor Modeling of Catalytic Hydrotreatment of Vegetable Oils," *Energy and Fuels*, vol. 32, no. 7, pp. 7245–7261, Jul. 2018, doi: 10.1021/acs.energyfuels.8b00947.

[7] M. Ameen, M. T. Azizan, A. Ramli, S. Yusup, and M. S. Alnarabiji, "Catalytic hydrodeoxygenation of rubber seed oil over sonochemically synthesized Ni-Mo/γ-Al2O3 catalyst for green diesel production," *Ultrason Sonochem*, vol. 51, pp. 90–102, Mar. 2019, doi: 10.1016/j.ultsonch.2018.10.011.

[8] A. Guzman, J. E. Torres, L. P. Prada, and M. L. Nuñez, "Hydroprocessing of crude palm oil at pilot plant scale," *Catal Today*, vol. 156, no. 1–2, pp. 38–43, Oct. 2010, doi: 10.1016/j.cattod.2009.11.015.

[9] M. Ameen, M. T. Azizan, S. Yusup, and A. Ramli, "Hydroprocessing of rubber seed oil over Ni-Mo/γ-Al2O3 for the green diesel production," *Chem Eng Trans*, vol. 61, pp. 1843–1848, 2017, doi: 10.3303/CET1761305.

[10] S. L. Douvartzides, N. D. Charisiou, K. N. Papageridis, and M. A. Goula, "Green diesel: Biomass feedstocks, production technologies, catalytic research, fuel

properties and performance in compression ignition internal combustion engines," *Energies*, vol. 12, no. 5. MDPI AG, Feb. 28, 2019. doi: 10.3390/en12050809.

[11] M. Ameen, M. T. Azizan, A. Ramli, S. Yusup, and M. S. Alnarabiji, "Catalytic hydrodeoxygenation of rubber seed oil over sonochemically synthesized Ni-Mo/γ-Al2O3 catalyst for green diesel production," *Ultrason Sonochem*, vol. 51, pp. 90–102, Mar. 2019, doi: 10.1016/j.ultsonch.2018.10.011.

[12] X. Li *et al.*, "Heterogeneous sulfur-free hydrodeoxygenation catalysts for selectively upgrading the renewable bio-oils to second generation biofuels," *Renewable and Sustainable Energy Reviews*, vol. 82. Elsevier Ltd, pp. 3762–3797, Feb. 01, 2018. doi: 10.1016/j.rser.2017.10.091.

[13] D. Kubička and V. Tukač, "Hydrotreating of Triglyceride-Based Feedstocks in Refineries," in *Advances in Chemical Engineering*, vol. 42, Academic Press Inc., 2013, pp. 141–194. doi: 10.1016/B978-0-12-386505-2.00003-1.

[14] P. Kittisupakorn, S. Sae-ueng, and A. Suwatthikul, "Optimization of Energy Consumption in a Hydrotreating Process for Green Diesel Production from Palm Oil," in *Computer Aided Chemical Engineering*, vol. 38, Elsevier B.V., 2016, pp. 751–756. doi: 10.1016/B978-0-444-63428-3.50130-2.

[15] T. J. Hilbers, L. M. J. Sprakel, L. B. J. van den Enk, B. Zaalberg, H. van den Berg, and L. G. J. van der Ham, "Green Diesel from Hydrotreated Vegetable Oil Process Design Study," *Chem Eng Technol*, vol. 38, no. 4, pp. 651–657, Apr. 2015, doi: 10.1002/ceat.201400648.

[16] S. L. Douvartzides, N. D. Charisiou, K. N. Papageridis, and M. A. Goula, "Green diesel: Biomass feedstocks, production technologies, catalytic research, fuel properties and performance in compression ignition internal combustion engines," *Energies*, vol. 12, no. 5. MDPI AG, Feb. 28, 2019. doi: 10.3390/en12050809.

[17] K. Landberg, "Experimental and kinetic modelling study of hydrodeoxygenation of tall oil to re-newable fuel."

[18] A. Srifa, K. Faungnawakij, V. Itthibenchapong, N. Viriya-empikul, T. Charinpanitkul, and S. Assabumrungrat, "Production of bio-hydrogenated diesel by catalytic hydrotreating of palm oil over NiMoS2/γ-Al2O3 catalyst," *Bioresour Technol*, vol. 158, pp. 81–90, 2014, doi: 10.1016/j.biortech.2014.01.100.

[19] P. Madejski, K. Chmiel, N. Subramanian, and T. Kuś, “Methods and Techniques for CO2 Capture: Review of Potential Solutions and Applications in Modern Energy Technologies,” *Energies*, vol. 15, no. 3. MDPI, Feb. 01, 2022. doi: 10.3390/en15030887.

[20] T. M. Pessanha, C. L. Quintanilha, C. N. Da Silva, and J. C. Afonso, “Characterization of several generations of nimo hydroprocessing catalysts employed in the same hydrotreater,” *Quim Nova*, vol. 42, no. 4, pp. 397–404, 2019, doi: 10.21577/0100-4042.20170323.

[21] C. Sowcharoensuk, “PALM OIL INDUSTRY.”

[22] Department of internal trade, “ปาล์มน้ำมัน ราคาผลปาล์มและน้ำมันปาล์มรายวัน.”

[23] LLC. Intratec Solutions, “Monitor Monoethanolamine Prices Worldwide.”

[24] Ltd. Zibo Yinghe Chemical Co., “Ni-Mo Catalyst /Al2O3 Catalyst For Fydrofining Desulfurization.”

[25] S. Skarlis, E. Kondili, and J. K. Kaldellis, “Small-scale biodiesel production economics: A case study focus on Crete Island,” *J Clean Prod*, vol. 20, no. 1, pp. 20–26, 2012, doi: 10.1016/j.jclepro.2011.08.011.

[26] W. Wu, H. Xu, B. Shi, and P. C. Kuo, “Techno-economic analysis of plastic wastes-based polygeneration processes,” *Chemical Engineering and Processing - Process Intensification*, vol. 184, Feb. 2023, doi: 10.1016/j.cep.2023.109297.

[27] Y. D. Publications, Y. Demirel, and Y. Demirel, “Cite this article: Demirel Y (2013) Sustainable Operations for Distillation Columns,” 2013. [Online]. Available: https://digitalcommons.unl.edu/cbmedemirel

[28] M. Alhajji and Y. Demirel, “Energy intensity and environmental impact metrics of the back-end separation of ethylene plant by thermodynamic analysis,” *International Journal of Energy and Environmental Engineering*, vol. 7, no. 1, pp. 45–59, Mar. 2016, doi: 10.1007/s40095-015-0194-9.

[29] Y. D. Rivera-Méndez, D. T. Rodríguez, and H. M. Romero, “Carbon footprint of the production of oil palm (Elaeis guineensis) fresh fruit bunches in Colombia,” *J Clean Prod*, vol. 149, pp. 743–750, Apr. 2017, doi: 10.1016/j.jclepro.2017.02.149.

[30] Y. A. Cengel and A. J. Ghajar, *Heat and Mass Transfer Fundamental and Application*, 5th ed., vol. 283. 2016.

[31] U.S. Energy Information Administration, “PETROLEUM & OTHER LIQUIDS.”

[32] S. P. de Souza, S. Pacca, M. T. de Ávila, and J. L. B. Borges, “Greenhouse gas emissions and energy balance of palm oil biofuel,” *Renew Energy*, vol. 35, no. 11, pp. 2552–2561, Nov. 2010, doi: 10.1016/j.renene.2010.03.028.

APPENDIX

Table A. 1 Costing specification for reactor in Design 1

Chemical reactor	**R-101**
Operating pressure (psig)	421.00
Design pressure (psig)	492.35
Inside shell diameter (in)	24.61
Max allowable stress (psi)	15,000
Fractional weld efficiency	0.85
Wall thickness (in)	0.49
Shell thickness (in)	0.74
Length, L(in)	399.61
Density of material (lb/in^3)	0.28
Weight (lb)	6981.19
Material factor	3.6
Purchase cost vessel ($)	25,850.91
Cost of the platforms and ladders ($)	8,309.38
Purchase cost ($)	15,245.23
Update purchase cost ($\$_{2022}$)	22,077.62

Table A. 2 Costing specification for pump in Design 1

Centrifugal Pump	**P-101**
Flow rate (gpm)	8.28
Pump head (ft)	49.01
Size factor	57.94
Bare cost ($)	7,622.61
Pump type factor	1
Material factor	2
Purchase cost ($)	15,245.23
Update purchase cost ($\$_{2022}$)	22,077.62

Table A. 3 Costing specification for compressor in Design 1

Compressor	**C-101**
Electric motor drive	1.25
Material factor	1.00
Consumed power (Hp)	21.77
Bare cost ($)	65,902.68
Purchase cost ($)	82,378.35
Update purchase cost ($$_{2022}$)	119,297.51

Table A. 4 Costing specification for heater in Design 1

Heater	**HX-103**
Heat duty (Btu/hr)	329,499.24
Operating pressure (psig)	421.00
Pressure factor	1.00
Material factor	1.70
Bare cost ($)	18,421.50
Purchase cost ($)	31,174.36
Update purchase cost ($$_{2022}$)	45,145.64

Table A. 5 Costing specification for heat exchanger in Design 1

Heat Exchanger	**HX-101**	**HX-102**
Surface area (ft^2)	90.84	5.74
Material factor	1	1
Operating pressure	419.49	419.49
Pressure factor	1.09	1.09
Tube length factor	1.25	1.25
Bare cost ($)	12,081.62	28,127.75
Purchase cost ($)	16,396.62	38,173.68
Update purchase cost ($$_{2022}$)	23,754.02	55,281.82

Table A. 6 Costing specification for reactor in Design 2

Chemical reactor	**R-101**
Operating pressure (psig)	420.94
Design pressure (psig)	492.29
Inside shell diameter (in)	24.61
Max allowable stress (psi)	15,000.00
Fractional weld efficiency	0.85
Wall thickness (in)	0.49
Shell thickness (in)	0.74
Length, L(in)	399.61
Density of material (lb/in^3)	0.28
Weight (lb)	6,980.57
Material factor	3.60
Purchase cost vessel ($)	25,849.60
Cost of the platforms and ladders ($)	8,309.38
Purchase cost ($)	101,367.95
Update purchase cost ($\$_{2022}$)	149,755.35

Table A. 7 Costing specification for pump in Design 2

Centrifugal Pump	**P-101**	**P-102**	**P-103**
Flow rate (gpm)	2.04	1.94	8.29
Pump head (ft)	36.28	3.73	427.04
Size factor	12.27	3.74	171.41
Bare cost ($)	18,717.80	49,300.42	5,206.46
Pump type factor	1	1	1
Material factor	2	2	2
Purchase cost ($)	37,437.60	98,600.83	10,412.93
Update purchase cost ($\$_{2022}$)	54,212.95	142,790.35	15,079.65

Table A. 8 Costing specification for compressor in Design 2

Compressor	**C-101**	**C-201**	**C-202**
Electric motor drive	1.25	1.25	1.25
Material factor	1.00	1.00	1.00
Consumed power (Hp)	22.29	206.48	32.64
Bare cost ($)	66,893.11	271,936.98	85,070.63
Purchase cost ($)	83,616.38	339,921.23	106,338.29
Update purchase cost ($$_{2022}$)	121,090.38	492,262.29	153,995.47

Table A. 9 Costing specification for heater in Design 2

Heater	**HX-103**
Heat duty (Btu/hr)	386,342.43
Operating pressure (psig)	420.94
Pressure factor	1.00
Material factor	1.70
Bare cost ($)	20,872.89
Purchase cost ($)	35,322.69
Update purchase cost ($$_{2022}$)	51,153.12

Table A. 10 Costing specification for heat exchanger in Design 2

Heat Exchanger	**HX-101**	**HX-102**	**HX-201**
Surface area (ft^2)	29.79	7.92	5.86
Material factor	1	1	1
Operating pressure	419.49	419.49	14.31
Pressure factor	1.09	1.09	0.98
Tube length factor	1.25	1.25	1.25
Bare cost ($)	14,199.52	23,610.65	27,788.81
Purchase cost ($)	19,270.93	32,043.28	34,142.40
Update purchase cost ($$_{2022}$)	27,907.50	46,403.99	49,443.86

Table A. 11 Costing specification for absorber and stripper in Design 2

Absorber and stripper	**AB**	**ST**
Operating pressure (psig)	-	14.50
Design pressure (psig)	10.00	21.49
Inside shell diameter (in)	12.60	13.78
Max allowable stress (psi)	15,000.00	15,000.00
Fractional weld efficiency	0.85	0.85
Wall thickness (in)	0.00	0.01
Shell thickness (in)	0.25	0.26
Length (in)	485.83	338.19
Density of material (lb/in^3)	0.28	0.28
Weight (lb)	1,450.06	1,144.60
Material factor	1.00	1.00
Purchase cost vessel	23,129.03	21,453.33
Cost of the platforms and ladders	5,815.16	4,809.65
Purchase cost ($)	28,944.19	26,262.98
Volume packing (ft^3)	35.04	29.15
Installed cost of packing ($/$ft^3$)	36.00	36.00
Area (ft^2)	0.87	1.04
Liquid Distributor Cost ($/$ft^2$)	140.00	140.00
C_{DR}	242.33	290.69
Total Purchase cost ($)	30,448.05	27,603.13
Update purchase cost ($\$_{2022}$)	44,093.83	39.973.90

Table A. 12 Costing specification for absorber and stripper in Design 2

Separators	**SEP-101**	**SEP-102**	**SEP-103**
residence time (hr^{-1})	0.08	0.08	0.08
Volumetric flow rate (cum/hr)	1.65	0.08	0.04
Volume vessel (m^3)	0.27	0.01	0.01
Volume vessel (in^3)	16736.55	780.95	359.13
L/D ratio	4	4	4
Operating pressure (psig)	421.00	421.00	421.00
Design pressure (psig)	492.35	492.35	492.35
Inside shell diameter (in)	17.47	6.29	4.85
Max allowable stress (psi)	15,000.00	15,000.00	15,000.00
Fractional weld efficiency	0.85	0.85	0.85
Wall thickness (in)	0.35	0.12	0.10
Shell thickness (in)	0.60	0.37	0.35
Length (in)	69.86	25.15	19.41
Density of material (lb/in^3)	0.28	1.28	2.28
Weight (lb)	804.05	303.56	300.64
Material factor	1.00	1.70	1.70
Purchase cost vessel	19,394.99	15,763.21	15,738.98
Cost of the platforms and ladders	1,879.75	428.89	294.90
Purchase cost ($)	21,274.74	27,226.34	27,051.16

Table A. 13 Bare module cost of Design 1 and Design 2

Equipment	Bare module factor	Purchase cost (M$)		BMC (M$)	
		Design 1	Design 2	Design 1	Design 2
Heat exchanger	3.17	0.124	0.175	0.394	0.554
Pump	3.3	0.022	0.212	0.073	0.700
Compressor	2.15	0.119	0.767	0.256	1.650
Stripper	4.16	-	0.040	-	0.166
Absorber	4.16	-	0.044	-	0.183
Separator	3.05	0.110	0.109	0.336	0.334
Reactor	4.16	0.147	0.147	0.611	0.611
ETSC	1	0.064	0.064	0.064	0.064
Land	1	0.012	0.030	0.012	0.030
Total		**0.598**	**1.589**	**1.746**	**4.198**

Table A. 14 Utility for Design 1

Utilities	Cost	Usage	Annual cost ($)
Water	0.067 $/1000kg	34,940 kg/hr	16,061
Refrigeration	0.190 $/1000kg	334,577 kg/hr	213,991
Electricity	0.120 $/kWh	21.59 kW/hr	18,614
Total			**248,666**

Table A. 15 Utility for Design 2

Utilities	Cost	Usage	Annual cost ($)
Water	0.067 $/1000kg	34,940 kg/hr	16,855
Refrigeration	0.190 $/1000kg	334,577 kg/hr	457,701
Electricity	0.120 $/kWh	21.59 kW/hr	18,652
Steam	29.970 $/1000kg	58.63 kg/hr	12,651
Total			**505,859**

Table A. 16 Impact analysis results

Impact categories	Design 1	Design 2
Abiotic depletion	0.0214	0.0218
Abiotic depletion (fossil fuels)	-0.1403	-0.1313
Acidification	0.2412	0.2429
Eutrophication	0.7952	0.7921
Global warming	0.6021	0.5988
Ozone layer depletion	-0.0007	-0.0005
Human toxicity	0.0671	0.0689
Fresh water aquatic ecotoxicity	7.2233	7.2118
Marine aquatic ecotoxicity	2.1632	2.1200
Terrestrial ecotoxicity	33.2359	33.2345
Photochemical oxidation	0.4342	0.2813

AUTHOR BIOGRAPHY

Name:	Mr. Nattapat Pongboriboon
Date of Birth:	December 14, 1998
Education:	(2021) Bachelor of Engineering Department of Chemical Engineering, School of Engineering King Mongkut's Institute of Technology Ladkrabang (2023) Master of Engineering Dual Degree Program, Department of Chemical Engineering, King Mongkut's Institute of Technology Ladkrabang and National Cheng Kung University
Specialized Skill:	1) Renewable energy system 2) Chemical process design and optimization 3) Simulation program (MATLAB, SimaPro, Aspen energy analyser and, Aspen Plus)
Working Experience:	2020 Process Engineer at SCG SHEMICALS CO., LTD. (SCG Excellent Internship Program 19th) Project: Analyzing Deviations from Standard: A Study on LS Consumption at E-3307
Publication:	Pongboriboon, N.; Wu, W.; Chandra-ambhorn, W.; Wongpromrat, P.; Bumrungthaichaichan, E. Simple Empirical Relation for an Evacuated-Tube Solar Collector Performance Prediction from Solar Intensity. *Energies* **2023**, *16*(17), 6256. https://doi.org/10.3390/en16176256